REPORT DOCUMENTATION PAGE

Form Approved
OMB No. 0704-0188

1. AGENCY USE ONLY (Leave blank)	2. REPORT DATE	3. REPORT TYPE AND DATES COVERED
	Dec 94	

4. TITLE AND SUBTITLE
Analysis of the Structural Characteristics & Intensity Evolution of Super Typhoon Flo (1990) in Special Sensor Microwave Imager Data

5. FUNDING NUMBERS

6. AUTHOR(S)

Edward C. Melton III

7. PERFORMING ORGANIZATION NAME(S) AND ADDRESS(ES)

AFIT Students Attending:

North Carolina State Univ

8. PERFORMING ORGANIZATION REPORT NUMBER
AFIT/CI/CIA

94-173

9. SPONSORING/MONITORING AGENCY NAME(S) AND ADDRESS(ES)

DEPARTNEMT OF THE AIR FORCE
AFIT/CI
2950 P STREET, BDLG 125
WRIGHT-PATTERSON AFB OH 45433-7765

10. SPONSORING/MONITORING AGENCY REPORT NUMBER

11. SUPPLEMENTARY NOTES

12a. DISTRIBUTION/AVAILABILITY STATEMENT

Approved for Public Release IAW AFR 190-1
Distribution Unlimited
BRIAN D. GAUTHIER, MSgt, USAF
Chief Administration

12b. DISTRIBUTION CODE

13. ABSTRACT *(Maximum 200 words)*

14. SUBJECT TERMS	15. NUMBER OF PAGES 112
	16. PRICE CODE

17. SECURITY CLASSIFICATION OF REPORT	18. SECURITY CLASSIFICATION OF THIS PAGE	19. SECURITY CLASSIFICATION OF ABSTRACT	20. LIMITATION OF ABSTRACT

ABSTRACT

MELTON, EDWARD C. III. Analysis of the Structural Characteristics and Intensity Evolution of Super Typhoon Flo (1990) in Special Sensor Microwave/ Imager (SSM/I) Data. (Under the direction of Sethu Raman and Simon W. Chang)

The purpose of this research has been to observe and analyze the structural details and intensity evolution of Super Typhoon Flo (1990) using SSM/I data. Flo's structural characteristics were observed with SSM/I imagery and then compared with conventional, infrared and visible satellite data to illustrate qualitative distinctions between the two types of data. High resolution 85-Ghz imagery showed more convective detail than operational line scan (OLS) data while low resolution 19-Ghz data afforded more realistic analysis of the active tropical cyclone region when compared with GMS data. Center locations determined in horizontally polarized 85-Ghz imagery offered improvement over the OLS fixes obtained from corresponding DMSP passes. However, the SSM/I derived 85 and 19-Ghz retrieval statistics, employed as intensity indicators in previous tropical cyclone research, were poorly correlated with changes in Flo's intensity.

Two over ocean SSM/I rainfall rate retrieval algorithms were compared for accuracy. The more accurate algorithm employing the 85-Ghz frequency was used to characterize Super Typhoon Flo's rainfall rate distribution and intensity evolution. Results are generally similar to previous studies. Maximum rainfall rates were usually confined to the eyewall and inner-core region. Furthermore, changes in Flo's average inner-core rainfall rate correlated reasonably well with intensity changes. However, the magnitude of Super Typhoon Flo's average rainfall rates within the eyewall and inner-core were significantly lower as compared to previous studies on similar tropical cyclones. Finally, the highest rainfall rates were generally concentrated in the forward sectors of Flo's inner-core region

relative to the direction of storm motion. These results were also consistent with similar research.

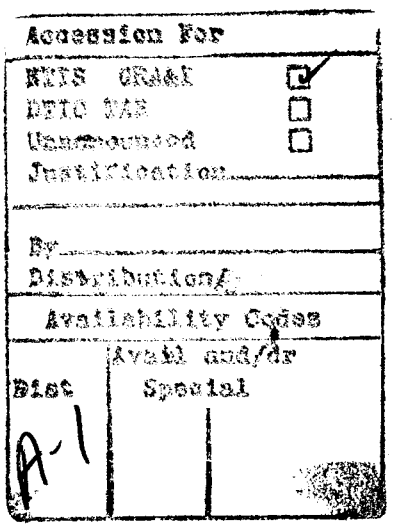

94-173

ANALYSIS OF THE STRUCTURAL CHARACTERISTICS AND INTENSITY EVOLUTION OF SUPER TYPHOON FLO (1990) IN SPECIAL SENSOR MICROWAVE/IMAGER (SSM/I) DATA

by

EDWARD C. MELTON III

A thesis submitted to the Graduate Faculty of
North Carolina State University
in partial fulfillment of the
requirements for the Degree of
Master of Science

MARINE, EARTH, AND ATMOSPHERIC SCIENCES

Raleigh

1994

APPROVED BY:

Dr. S. Raman Committee Chairman	Dr. S. W. Chang Committee Co-Chairman
Dr. R. Madala	Dr. L. Xie

BIOGRAPHY

Edward C. Melton III (Ted) is the son of Captain Edward C. Melton, Jr., USN (Retired), and Rebecca L. (Smith) Melton and was born on the 20th of September 1962 in Monterey, California. He graduated from Manteo High School, Manteo, North Carolina in 1981. The author has one younger brother, Craig B. Melton.

He received a Bachelor of Science degree in Meteorology in December of 1985 from North Carolina State University, Raleigh, North Carolina. After completing Officer Training School in June of 1987, the author was commissioned a second lieutenant in the United States Air Force. In January of 1993, after two operational assignments, he entered Graduate School at North Carolina State University to pursue a Master of Science degree in Meteorology.

The author is married to the former Barbara Anne Burrow of Virginia Beach, Virginia.

ACKNOWLEDGMENTS

The author wishes to extend his gratitude to the United States Air Force and the Air Force Institute of Technology, for providing the opportunity to pursue a postgraduate education. Dr. Sethu Raman of North Carolina State University deserves special aknowledgment for excepting a mid-year graduate student on relatively short notice. In addition, without the help and guidance of Dr. Simon W. Chang of the Naval Research Laboratory, completing this thesis would not have been possible.

Sincere appreciation is extended to members of the Remote Sensing Branch of the Naval Research Laboratory for their hospitality and help during the many visits to Washington D.C. Dr. Jainn-Jong (Roger) Shi's knowledge and assistance in data processing and graphics support proved critical to the completion of this work. Also, special thanks to Mr. Glen Sandlin for providing the SSM/I data used in this research.

Many thanks also go out to Dr. Melinda Peng and Dr. Pat Harr of the Naval Postgraduate School for providing analysis data from the TCM-90 field experiment. Invaluable GMS satellite data was provided by Dr. Chris Velden of the University of Wisconsin. The DMSP polar orbiting satellite images and best track data were graciously furnished by Captain Brooks and Captain Borelli of the Joint Typhoon Warning Center.

Finally, the author wants to thank his friends and family for supporting and encouraging his efforts for the past two years. He is especially grateful to his wife for having faith and confidence in his abilities even during the times when he did not.

This research was supported by funding from the Naval Research Laboratory, Washington, D.C.

TABLE OF CONTENTS

LIST OF TABLES

LIST OF FIGURES

LIST OF ABBREVIATIONS

(D) ..... V-H Polarization Difference
(H) ..... Horizontal Polarization
(V) ..... Vertical Polarization
AOR ..... Area of Responsibility
AVHRR ..... Advanced Very High Resolution Radiometer
BT ..... Brightness Temperature
CDO ..... Cold Dense Overcast
DMSP ..... Defense Meteorological Satellite Program
EDR ..... Environmental Data Record
ESCAP ..... Economic and Social Commission For Asia and the Pacific
Ghz ..... Gigahertz
GMS ..... Geostationary Meteorological Satellite
IOP ..... Intensive Observation Period
IR ..... Infrared
JTWC ..... Joint Typhoon Warning Center
km ..... kilometer
km h^{-1} ..... kilometer per hour
kts ..... nautical miles per hour
LLCC ..... Low Level Circulation Center
m s^{-1} ..... meters per second
mb ..... millibar
mm ..... millimeter
mm h^{-1} ..... millimeter per hour
nm ..... nautical mile
NMC ..... National Meteorological Center
NOAA ..... National Oceanic Space Administration
NOGAPS ..... Naval Operational Global Atmospheric Prediction System
OI ..... Optimum Interpolation
OLS ..... Operational Line Scan
SDR ..... Sensor Data Record
SPECTRUM ..... Special Experiment Concerning Recurvature and Unusual Motion
SRP ..... Selective Reconnaissance Program
SSM/I ..... Special Sensor Microwave/Imager
SST ..... Sea Surface Temperature
TATEX ..... Taiwan Area Typhoon Experiment
TCM-90 ..... Tropical Cyclone Motion Experiment 1990
TUTT ..... Tropical Upper-Tropospheric Trough
VIS ..... Visible
WMO ..... World Meteorological Organization

1. INTRODUCTION

A joint U.S. Navy-Air Force effort launched the first Special Sensor Microwave Imager (SSM/I) on board the Defense Meteorological Satellite Program (DMSP) F-8 Satellite in 1987 (Hollinger et al. 1987). This event was another major milestone in the ongoing development and implementation of remote sensing from space. Since that time the SSM/I has proven its potential as an invaluable source of meteorological information, particularly over the data sparse tropical oceans.

SSM/I data is now operationally available to the military and other government agencies. Among other applications, microwave data has been used effectively as an aid in the analysis of tropical weather systems. Microwave data offers significant advantages over conventional visible (VIS) and infrared (IR) satellite data, particularly when analyzing tropical cyclones (Alliss et al. 1992,1993; Rodgers et al. 1994). Sensor data records (SDRs), depicted as calibrated brightness temperatures (BTs), provide measurements of upwelling microwave energy at several dual polarized frequencies. Combinations of SDRs have been applied in extensively calibrated algorithms to develop environmental data records (EDRs) of various atmospheric parameters. These parameters include rainfall rate, wind speed, integrated water vapor, and cloud liquid water content. Some of the same meteorological information directly observed over land can now be derived from SSM/I over the open ocean where there is a general scarcity of in situ data. Obviously, these capabilities indicate SSM/I would provide a unique tool to facilitate tropical cyclone analysis. SSM/I data reveals the structural details of tropical cyclones where conventional data may not. Satellite sensors that monitor only reflectivity and cloud top temperatures

often detect the presence of high cirrus outflow that may obscure a tropical cyclone's important convective features.

Similar to conventional meteorological satellite data, an extensive effort has been focused on investigating and documenting the potential applications of SSM/I data for operational use. Many studies have demonstrated how SSM/I data may be used to fill the significant in situ data void over the open oceans. In addition to research, SSM/I data has already been incorporated into operational tropical cyclone analysis programs. Both the National Hurricane Center, and most of the satellite reconnaissance network of the Joint Typhoon Warning Center now apply SSM/I data in various areas of the analysis process.

1.1 Data Background and Research Overview

The Joint Typhoon Warning Center (JTWC), located on the island of Guam in the western North Pacific, is the Department of Defense equivalent to the National Hurricane Center in Coral Gables, Florida. Their warning area of responsibility (AOR) covers the western North and South Pacific (west of 180°), and the Indian Ocean including the Bay of Bengal. On 1 April 1960, NASA ushered in a new era in weather observing with the launch of the world's first meteorological satellite, TIROS I. However, it was May 1971, before the first real-time satellite imagery was available to JTWC. This new data was carefully tested through extensive comparisons between satellite and aircraft fixes. After successful validation, satellite fixes were integrated with aircraft fixes marking the beginning of JTWC's Selective Reconnaissance Program (SRP).

In 1987, the last official tropical cyclone aircraft reconnaissance missions were flown by the U.S. Air Force in JTWC's AOR. From 1986 to 1988, JTWC underwent a dramatic transition from a tropical cyclone warning system that relied heavily on aircraft (intensity and position) fixes to an approach based almost entirely on remote sensing from meteorological satellites (McMorrow 1989). During this period, JTWC gained access to Japanese Geostationary Meteorological Satellite (GMS) data while also upgrading their existing DMSP satellite processing capability. Along with the progress in data resources and processing capability, JTWC has continued to refine objective guidelines to help compensate for the absence of "ground truth" aircraft observations. To evaluate their performance without aircraft data, JTWC looked at storm cases from previous years' warnings when aircraft fixes where avialable. With the help of experienced satellite analysts, aircraft/satellite versus satellite only fixes where used to initialize warnings to compare forecast results. The tests showed that there was no significant degradation in tropical cyclone track or intensity forecasts at 24, 48, and 72 hours for the sample cases. However, when compared to best track data, the average position fix error using satellite imagery was 42 km while average aircraft fix error was 33 km.

In 1990, the JTWC and other DMSP direct read out (DRO) sites in the western North Pacific gained access to SSM/I data for operational use. With hardware and software provided by a Hughes Aircraft Corporation contract, DMSP DRO sites could process real time SSM/I data on Sun Sparc2 work stations. The primary application of this data was using SSM/I wind speed EDRs to determine the approximate gale force (>15 ms^{-1}) wind boundaries associated with tropical cyclones. The high resolution SSM/I SDR sensitivity

to convective structure provided an excellent supplement to conventional geostationary and polar orbiting satellite data as a tool for tropical cyclone positioning. In addition, SSM/I rainfall rate imagery was used to qualitatively evaluate tropical cyclone convective structure.

During the peak of the 1990 Typhoon Season, the western North Pacific was the focus of a concerted effort to study tropical cyclone motion for the purpose of improving forecasting capability. The Tropical Cyclone Motion (TCM-90) field experiment was conducted during August and September of 1990. Elsberry (1990) gives a detailed overview of the experiment's mission and objectives. TCM-90 was part of a larger five year Office of Naval Research Tropical Cyclone Motion initiative to improve basic understanding of tropical cyclone motion. Through the efforts and cooperation of many agencies, large amounts of data were collected, processed, and archived for the purpose of facilitating tropical cyclone research. The JTWC served as the command center for the field experiment while data was collected at a variety of locations by an extensive array of observing platforms.

During TCM-90, a series of seven intensive observing periods (IOPs) were directed on six typhoons. Super Typhoon Flo (20W) was the last in the series and the subject of IOPs 6 and 7 during September 1990. The data collected, processed, and archived from these IOPs included aircraft (NASA DC-8), rawinsonde, radar wind profiler, buoy, Doppler radar, and satellite data. Data from the enhanced observation network collected during TCM-90 was used by the National Meteorological Center (NMC) to produce model

analyses for each of the six tropical cyclones. The TCM-90 field experiment is discussed in greater detail in Chapter 3.

1.2 Literature Review

Since the launch of the first SSM/I in 1987, there has been considerable effort concentrated on investigating the various applications of SSM/I data in the analysis of tropical cyclones (Alliss et al. 1992, 1993; Burpee and Black 1989; Felde and Glass 1991; Holiday and Waters 1989; Olson 1989; Rappaport 1991; Rappaport and Black 1989; Rodgers et al. 1994). These studies have illustrated the importance of this data and its potential applications. Specific research initiatives have documented the application of SSM/I SDR and EDR retrievals in the analysis of tropical cyclone convective and horizontal structure. Alliss et al. (1992,1993) used SSM/I EDRs to qualitatively examine the precipitation patterns of Hurricane Hugo (1989) and Hurricane Florence (1988). Felde and Glass (1991) SSM/I SDRs to define the outer boundary of the active tropical cyclone region and to provide information about tropical cyclone horizontal structure.

Some recent studies have also demonstrated favorable correlations between SSM/I data and tropical cyclone intensity. Changes in area averaged SSM/I rainfall rates and derived latent heating parameters have been shown to coincide with intensity changes and in some cases indicate subsequent intensity changes in tropicl cyclones. Rodgers et al. (1994) derived area averaged latent heat measurements from SSM/I rainfall rate EDRs of 18 named western North Atlantic tropical cyclones and determined a relationship between

their inner-core diabatic heating and subsequent intensity changes. Alliss et al. (1992,1993) analyzed SSM/I area averaged rainfall rates and derived total latent heat release from Hurricanes Hugo and Florence correlated well with tropical cyclone intensity. In addition, Alliss et al. (1992) and Felde and Glass (1991) have similarly identified significant associations between tropical cyclone intensity and certain SSM/I SDR derived statistics.

High resolution SSM/I retrievals have also showed promise as an alternative or complimentary source of data for position fixes. Some studies have shown superior accuracy in tropical cyclone center estimates determined from SSM/I data compared to center fixes resolved from conventional VIS or IR satellite imagery (Alliss et al. 1992, 1993; Sandlin and Spangler 1989; Velden et al. 1989). A significant emphasis has also been placed on validating the accuracy of SSM/I wind speed retrievals in the vicinity of tropical cyclones (Alliss et al. 1993; Holliday and Waters 1989).

SSM/I research has also been concentrated in the area of improving model initialization. Numerical weather prediction models have long been used to forecast the motion and intensity of tropical cyclones. However, as noted by Chang and Holt (1991), many numerical weather prediction models continue to experience difficulty in accurately depicting the timing, intensity, and horizontal and vertical distributions of latent heating. Specifically, horizontal divergence and the moisture field are usually the least accurately analyzed in the model initialization process. This difficulty causes an artificial delay in the onset of precipitation also known as the spin up problem. The relative importance of latent heating as a mechanism responsible for the development and maintenance of tropical

cyclones has inspired more research in this area. In several studies, increases and decreases in latent heating rates have been shown to be precursors for intensity changes in tropical cyclones (Alliss et al. 1992; Rodgers 1992). If forecast models could accurately assimilate rainfall rates or the idealized total latent heating distribution either directly or through dynamic initialization, then improvements in both the track and intensity forecasts of tropical cyclones should be expected. This has indeed been the case. Studies have shown the benefits of assimilating idealized rainfall rates into hurricane models. Molinari (1981) assimilated radar observed rainfall rates to improve hurricane model track and intensity forecasts. Assimilating idealized total latent heating as a forcing function and as a dynamic initialization parameter has also been shown to have a positive impact on hurricane track and intensity forecasts (Fiorino and Warner 1981; Adler and Rodgers 1977). Model initialization with SSM/I data has been studied in cases involving mesoscale models and midlatitude marine cyclones (Chang and Holt 1991). Additionally, recent research has also demonstrated improved results by initializing a mesoscale tropical cyclone model with SSM/I data. Specifically, Peng and Chang (1994) have confirmed a positive impact on the numerical prediction of Super Typhoon Flo's track and intensity when their model's physical initialization included SSM/I rainfall rate retrievals.

1.3 Thesis Objectives

The focus of this thesis is to investigate the structure and intensity evolution of Super Typhoon Flo (1990). Flo provides a significant case study in many respects. It was the only storm to reach super typhoon strength during the TCM-90 field experiment. Flo was

also called the most powerful and devastating typhoon to strike mainland Japan in 19 years. However, it was also responsible for some favorable effects. During the period of peak intensity between 16-18 September, Flo caused only minor damage as it passed within 60 nm (110 km) of Okinawa, Japan. According to research aircraft reports, the most intense winds were just offshore, apparently confined to within the immediate eyewall region. Flo's close proximity to the island actually provided some benefit. For the two day period, enough rain fell to end government mandated day-on-day-off water rationing. However, considering the extreme intensity of Super Typhoon Flo and it's slow translation speed as it skirted Okinawa, rainfall totals were much lower than expected.

SSM/I retrievals and data from other sources collected during TCM-90 were used to document the structure and intensity evolution of Super Typhoon Flo. Comparisons were made to provide evidence of the benefits of incorporating SSM/I data into the tropical cyclone analysis process. Conclusions from recent tropical cyclone research were also applied in an effort to evaluate the intensity evolution of Super Typhoon Flo. Finally, careful attention was paid to the accuracy of SSM/I data in tropical cyclone positioning and in evaluating Flo's precipitation structure at peak intensity during it's recurvature near the island of Okinawa, Japan.

Tropical cyclones in general and specifically western North Pacific tropical cyclone activity are discussed in Chapter 2. An overview of Super Typhoon Flo's synoptic background and evolution are also provided. Chapter 3 gives an outline of the data used to analyze Super Typhoon Flo. In addition to SSM/I, selected data from the TCM-90 data set are applied in the analysis.

In Chapter 4, the convective structure of Super Typhoon Flo is examined using 85-Ghz sensor data records. Results from recent investigations demonstrating favorable correlations between tropical cyclone intensity and 85-Ghz data are applied to determine their validity for this storm. As with previous studies, the Super Typhoon Flo example is used to demonstrate the advantage of utilizing horizontally polarized (H) 85-Ghz SDRs to compliment other satellite data resources to improve position fix accuracy.

Felde and Glass (1991) define the active tropical cyclone region as the area covered by gale wind driven seas, high water vapor content, and weather conditions that can include anything from clear skies to convective precipitation. The horizontal structure of Flo's active tropical cyclone region is investigated in Chapter 5. The 19-Ghz SDRs have been used to provide a more accurate description of the size and shape distribution of the active tropical cyclone region. The lower sensor resolution of the 19-Ghz data makes it uniquely suited for this purpose. The Super Typhoon Flo case also provides an opportunity to further test findings from earlier research that show an association between 19-Ghz data and tropical cyclone intensity.

Chapter 6 examines the precipitation structure of Super Typhoon Flo in SSM/I rainfall rate EDRs. The performances of two over ocean SSM/I rainfall rate algorithms are evaluated first. This is accomplished by comparing the SSM/I data to TCM-90 enhanced NMC model analyses, NOGAPS analysis output, as well as rainfall measurements that were recorded on the island of Okinawa during Super Typhoon Flo's recurvature. Once evaluated, the most realistic rainfall rate EDR algorithm is used to investigate the

evolution of Flo's precipitation structure as it compares to similar tropical cyclone precipitation distribution studies.

This thesis concludes by examining the benefits of incorporating SSM/I data, where available, in the tropical cyclone analysis process. Statistically derived SSM/I tropical cyclone intensity parameters, described in other SSM/I research, are examined using Super Typhoon Flo data and their validity is discussed. In addition, the two originally designed SSM/I rainfall rate algorithms compared in this study are shown to be quite different in terms of area averaged values when compared to results from model analyses and raingage information. Finally, the precipitation structure appears to characterize Flo as an abnormally dry typhoon in terms of the SSM/I retrieved rainfall rates and available raingage measurements.

2. SUPER TYPHOON FLO (1990)

2.1 Typhoon Activity

Of all natural disasters, the tropical cyclone is recognized as one of the most destructive. The strong winds, storm surge, and torrential rains associated with tropical cyclones have been responsible for many deaths and enormous destruction. Many of the worlds' population and industrial centers are located in coastal areas vulnerable to tropical cyclone strikes. For this reason, there has been a continued emphasis concentrated on improving our analysis and forecasting capabilities as well as increasing our general understanding of these devastating storms.

Tropical cyclones are warm core mesoscale low pressure systems that form over warm tropical ocean basins. They derive their energy from the release of latent heat. Studies have shown the following conditions should be present for tropical cyclogenesis:

1) Large body of warm SSTs ($\geq 27.5^{0}C$)
2) Conditional instability
3) Midtropospheric moisture
4) Absolute vorticity
5) Weak vertical wind shear and
6) Upper-level divergence

In addition, tropical cyclone formation is also dependent upon Coriolis force. Rarely do these storms form within the latitude belt between 5 degrees south and 5 degrees north. Although the magnitude Coriolis forces is small at low latititudes, it is critical to the

initiation of rotation. Coriolis plays a key role in the generation of absolute vorticity, a parameter critical to tropical cyclogenesis.

The conditions listed above prevail both temporally and spatially over the tropical western North Pacific basin. Approximately 40% of the earth's tropical cyclone activity occurs in this region where an average of 26 named tropical storms and typhoons form annually. Activity is concentrated during the late summer and fall but may occur at anytime during the year. Tropical cyclones in this region vary considerably in terms of intensity and horizontal scale. Western North Pacific tropical cyclones are referred to as typhoons when their maximum sustained winds reach or exceed 33 ms^{-1} (65 kts). Super typhoon intensity is reached when maximum sustained wind velocity exceeds 66 ms^{-1} (134 kts). According to Holliday and Thompson (1979), most super typhoons undergo a period of explosive deepening during their evolution with average pressure falls of 42 mb in 24 hours. An average of three tropical cyclones reach super typhoon intensity each year in the western North Pacific. However, the frequency of super typhoons is highly variable from year to year. The horizontal scale defined by the wind structure is also highly variable among super typhoons. For example, Super Typhoon Gay (1989) had a gale wind (>15 ms^{-1}) diameter of approximately 200 km while Super Typhoon Tip's (1979) gale force wind diameter was close to 2200 km (Guard et al. 1992).

Most of the tropical cyclone activity in the western North Pacific develops within the monsoon trough. After formation, intensification continues as most systems track toward the west-northwest around the southern boundary of subtropical high pressure. Depending on the position, extent, and intensity of the subtropical high, tropical cyclones

reaching typhoon intensity normally follow one of two preferred tracks. When the subtropical ridge weakens, breaks, or retreats eastward, typhoons recurve toward cooler waters of the North Pacific sometimes striking the Japanese Islands, Taiwan, Korea, or the east coast of mainland China. Climatologically, typhoons more frequently follow this preferred recurvature track during the period between the end of summer through fall as midlatitude features begin to influence the position and intensity of the subtropical high. However, through the peak of summer, the subtropical ridge remains firmly in place over the southwestern North Pacific. During this period, climatology indicates typhoons tend to frequently follow a more westward track through the Philippine Sea, possibly striking the Philippines before entering the South China Sea and making final land fall on the coast of Vietnam, Hianan, Hong Kong, or southern mainland China.

2.2 Evolution of Super Typhoon Flo (20W)

Flo was the first of four super typhoons and the twentieth of thirty-two numbered storms to form in the western North Pacific during 1990. After a few days of observing a persistent area of convection within the monsoon trough well east of Guam near the Marshall Islands, the Joint Typhoon Warning Center (JTWC) issued the first warning on tropical depression 20W at 1800 UTC 12 September 1990. Twenty-four hours after the first warning, tropical depression 20W became Tropical Storm Flo. It formed south of the subtropical ridge within the monsoon trough in Typhoon Ed's (19W) wake.

For four and a half days before the first warning was issued on Flo, meteorological satellite analysts at JTWC continued monitoring an area of disorganized convection

within the monsoon trough near the Marshall Islands. A few days earlier, on 7 September, the first warnings were issued on Typhoon Ed (19W) as it formed 1390 km (750 nm) east of Guam. Ed tracked west passed Guam as a minimal tropical storm before continuing around the southern extent of the subtropical ridge. The disturbance that was to become Flo was located east of Ed's point of origin and did not begin to organize until Ed intensified well west of Guam. The strong southwesterly monsoon flow, apparently enhanced by Ed's wake, provided the stimulus needed to consolidate the convection and low-level circulation that led to Flo's eventual development. Flo continued to intensify at the Dvorak (1984)-derived average rate of one T-number per day (the Dvorak T-number is determined from cloud top temperatures in enhanced infrared satellite imagery and directly corresponds to current tropical cyclone intensity), reaching typhoon strength at 0600 UTC, 15 September 1990. Following in Typhoon Ed's wake, Flo tracked west-northwest at 22 kmh^{-1} (12 kts) around the southern extent of the subtropical ridge. Once a typhoon, Flo experienced rapid intensification for the following 36 hours and was upgraded to super typhoon status at 1200 UTC, 16 September 1990. It was also at this time that Super Typhoon Flo turned more northwestward toward a break in the subtropical ridge induced by a passing short-wave north of Okinawa, Japan. On 17 September, dropsonde data from the second TCM-90 aircraft reconnaissance mission revealed an uncorrected central pressure of 891 mb. Super Typhoon Flo's observed central pressure was very close to the Dvorak (1984) current intensity estimates derived from enhanced infrared satellite imagery. Based on the aircraft information, JTWC increased the maximum sustained winds from 135 kts (69 ms^{-1}) to 145 kts (75 ms^{-1})

on their 0600 UTC warning. It was near this time that Flo decreased it's forward speed and began to recurve in response to the deepening and eastward migrating short-wave. During recurvature, Flo passed 110 km (60 nm) east of Okinawa. Although it skirted the island, damage was minimal because the most extreme winds remained concentrated within the eyewall. Remaining over the warm waters of the Kuroshio Current, Flo began to track northeast toward the short-wave induced break in the subtropical ridge in the direction of the southern Japanese mainland. Although Super Typhoon Flo weakened quickly under the influence of an unfavorable shear environment and slightly cooler ocean temperatures, it still made landfall near Osaka with sustained winds of 90 kts (45 ms^{-1}). Flo was the most powerful typhoon to strike southern Honshu in 19 years and was blamed for 32 deaths along with damage estimates totalling in the millions of dollars. After continued weakening over the rugged terrain of mainland Japan, Typhoon Flo was downgraded to tropical storm status at 0000 UTC, 20 September 1990. A day later, Flo proceeded to track northeast over the cooler waters of the northern Pacific ocean finally transitioning to an extratropical system. Super Typhoon Flo's track and intensity evolution are summarized in the final JTWC best track shown in Figure 2.1.

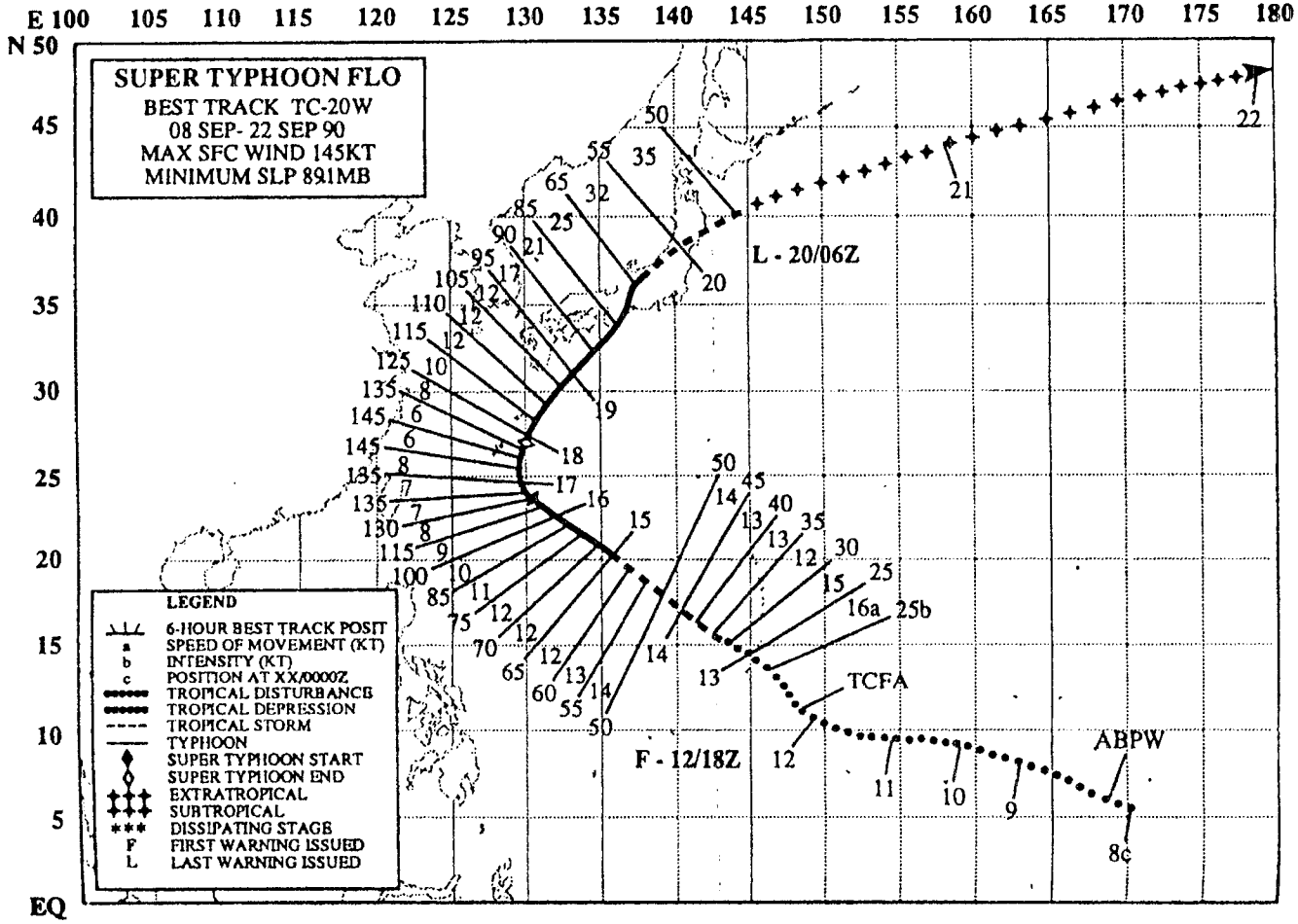

Figure 2.1. Super Typhoon Flo (20W) best track representation with maximum sustained winds (kts) and foreward speed.

3. DATA

3.1 SSM/I Data

3.1.1 General Description

The first Special Sensor Microwave/Imager (SSM/I) was launched 19 June 1987 aboard the Defense Meteorological Satellite Program (DMSP) Block 5D-2 Spacecraft F-8 (Hollinger et al. 1987). Since that time, two more DMSP launches have included similar SSM/I equipment. All DMSP spacecraft follow a circular sun-synchronous near-polar orbit completing 14.1 revolutions per day (one revolution every 102 minutes). Each spacecraft orbits at an altitude of 833 km with an inclination angle of 98.8 degrees. Nodal times for all operating DMSP spacecraft take place in the mid to late morning and again in the mid to late evening.

The SSM/I passively measures emitted and scattered microwave energy from the earth and atmosphere at 4 frequencies. Upwelling radiation is measured at dual polarized frequencies of 19, 37, 85-Ghz, and only vertically polarized at 22-Ghz. These seven channels are referred to as sensor data records or SDRs. Combinations of these channels provide important information on a number of meteorological parameters. The SDR resolution is approximately 15 km, 30 km, and 50 km for the 85-Ghz, 37-Ghz, and 22/19-Ghz frequencies, respectively. The SSM/I's 85-Ghz channel provides the highest microwave resolution ever flown aboard an orbiting satellite platform. The seven channels express measurements of microwave energy in terms of calibrated brightness temperatures (BTs). SSM/I data is extremely valuable for meteorological applications over oceans because the open ocean appears as a relatively uniform background in terms of BTs.

The seven channel SSM/I instrument detects energy scattered and emitted by atmospheric constituents creating a significant contrast between the ocean and atmosphere in the presence of meteorological parameters . Environmental data records (EDRs) developed were developed from extensively calibrated algorithms determined from combinations of SDRs. They provide a more direct approach to measure atmospheric parameters such as rainfall rate, marine surface wind speed, integrated water vapor, and cloud liquid water than has previously been available. These capabilities are particularly useful for observing tropical weather systems over open tropical oceans. Specifically, a general scarcity of in situ data collected in the vicinity of intense tropical cyclones makes SSM/I data an excellent analysis tool. The upwelling microwave energy in the channels measured by SSM/I easily passes through cirrus clouds without attenuation revealing important structural features often obscured in visible and infrared satellite data. The SSM/I provides improvements in the ability to discern features such as convective bands and eyewall structure often undetectable in conventional satellite imagery.

Initially, one of the key weaknesses of SSM/I was it's limited swath width (1400 km). Data gaps over the tropics meant only an 89% probability of observing a particular tropical cyclone at least once per day. However, there are now SSM/I sensors aboard two orbiting DMSP spacecraft improving the probability of daily tropical cyclone observations to 99% for one overpass, 89% for two overpasses, and 59% for three overpasses.

The SSM/I SDRs most sensitive to the scattering and emission from atmospheric conditions associated with tropical cyclones were used to analyze the structural characteristics and intensity evolution of Super Typhoon Flo. These included the 85 and

19-Ghz frequencies. The 19-Ghz frequency has been shown to be sensitive to microwave attenuation by atmospheric constituents. For this reason, both the vertically and horizontally polarized 19-Ghz channels are included as variables in the two SSM/I rainfall rate algorithms used in this study. The high resolution horizontally polarized 85-Ghz channel has been shown to be very sensitive to convection. This is demonstrated in qualitative comparisons with conventional satellite data and by showing the channel's impact on the accuracy of two rainfall rate algorithms. SSM/I rainfall rate EDRs are also very important in tropical cyclone analysis. The data can be used to investigate the precipitation structure and sometimes the intensity evolution of tropical cyclones. The following section describes the two rainfall rate algorithms used later in this study.

3.1.2 SSM/I Rainfall Rate Algorithms

Since the advent of SSM/I in 1987, passive microwave data has evolved as a more direct method of evaluating precipitation over the open ocean. At microwave frequencies, clouds are often transparent, while larger precipitation size particles provide the only significant source of attenuation. At lower microwave frequencies ($\leq$22-Ghz) emission and absorption radiances dominate for liquid precipitation, while the higher frequencies ($\geq$60-Ghz) are more sensitive to microwave scattering by frozen precipitation. The frequencies between 22-60 Ghz effectively detect both liquid and frozen precipitation. The SSM/I instrument covers this frequency spectrum and is sensitive to emission and scattering by both liquid and frozen hydrometeors.

SSM/I rainfall rate algorithms have been developed from statistical regression equations based on combinations of the seven microwave channels' calibrated brightness temperatures measured by the sensor. Considerable time and effort have been invested in instrument calibration and statistical validation of all SSM/I products including the rainfall rate algorithms. All SSM/I products including integrated water vapor, cloud liquid water, wind speed, as well as rainfall rate, are expected to be accurate within individual specification approximately 67% ($\pm 1\sigma$) of the time (Sandlin and Spangler 1989). For rainfall rate, the accuracy specification is a standard deviation of 5 mmh^{-1} for estimates between 0 and 25 mmh^{-1} (Hollinger 1991).

In Chapter 5, the performance of two rainfall rate algorithms is tested by comparisons with area averaged budget approximations from NOGAPS data, NMC analyses, and sparse raingage derived rainfall rates for the Super Typhoon Flo case study. The algorithms used in this study are described in detail by Olson (1989), and Hollinger (1989, 1991). Unfortunately, the rainfall rate algorithms used in this study did not include the 85-Ghz (V) SSM/I channel because it failed aboard the DMSP F-8 satellite permanently after 3/20/90 due to heating problems. However, the 85-Ghz (H) SSM/I channel did remain marginally within the ± 1 K tolerance range and is included in one of the rainfall rate algorithms (Sandlin 1993, personal communication).

Although rainfall rate algorithms have been developed for measurements over both land and water, this study will make use of algorithms developed for the open ocean only. For SSM/I data covering both land and ocean, pixels within 100 km of land are not processed because large gradients in microwave emissions exist in the coastal regions.

This difficulty is minimized in our study as Super Typhoon Flo remained over the open western North Pacific with only limited contact with the Ryukyu Islands and southern mainland Japan. The first rainfall rate algorithm used in this study is the original Calibration Validation (CAL/VAL) Volume I alternate (Hollinger 1989) version calculated without the 85-Ghz (V) channel:

$$\textbf{Rainfall Rate} = exp\,(-0.42383 - 0.0082985\ T_{B85H} + 0.01496\ T_{B19V} + 0.00583\ T_{B19H}) - 4.0\ mmh^{-1}$$

The second rainfall rate algorithm is the alternate version from the Volume II CAL/VAL effort described by Hollinger (1991). This algorithm does not contain either of the 85-Ghz channels:

$$\textbf{Rainfall Rate} = exp\,(5.10196 - 0.05378\ T_{B37V} + 0.2766\ T_{B37H} + 0.01373\ T_{B19V}) - 2.0\ mmh^{-1}$$

The variables T_{B19H}, T_{B19V}, T_{B37H}, T_{B37V}, and T_{B85H} are the BTs of the 19-Ghz (H), 19-Ghz (V), 37-Ghz (H), 37-Ghz (V), and 85-Ghz (H) polarized channels, respectively. If computations result in a negative rainfall rate, the value is set to zero. The SSM/I data obtained for this study was provided courtesy of the Fleet Numerical Meteorology and Oceanography Center and was preprocessed by the Center for Advanced Space Sensing of the Naval Research Laboratory. Processing the data for display required resampling the

unformatted files, smoothing, and gridding over the desired domain. The two SSM/I algorithms were used to calculate area averaged rainfall rates. These values were then compared to computations of average rainfall rates derived from NOGAPS and NMC analyses determined over an equal area.

3.2 TCM-90 DATA

3.2.1 Experiment Overview.

The Tropical Cyclone Motion (TCM-90) experiment was the field phase of the Office of Naval Research Tropical Cyclone Motion initiative to improve basic understanding of tropical cyclone motion (Elsberry et al. 1990). The TCM-90 field experiment was conducted during August and September of 1990 in the western North Pacific. Three additional international typhoon related field experiments occurred in concert with TCM-90 ensuring a wealth of data during the two month period. The Special Experiment Concerning Recurvature and Unusual Motion (SPECTRUM) organized by the World Meteorological Organization (WMO) and the Economic and Social Commission for Asia and the Pacific (ESCAP) was designed to improve real time track prediction. The USSR organized TYPHOON-90 with the primary objective of investigating the oceanic response to tropical cyclone passage. Finally, the Taiwan Area Typhoon Experiment (TATEX) was directed to improve wind and precipitation forecasts associated with tropical cyclones threatening Taiwan. Although each experiment may have had different objectives, data gathering was coordinated among the countries and agencies involved to maximize the

amount of information collected to ensure each of the four experiments received the maximum benefit.

To improve the basic understanding of tropical cyclone motion, the TCM-90 field experiment focused on the following set of related hypotheses (Elsberry et al. 1990):

Hypothesis I

Interaction between large intense tropical cyclones and subtropical ridge will modify both circulation's and cause significant departures in the tropical cyclone track compared to an unmodified ridge-cyclone situation.

Hypothesis II

Significant turns in the tropical cyclone occur when the interaction with transient synoptic-scale features, such as midlatitude troughs or TUTT cell and causes a response that extends the effects over a deep layer.

Hypothesis III

A limited set of propagation vectors, which are departures of the storm motion from a specifically defined steering flow, may be defined for particular cyclone characteristics and environmental configurations.

To meet the experiment's objectives, intensive observation periods (IOPs) were initiated when tropical cyclones entering the TCM-90 domain were expected to allow appropriate tests for one or more of the three hypotheses. Figure 3.1 shows the experiment domain along with the observing network locations and platform descriptions. For the duration of the two month field experiment, seven IOPs were directed on six typhoons. These IOPs are summarized in Table 3.1.

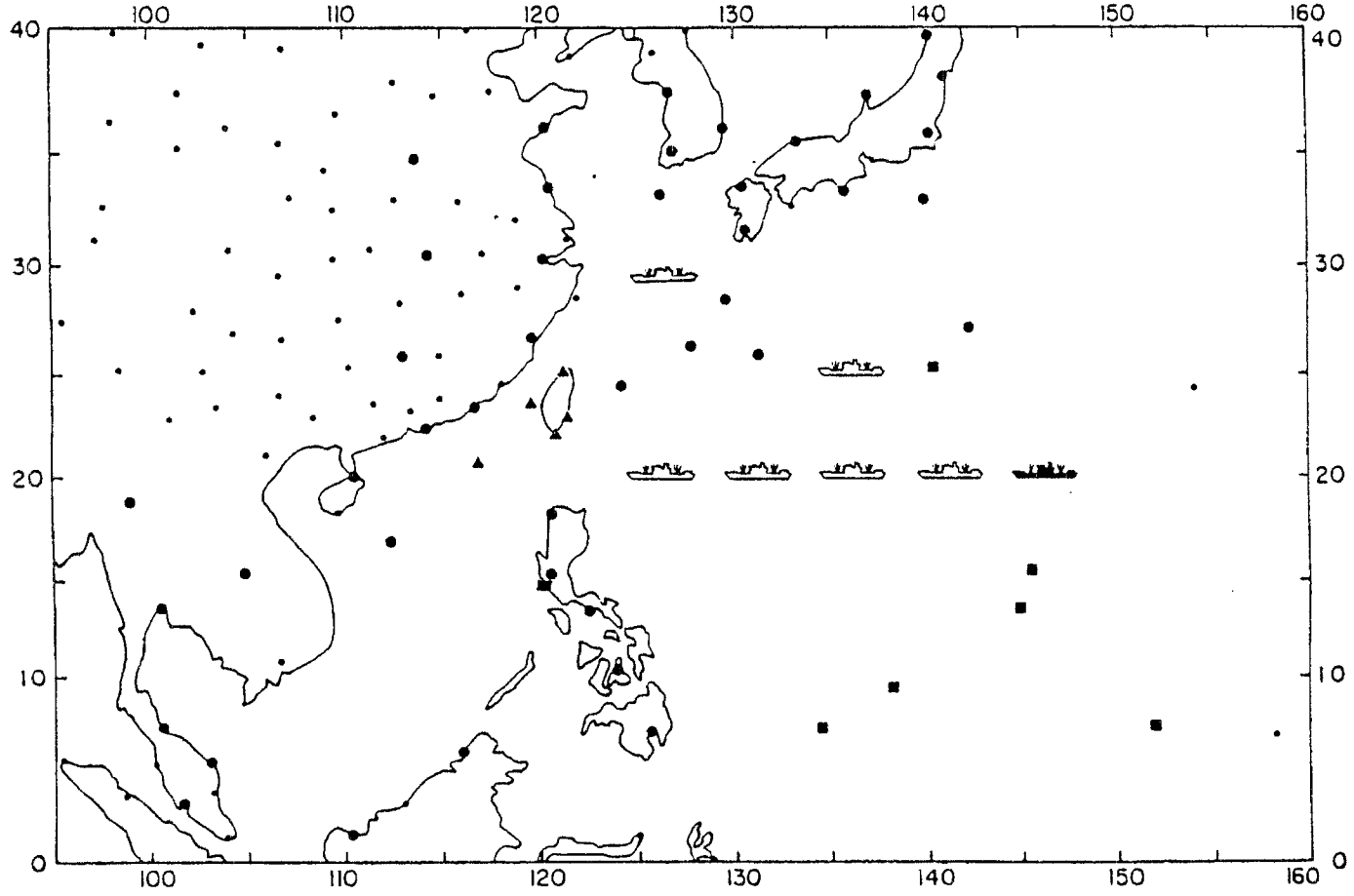

Figure 3.1. TCM-90 field experiment domain. Upper-air sounding network included assets from SPECTRUM and TATEX stations and TYPHOON-90 ships. The large circles, squares and triangles represent the special rawinsonde stations with soundings at 0600 and 1800 UTC. The ship symbols show the fixed positions of the participating ships (Elsberry et al. 1990).

Table 3.1. Intensive Observing Periods (IOPs) during the TCM-90 field experiment with target storm name(s) and the hypotheses that might be addressed (Elsberry et al. 1990).

IOP	STORM	HYPOTHESIS
1	Winona	-Interaction with ridge to east
2-3	Yancy	-Interaction with subtropical ridge -Outer wind structure effects on motion -Interaction with orography -Embedded mesoscale circulations in early stage motion
3	Zola	-Interaction with ridge to east -Tropical Upper Tropospheric Trough (TUTT) effect -Embedded mesoscale circulations in early stage motion
4	Dot	-Interaction with subtropical ridge -Embedded mesoscale circulations in early stage motion -Interaction with orography
5	Ed	-Interaction with a monsoon trough -Interaction with a ridge to the north
6	Flo-Ed	-Interaction with a ridge to the north -Embedded mesoscale circulation in early stage motion
7	Flo-Ed	-Interaction with monsoon trough -Interaction with midlatitude trough during recurvature -Interaction with ridge to east -TUTT effect

Some of the data collected during IOPs 6 and 7 were used in the analysis of Super Typhoon Flo. For example, SSM/I retreivals were qualitatively compared to TCM-90 field experiment data resources such as conventional geostationary and polar orbiting satellite imagery. In addition, the accumulated precipitation analyses from the TCM-90 enhanced National Meteorological Center (NMC) model were contrasted with SSM/I data to characterize Flo's precipitation structure.

3.2.2 NMC Analysis Data

The National Meteorological Center (NMC) was the agency responsible for producing the analysis record for TCM-90 with the purpose of meeting the ultimate goal of the initiative, a better understanding of tropical cyclone motion. Data was collected and assimilated from a variety of platforms including 6-hourly land and ship based rawinsondes, radar wind profilers, dropwindsondes, and meteorological satellites. The three dimensional, hydrostatic, primitive equation NMC model was employed to produce the TCM-90 analysis record. The regional NMC model uses the ETA vertical coordinate system described by Mesinger (1984) and Black (1988). The mesoscale model has a horizontal resolution of 50 km and resolves 20 vertical layers. The analysis was prepared using Regional Optimum Interpolation (ROI) over a 12 hour assimilation period with the six hour forecast from the NMC global spectral model as a starting background (Rogers et al. 1991).

The final analysis consists of the T-0 initialization passed through the ETA model for one time step to compute precipitation, vertical motion, surface fluxes, and radiative

fluxes. Vertically, the model interpolates the analyzed fields onto ETA surfaces at constant pressure levels from 1000 mb to 100 mb at 50 mb intervals. Surface fields and fluxes are interpolated to the final analysis grid of 186 by 112 at 0.5 degree resolution. The TCM-90 analysis domain covers an area from 10° south to 60° north latitude and 60° to 180° east longitude. The data structure of the special NMC analysis includes 126 analyzed fields. The NMC six hour accumulated precipitation (mm) field was used as a source of comparison with SSM/I rainfall rate retrievals.

3.2.3 In Situ Observations

As a result of the two month TCM-90 field experiment, a comprehensive data set was archived for the purpose of future research. However, during the experiment observations from numerous data sources were also disseminated real time to assist the many agencies involved in the tropical cyclone warning process. In addition, real time screened and quality controlled data was used by the Fleet Numerical Meteorology and Oceanography Center in the global analysis and forecast cycle for their numerical weather prediction model. In situ data sources employed during the field experiment included; aircraft dropwindsonde, radar wind profiler, surface observations, and radiosonde data. In analyzing the precipitation distribution of Super Typhoon Flo in SSM/I data, comparisons were first made with rainfall rates determined from rainfall measurements recorded at U.S. Military installations on Okinawa participating in TCM-90. Qualitative aircraft observations were also used to assist in characterizing the evolution of Flo's convective structure.

3.2.4 Conventional Satellite Data

During TCM-90 conventional visible and infrared meteorological satellite data were collected from several sources. Meteorological satellite platforms available during the two month experiment included polar orbiting DMSP and NOAA satellites, and the geostationary Japanese GMS satellite. Geostationary data was available on an hourly basis while each of the polar orbiting satellites provided at least four passes per day over the experiment's domain.

Archived GMS data for the period between 12-18 September 1990 was furnished by the University of Wisconsin (satellite data center for TCM-90). The images document Super Typhoon Flo's evolution from tropical depression through dissipation before Flo finally obtained extra-tropical characteristics as it tracked across the western North Pacific. DMSP Operational Line Scan (OLS) infrared, enhanced infrared, and visible products were also available from the F-8 satellite that carries the SSM/I. Some of these products were available for comparisons with the corresponding SSM/I images.

DMSP polar orbiting and GMS geostationary metsat data were compared to SSM/I data to reveal differences and similarities between the two when evaluating tropical cyclone structure and organization.

3.3 NOGAPS Data

The Navy Operational Global Atmospheric Prediction System (NOGAPS) model is described in detail by Hogan and Rosmond (1991) and Hogan et al. (1990). In summary, NOGAPS is a global spectral model with 18 vertical levels (σ surfaces) and a T79

horizontal resolution in 1990. However, the NOGAPS analyses were archived at a standard horizontal resolution of 2.5 degrees latitude and longitude. Boundary layer parameters, stable and convective precipitation parameterizations, and long- and short-wave radiation comprise the physics employed in the NOGAPS model. NOGAPS includes a quality control routine, an objective analysis, initialization, and a prediction model.

Several output fields from NOGAPS model analysis data are used later in this study to calculate spatially averaged rainfall rates by applying a water vapor budget calculation. Output fields used in the computation include, moisture (q), temperature (T), pressure (p), sea-level pressure (s), and the u and v wind components. The NOGAPS output fields provided for this study were interpolated to a resolution of 0.5 degrees.

4. SSM/I 85-GHZ SENSOR DATA RECORDS

The horizontally polarized (H) SSM/I 85-Ghz channel is very effective at detecting convection over the open ocean. At this frequency, microwave energy is scattered by suspended ice particles and large water droplets present in deep convection. This results in the attenuation of upwelling microwave energy emitted from the ocean surface. Therefore, the sensor detects the convection as cold BTs relative to a warmer ocean surface. The relatively high resolution (near 15 km) of this data rivals conventional visible and infrared satellite analysis tools with resolution near 1 km and 2 km, respectively. These sensor capabilities allow for many applications including the analysis of convective structure, center position fixing, and the examination of tropical cyclone intensity evolution.

4.1 85-Ghz (H) Observations of Flo's Convective Structure

Glass and Felde (1989) demonstrated one application of SSM/I 85-Ghz (H) SDRs when they examined the convective structure of Typhoon Freda (1987) and Typhoon Skip (1988) in the western North Pacific. Likewise, SSM/I 85-Ghz (H) data was used in this study to qualitatively analyze the convective structure of Super Typhoon Flo. Where possible, this data was further compared to enhanced infrared OLS products from the same DMSP passes to demonstrate the differences and similarities between the two types of imagery.

Super Typhoon Flo began like the majority of western North Pacific tropical cyclones. During mid-September, it developed within the monsoon trough between the Marianas

and Marshall Islands. Except for Flo's extreme intensity, it's evolution followed a typical pattern for recurving tropical cyclones. A time versus intensity plot of Super Typhoon Flo is depicted in Figure 4.1. Development to typhoon strength occurred at a predictable one T-number per day (Dvorak 1984) between 0000 UTC, 13 September and 0600 UTC, 15 September 1990. A little while later, Flo began period of explosive deepening before reaching super typhoon intensity 36 hours later at 1200 UTC, 16 September.

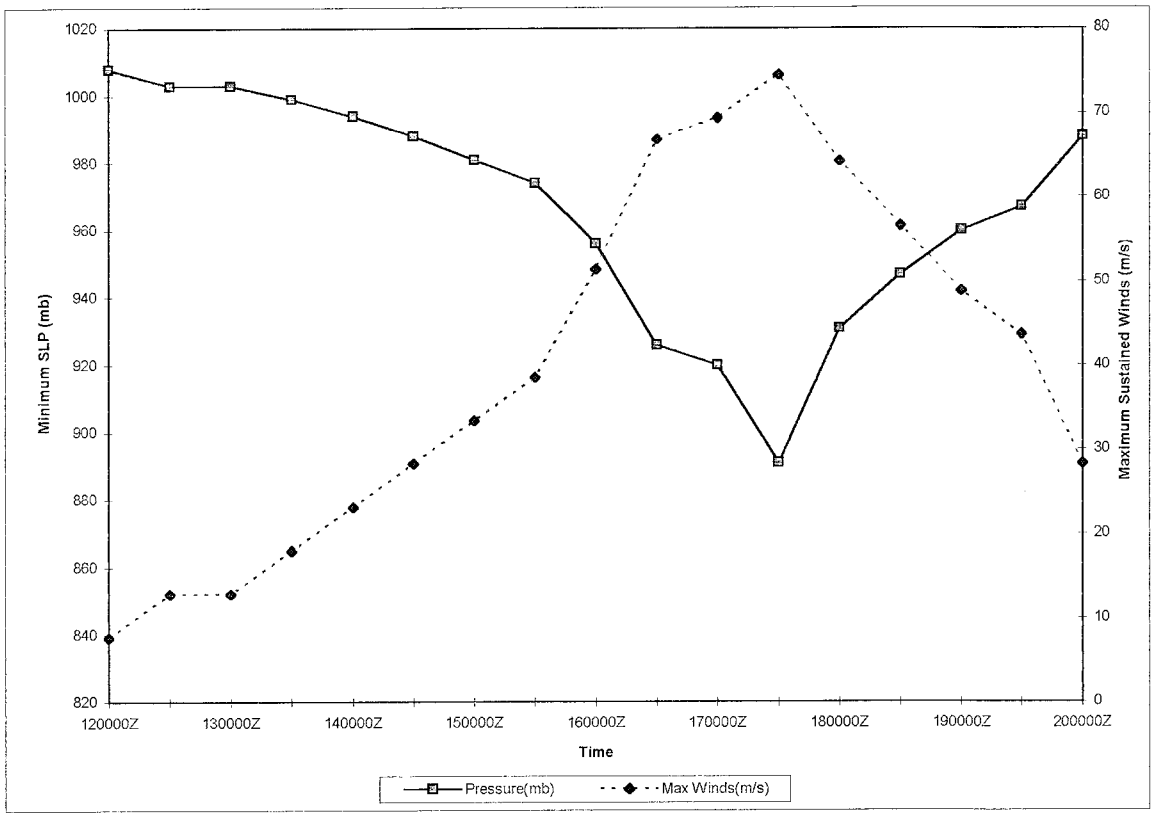

Figure 4.1. Maximum sustained winds (ms^{-1}) and minimum sea-level pressure (mb) as a function of time showing the intensity evolution of Super Typhoon Flo. Maximum sustained wind speed data was determined directly from the JTWC final best track and sea-level pressure data was derived from the Atkinson and Holliday (1977) relationship. The peak intensity of 891 mb represented in the minimum sea-level pressure data was provided by a dropsonde observation during a TCM-90 aircraft mission.

Flo's peak strength was recorded at 0600 UTC on 17 September as it began to recurve around a trough induced break in the subtropical ridge east of Okinawa, Japan. In the upper-levels, Flo exhibited an unusual structure. According to information from the second NASA DC-8 mission on 17 September, flight level data (200 mb) revealed an intense cyclonic flow near the vortex center with little direct outflow apparent near the eye. Slow weakening commenced after recurvature while rapid weakening occurred shortly thereafter as Flo tracked across the Japanese mainland. The system was finally downgraded to tropical storm status at 0000 UTC on 20 September 1990.

The following qualitative SSM/I analysis documents the evolution of Super Typhoon Flo's convective structure. The SSM/I 85-Ghz (H) images follow Flo from tropical storm stage near Guam to weakening typhoon status over the Japanese mainland. Figure 4.2 (a) shows the SSM/I 85-Ghz (H) brightness temperature (BT) imagery of Flo at 2030 UTC, on 13 September 1990, just two hours after being upgraded to tropical storm status. just two hours after upgrade to tropical storm status. Low brightness temperature values indicate areas of deepest convection. The cooler 85-Ghz (H) BTs observed in this pass reveal an area of organized convective banding around what appears to be the center of circulation located approximately 120 nm west of Guam. Also note the banding feature detached south of the main convective core region. Figure 4.2 (b) is the accompanying DMSP OLS enhanced IR imagery. This imagery gives a more general impression of the possible center of circulation while offering a less detailed observation of the convective features and inner-core banding. However, in the OLS imagery, a tropical upper-

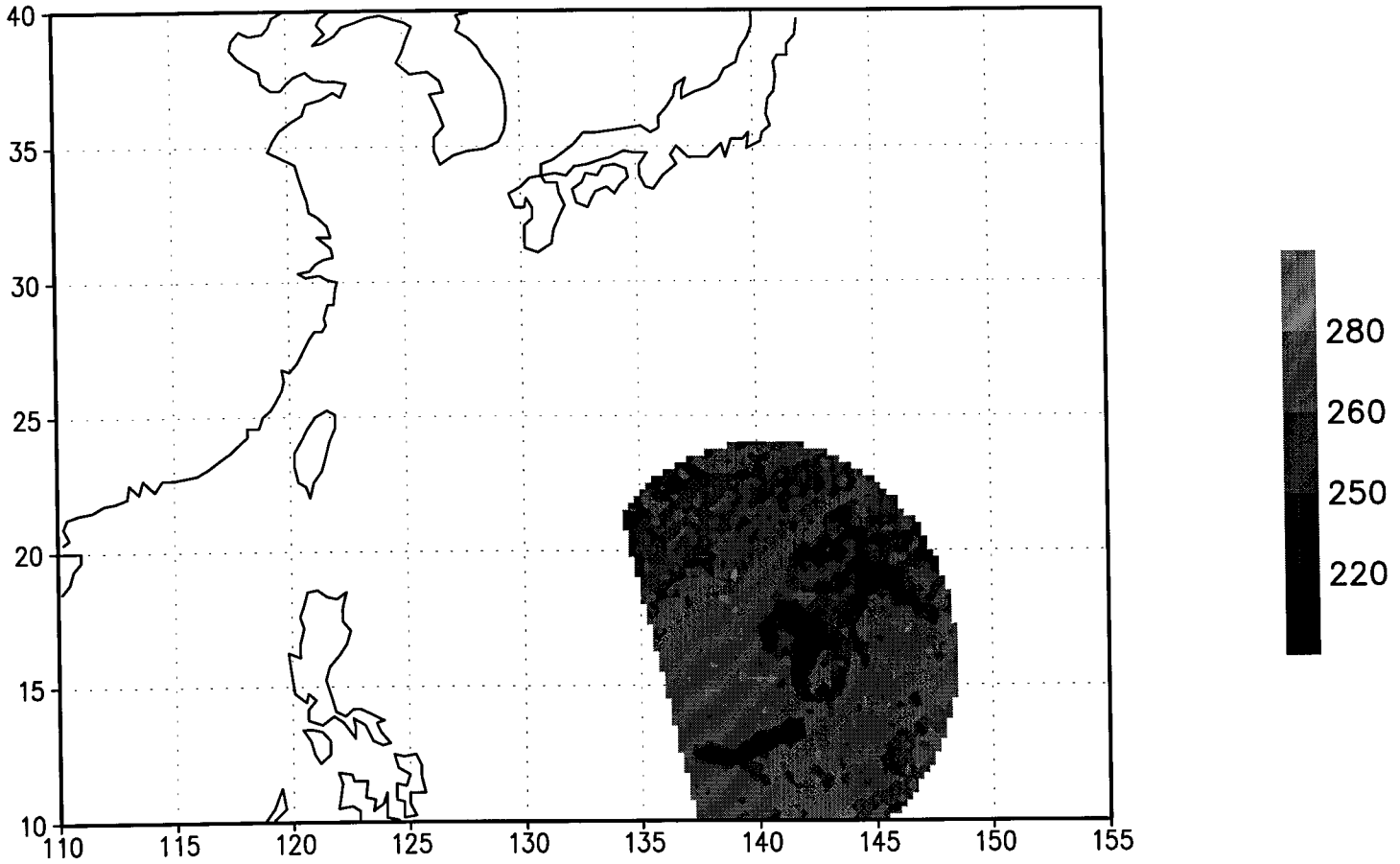

Figure 4.2 (a) SSM/I 85-Ghz (H) imagery from 2030 UTC, 13 September 1990. The imagery shows a tight convective banding region around what appears to be the center of circulation.

Figure 4.2. (b) DMSP OLS enhanced infrared imagery for 2030 UTC, 13 September 1990. The imagery shows less convective detail than revealed in SSM/I data. The TUTT is visible to the northwest of Flo.

tropospheric trough (TUTT) is easily observed off Flo's northwest quadrant. This TUTT cell eventually migrated westward, then orbited to the southwestern flank of Tropical Storm Flo before dissipating (Elsberry et al. 1990). The proximity of the TUTT suggests the outflow may have been enhanced, possibly providing further impetus for intensification. Rodgers et al. (1991) suggested the initiation and maintenance of intense convection in tropical cyclones during the mature stage are related to the channeling and strengthening of their outflow by upper-tropospheric troughs. However, Rodgers et al. (1991) also observed the cessation of convection during episodes when TUTT cells were positioned very close or over the tropical cyclone. If this occurred, the TUTT usually inhibited outflow and entrained dry upper-tropospheric air into the inner-core region. In the break between available DMSP passes, GMS imagery revealed how the TUTT rotated counter-clockwise around the western and southern quadrants of Tropical Storm Flo before dissipating. During this time, outflow may have been inhibited in the western sector of the storm. There were also indications that dry upper-tropospheric air may have been entrained into the inner-core region, possibly slowing the intensification process.

The next SSM/I 85-Ghz imagery available at 0900 UTC on 14 September is shown in Figure 4.3 (a). At this time, Tropical Storm Flo was located approximately 500 nm west of the Marianas Islands in the Philippine Sea. Flo's maximum sustained winds were 55 kts (27 ms^{-1}) according to Dvorak (1984) current intensity estimates. The imagery shows two convective bands displaced north and east of the apparent center of circulation. The first indication of partial eyewall formation may also be inferred. The corresponding DMSP F-8 enhanced IR imagery shown in Figure 4.3 (b) agrees well in it's depiction of the same

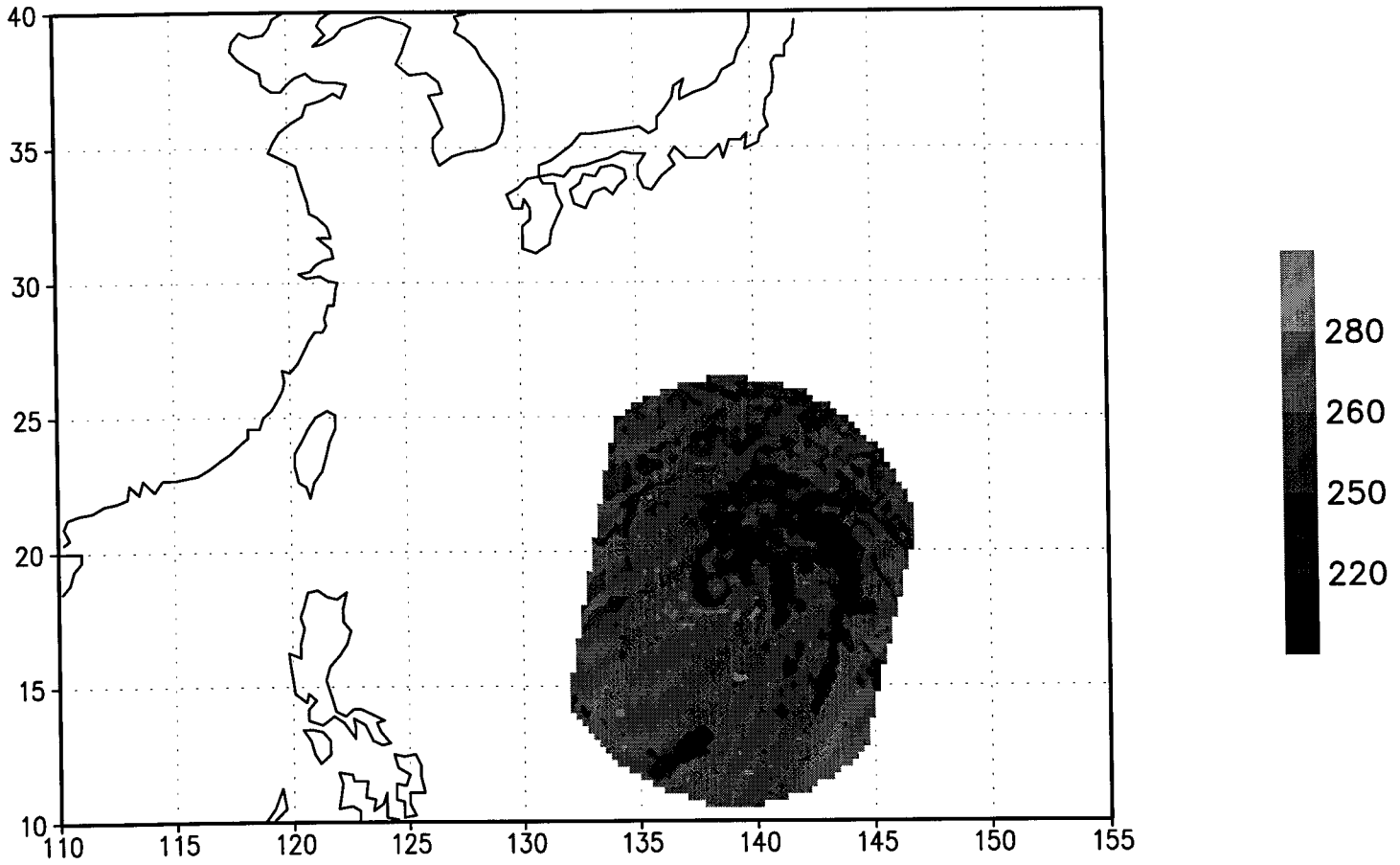

Figure 4.3. (a) SSM/I 85-Ghz imagery at 0900 UTC on 14 September 1990. The imagery shows two convective bands displaced north and east of the apparent center of circulation. The first indication of partial eyewall formation may be inferred.

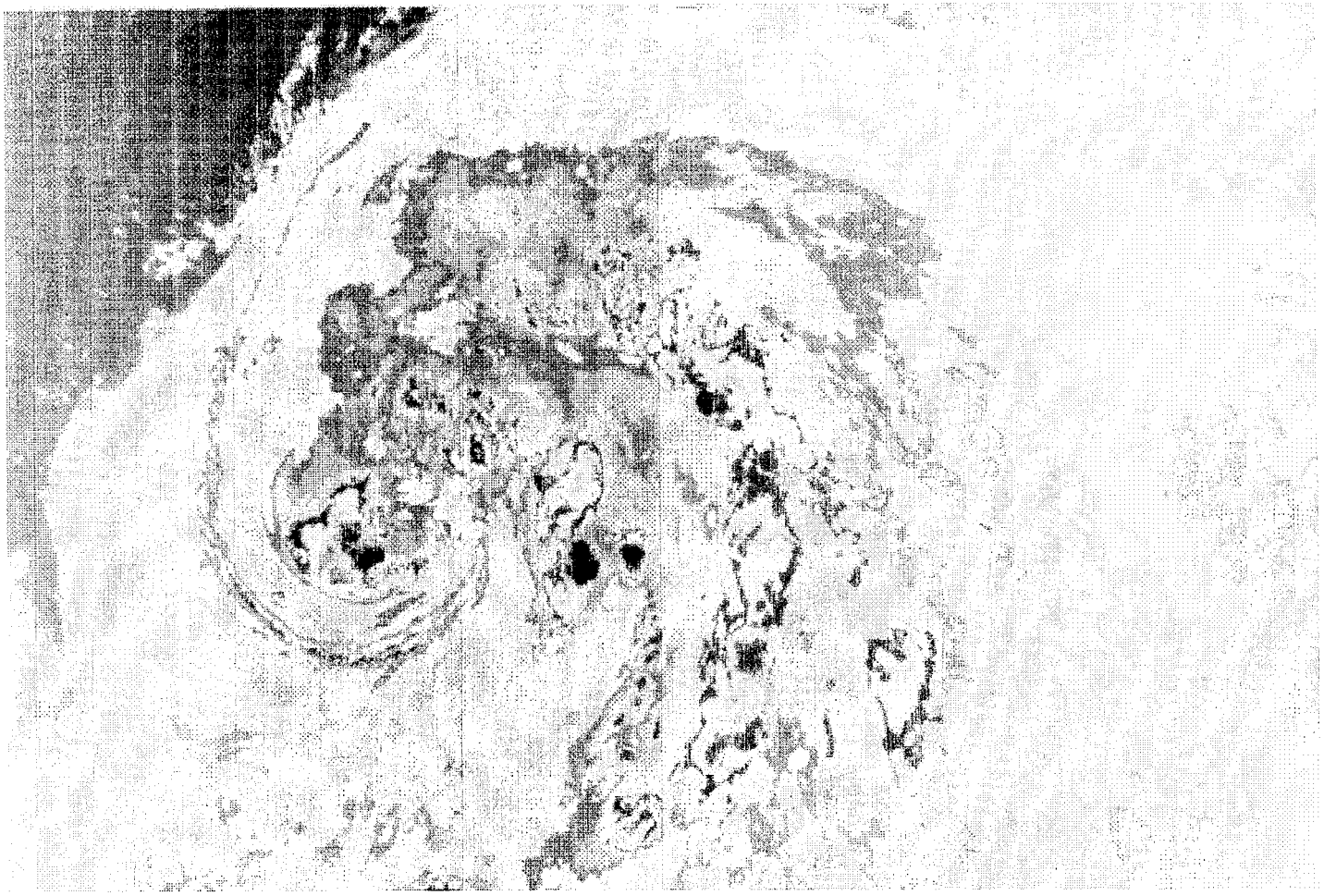

Figure 4.3. (b) Corresponding DMSP F-8 enhanced IR imagery also reveals the prominent convective bands identified in the 85-Ghz SSM/I data.

prominent convective bands revealed in the 85-Ghz data. By using the DMSP OLS and SSM/I 85-Ghz data to compliment one another, Flo's center of circulation can be accurately located just northeast of the apparent partial eyewall.

The next SSM/I imagery was available from the DMSP F-8 pass at 2130 UTC, 16 September. During the 2 1/2 days since the previous pass, it was indicated that Flo experienced a period of rapid intensification. JTWC upgraded Flo to typhoon status at 0600 UTC, 15 September or about 24 hours after the last available SSM/I data. As previously mentioned, GMS IR imagery spanning the 60 hour gap in SSM/I coverage revealed how the evolution of Flo's outflow pattern may have inhibited development. Additionally, the migrating upper-tropospheric trough appeared to have caused a main outer convective band east of Flo's circulation center to break away before the TUTT finally dissipated. For 36 hours following initial typhoon classification, Flo intensified at the accelerated pace of two T-numbers (Dvorak 1984) per day. The start of this explosive period of intensification seemed to coincide with the disintegration of the TUTT. The Joint Typhoon Warning Center classified Flo as a super typhoon at 1200 UTC, 16 September. The status upgrade was based on enhanced IR satellite derived Dvorak (1984) current intensity estimates that corresponded to maximum sustained winds of 130 kts (65 ms^{-1}). According to Elsberry et al. (1990), the period of explosive deepening was associated with improved outflow enhanced by the proximity of the midlatitude westerlies located just north of Super Typhoon Flo and by the presence of a new TUTT that developed in a more favorable location.

The SSM/I 85-Ghz (H) from 2130 UTC, 16 September presented in Figure 4.4 (a) depicts a tightly wrapped inner-core convective region with a concentric eyewall surrounding a small well defined eye. A moderate area of convection depicted in the medium gray shades appears in the form of a broad outer curved band feature oriented in a counter-clockwise fashion west through southeast. This area is separated by warmer BTs surrounding the inner convective comma and eyewall regions. Figure 4.4 (b) is the accompanying OLS enhanced IR imagery from the same DMSP pass and shows a classic super typhoon signature. An eyewall surrounding gray shade of unbroken white with a warm dark gray eye temperature yields an objective Dvorak (1984) current intensity estimate of 7.0 corresponding to maximum sustained winds of 135 kts (67 ms^{-1}). In this imagery, it is interesting to note the concave nature of eyewall's eastern semicircle. In contrast, the top of the western semicircle of the eyewall appears to overhang the lower, warmer gray shades of the inner eyewall. Approximately six hours later, the NASA DC-8, participating in TCM-90, completed two upper-level eye penetrations of Super Typhoon Flo on the second day of airborne reconnaissance. The research aircraft measured an eye diameter of approximately 20 NM (37 km). According to the crew, the western semicircle of the eye had a definite "fishbowl" appearance, i.e., the top part of the eyewall was over hanging to form a concave surface appearing as a fishbowl from the inside (Dunnavan et al. 1991).

At 0600 UTC on 17 September, later in the same mission mentioned above, the NASA DC-8 observed Super Typhoon Flo at peak intensity. A dropwindsonde deployed within the geometric center of Flo's eye recorded an uncorrected minimum sea-level pressure of

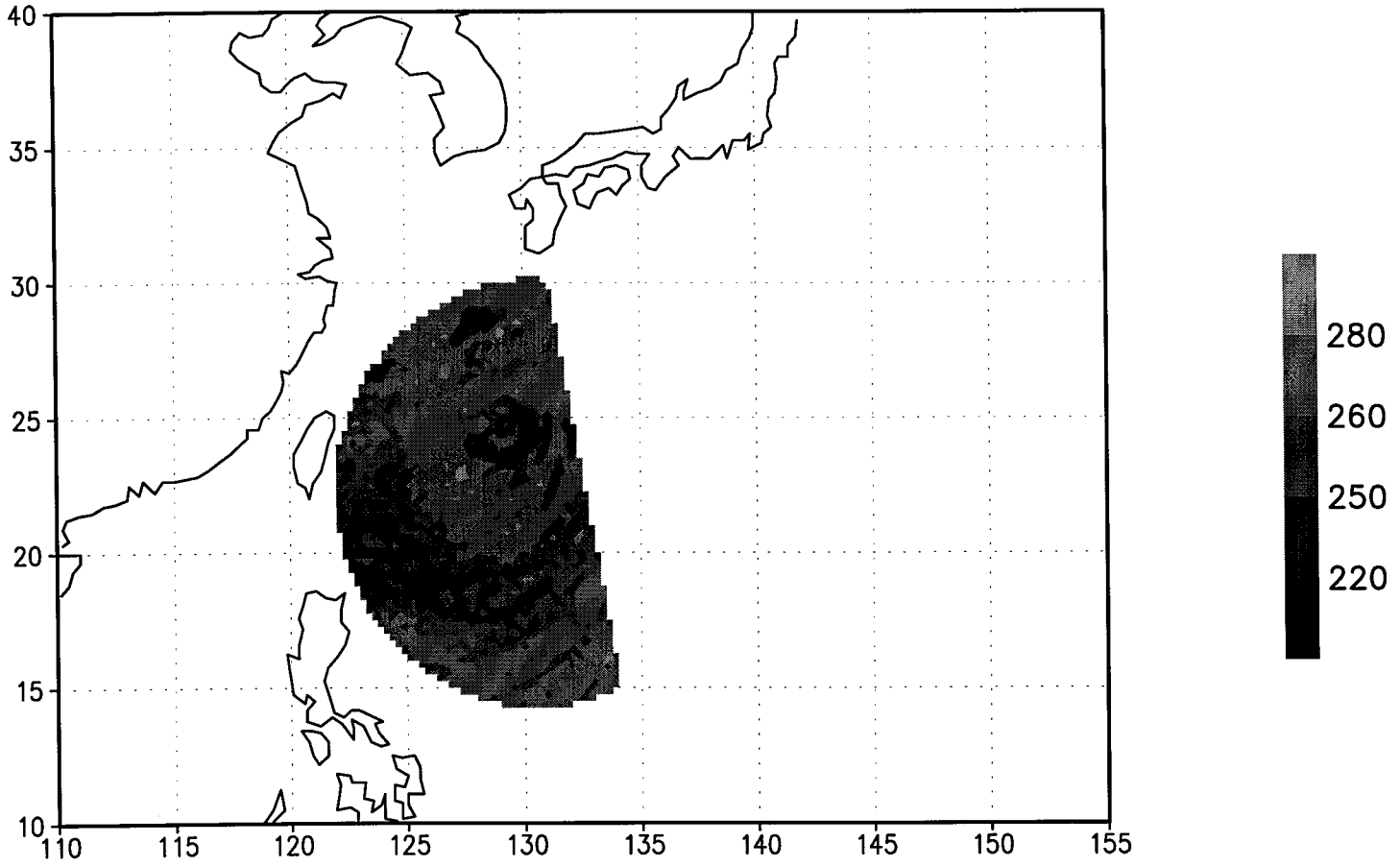

Figure 4.4. (a) SSM/I 85-Ghz (H) imagery from 2130 UTC, 16 September 1990, depicts a tightly wrapped inner convective core region with a concentric eyewall surrounding a very small well defined eye.

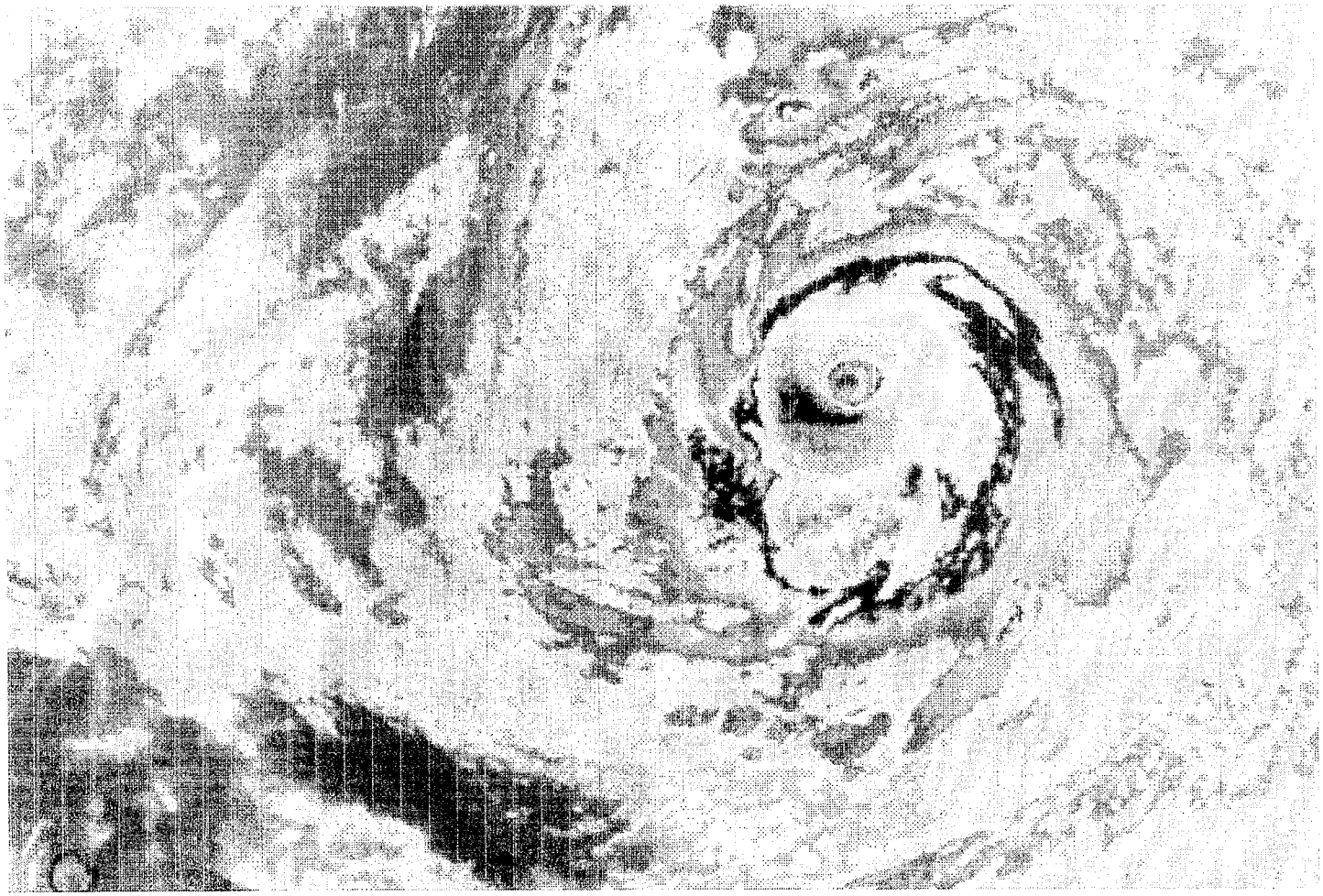

Figure 4.4. (b) DMSP OLS enhanced IR imagery at 2130 UTC, 16 September 1990 shows the classic super typhoon signature defined by the Dvorak (1984) technique.

891 mb (Dunnavan et al. 1991). Based on the information provided by the first ever upper-tropospheric typhoon reconnaissance mission in the western North Pacific, JTWC increased the maximum sustained winds from 135 kts (69 ms^{-1}) to 145 kts (75 ms^{-1}) on their 0600 UTC, 17 September warning.

Figure 4.5 shows the SSM/I 85-Ghz (H) retrieval available at 1000 UTC, 17 September. In this image, a concentric ring of convection forms a secondary eyewall outside the primary eyewall region that surrounds the tiny eye not visible in the SSM/I data. The lighter gray shade appearing within the secondary eyewall might be confused with the location of the eye. However, the eye is actually placed just south of the small prominant area of convection within the region surrounded by the secondary eyewall. At the time, WSR-57 weather radar observations from Okinawa measured an eye diameter of approximately 17 nm, to small to resolve with any detail given the 25 km maximum resolution of the SSM/I sensor (by personal communication). A rotated convective comma configuration can be seen curving inward toward the circulation center joining the secondary eyewall in the northern quadrant of the cyclone. According to Willoughby et al. (1982), this feature is indicative of large intensity changes attributed to the contraction and reformation of convective rings around the eye. The time of this overpass also coincides with Flo's closest point of approach (CPA) to the island of Okinawa, Japan at 1200 UTC, 17 September. At CPA, the Kadena Air Base weather radar also observed two concentric ring shaped eyewalls surrounding a very small eye. As Flo skirted Okinawa, the TCM-90 reconnaissance aircraft estimated the 100 kt (50 ms^{-1}) winds were just off the east coast.

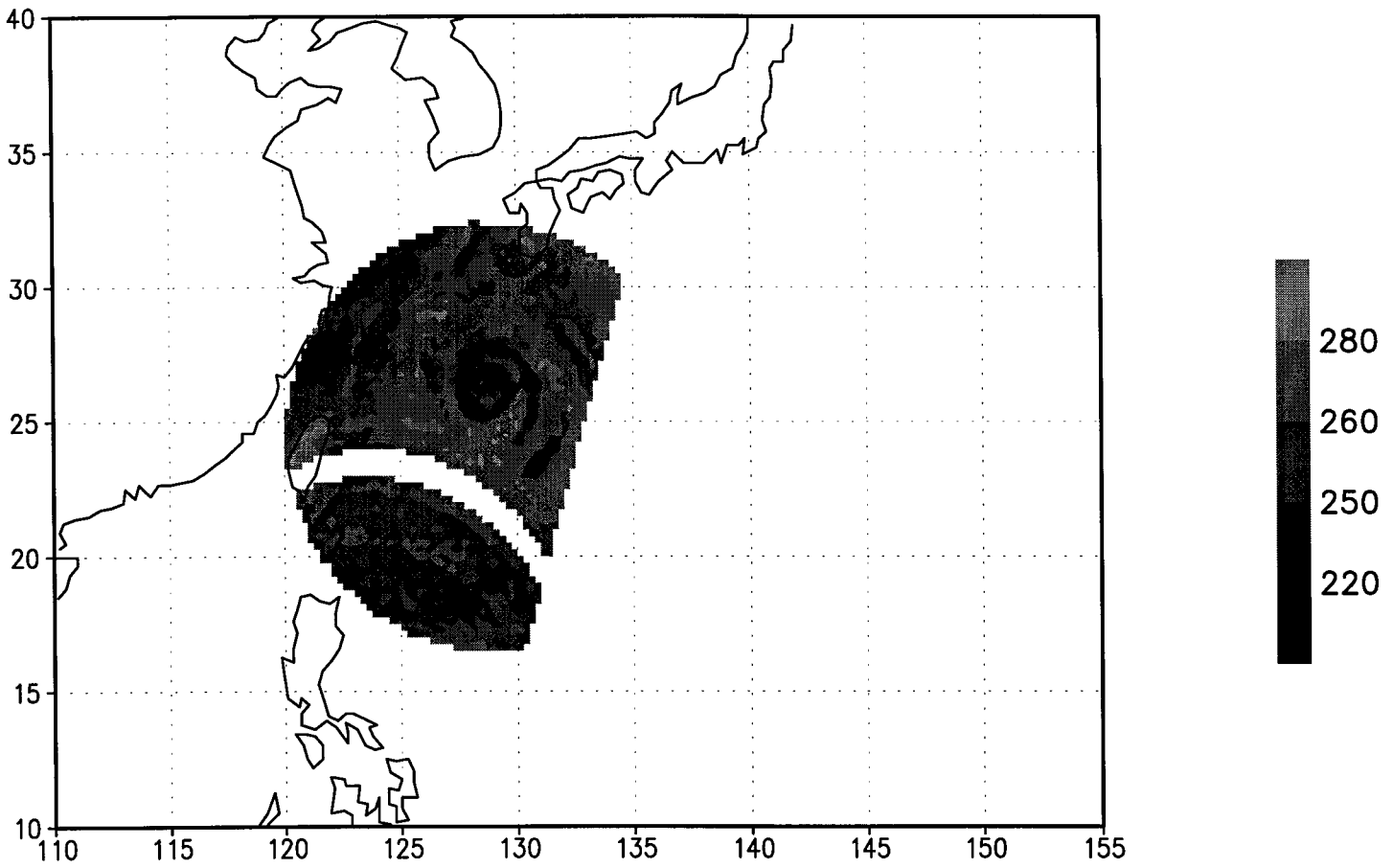

Figure 4.5. SSM/I 85-Ghz (H) at 1000 UTC, 17 September 1990, shows a concentric ring of convection forming a second eyewall region outside the primary eyewall surrounding the actual eye barely visible in the SSM/I data.

However, observing stations on the island measured maximum winds of only 66 kts (35 ms^{-1}).

The next SSM/I 85-Ghz imagery at 2120 UTC, 17 September is shown in Figure 4.6 (a). At the time of this pass, Super Typhoon Flo was weakening and moving north-northeast toward mainland Japan. The SSM/I data provides evidence of this weakening. The secondary eyewall has disappreared leaving only a primary eyewall surrounding the larger eye. As Willoughby et al. (1982) has also suggested, the disappearance of an inner eyewall region usually indicates the end of intensification and the beginning of the weakening phase. A noticable decrease in the intense convection (darkest gray shades) is also observed around most of the western semicircle of the primary eyewall. In addition, detached convective bands are also detected northwest and southeast of Flo's eye. The eye diameter is approximately 43 nm (68 km) when measured in this 85-Ghz data. Flo's signature in the OLS enhanced IR image from the same DMSP pass, presented in Figure 4.6 (b), is also characteristic of a weakening system. In this imagery, a dry slot appears to be rotating into the central core region. Although not reclassified, the satellite signature also indicates Flo is no longer a super typhoon. In fact, JTWC downgraded Flo to typhoon status on the next warning issued at 0000 UTC, 18 September by reducing the maximum sustained winds to 125 kts (62 ms^{-1}). The dry slot rotating into the inner-core region from the north is also apparent in the corresponding low-light VIS imagery shown in Figure 4.6 (c). In this image, there appears to be a break in the intense convection within the southwest quadrant of the eyewall. This observation is similar to the

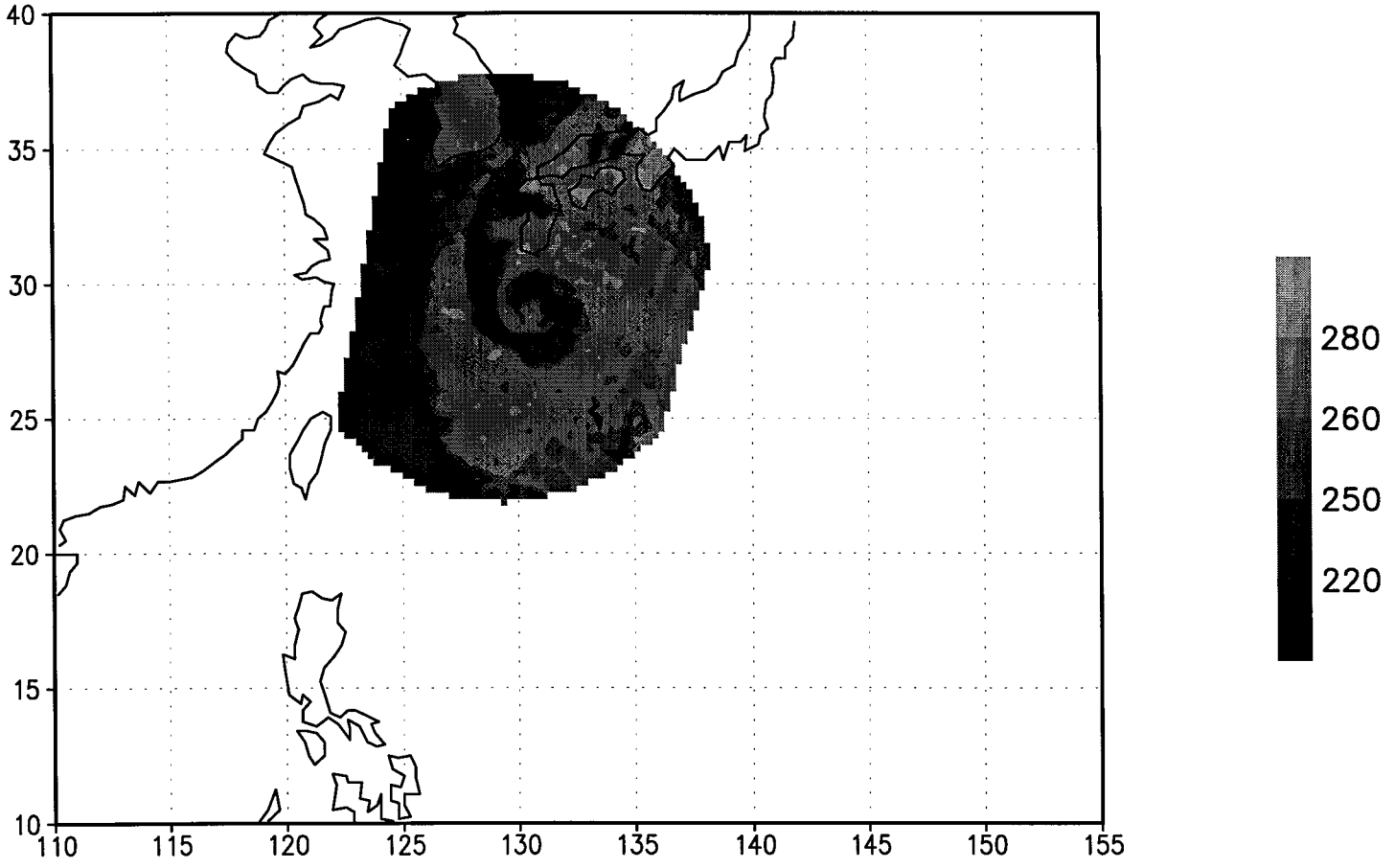

Figure 4.6. (a) SSM/I 85-Ghz (H) imagery at 2120 UTC, 17 September 1990, provides evidence of Flo's weakening as it was moving north-northeast toward mainland Japan.

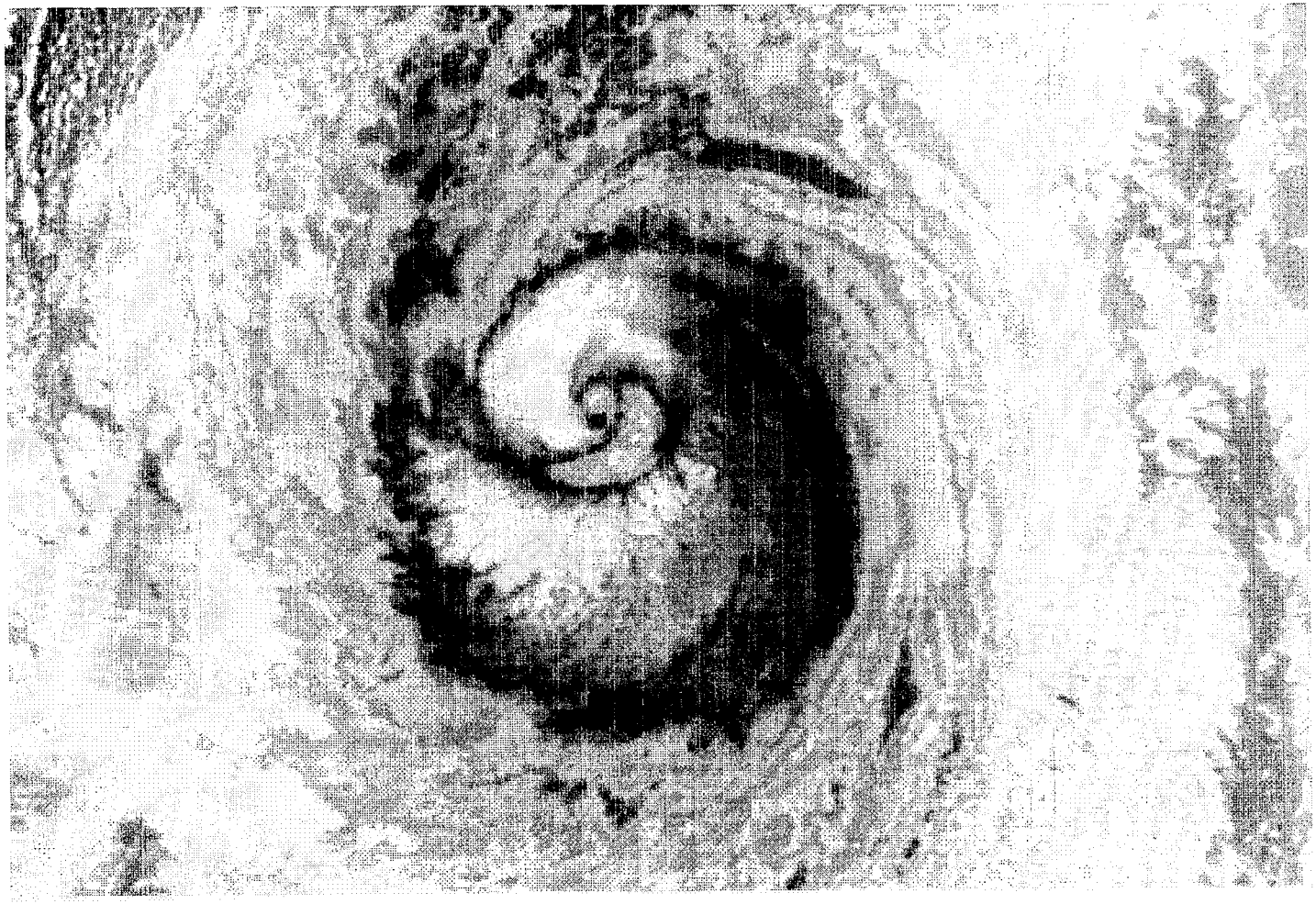

Figure 4.6. (b) Enhanced OLS IR image from the same DMSP pass is also indicative of a weakening system. In this imagery, a dry slot appears to be rotating into the central core region.

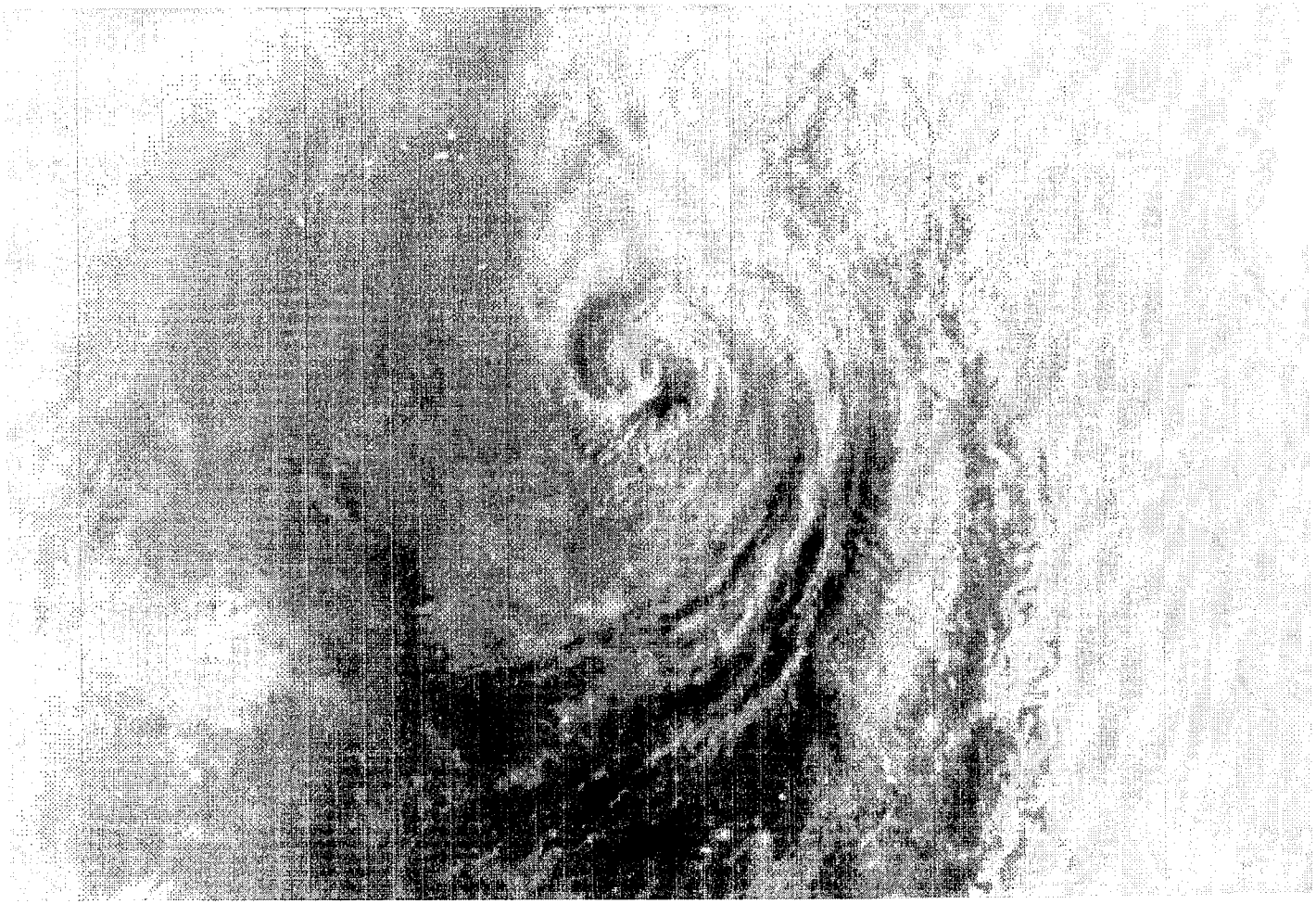

Figure 4.6. (c) The dry slot rotating into the inner-core region from the north can also be seen in corresponding low-light VIS imagery.

corresponding SSM/I data where reduced convection was also noted in the western semicircle of Flo's eyewall.

The SSM/I data available approximately 12 hours later captures Typhoon Flo located approximately 130 nm (210 km) south of Kyushu (southern mainland Japan). The high resolution 85-Ghz (H) microwave retrieval from 1000 UTC, 18 September is displayed in figure 4.7. In this image, a definitive closed eyewall feature is no longer evident. However, there is an organized and tightly wrapped convective comma surrounding the eye remnants. A similar eye diameter of 43 nm (68 km) was found by measuring across the partial eyewall. More evidence of weakening is also exposed in this image. A dry slot, represented by a comma shaped band of comparatively warm BTs, is evident and dry air entrainment is resulting in Flo's rapid dissipation.

The last available SSM/I 85-Ghz image at 2100 UTC, 18 September is presented in Figure 4.8 (a). At this time, there are additional signs of continued weakening. In this image, there is no longer an eyewall or eye feature evident. Most of the convection has been displaced toward the northeast quadrant of Typhoon Flo. A strong shear signal on the western semicircle of Flo appears as a sharp edge between convection and the sea surface characterized as lower BTs in the 85-Ghz retrieval. The OLS enhanced IR imagery from the same DMSP satellite pass shown in Figure 4.8 (b) provides better detail of Flo's central features than the SSM/I image. Two prominent curved bands north and south provide a reasonable estimate of Flo's low-level circulation center.

Typhoon Flo made landfall 15 hours later at 1200 UTC 19 September near Osaka, Japan with winds of 90 kts (45 ms^{-1}). The typhoon was responsible for 32 deaths and

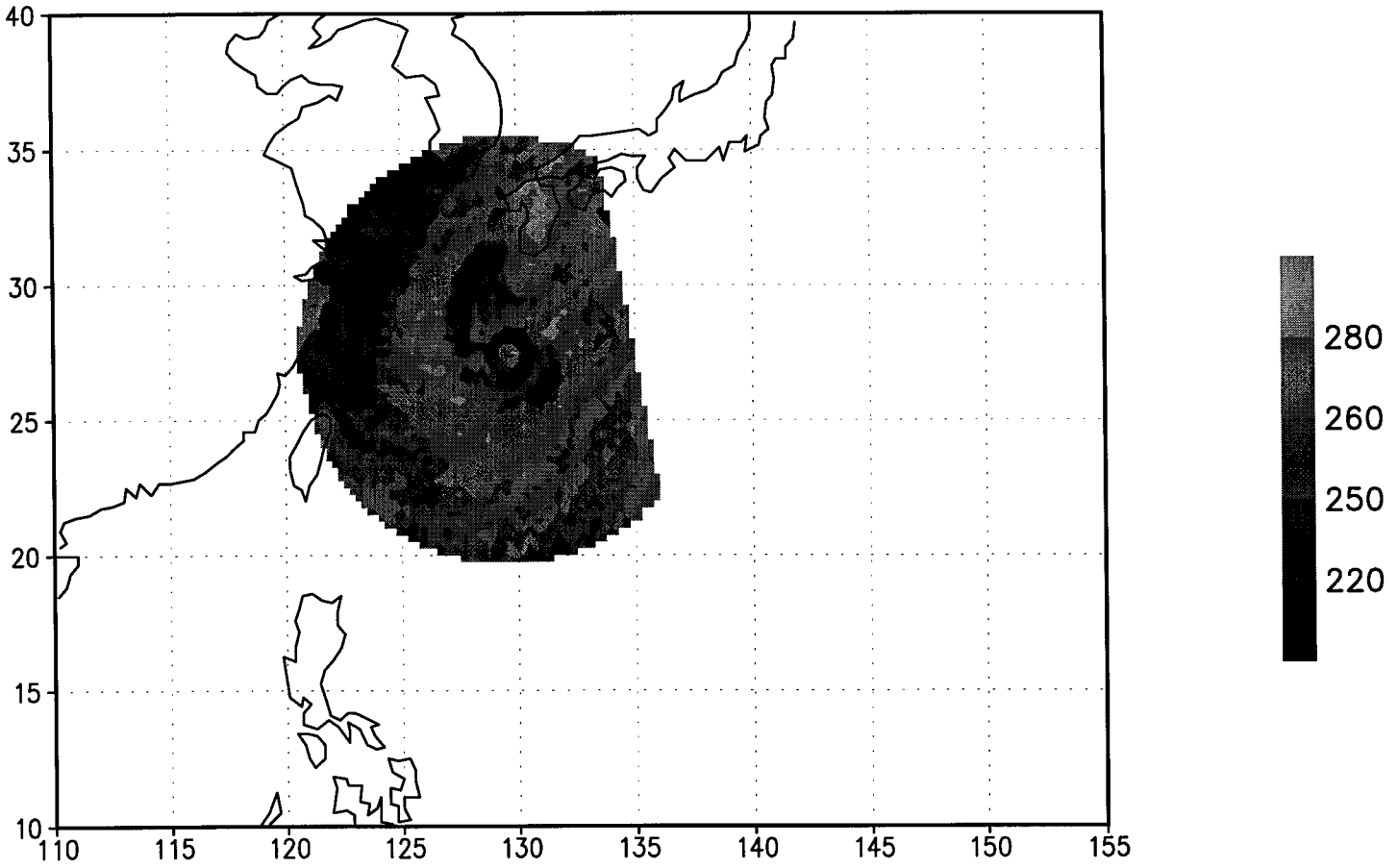

Figure 4.7. 85-Ghz (H) microwave retrieval from 1000 UTC, 18 September 1990. There is no longer a definitive closed eyewall feature. However, there is an organized and tightly wrapped convective comma surrounding the eye remnants.

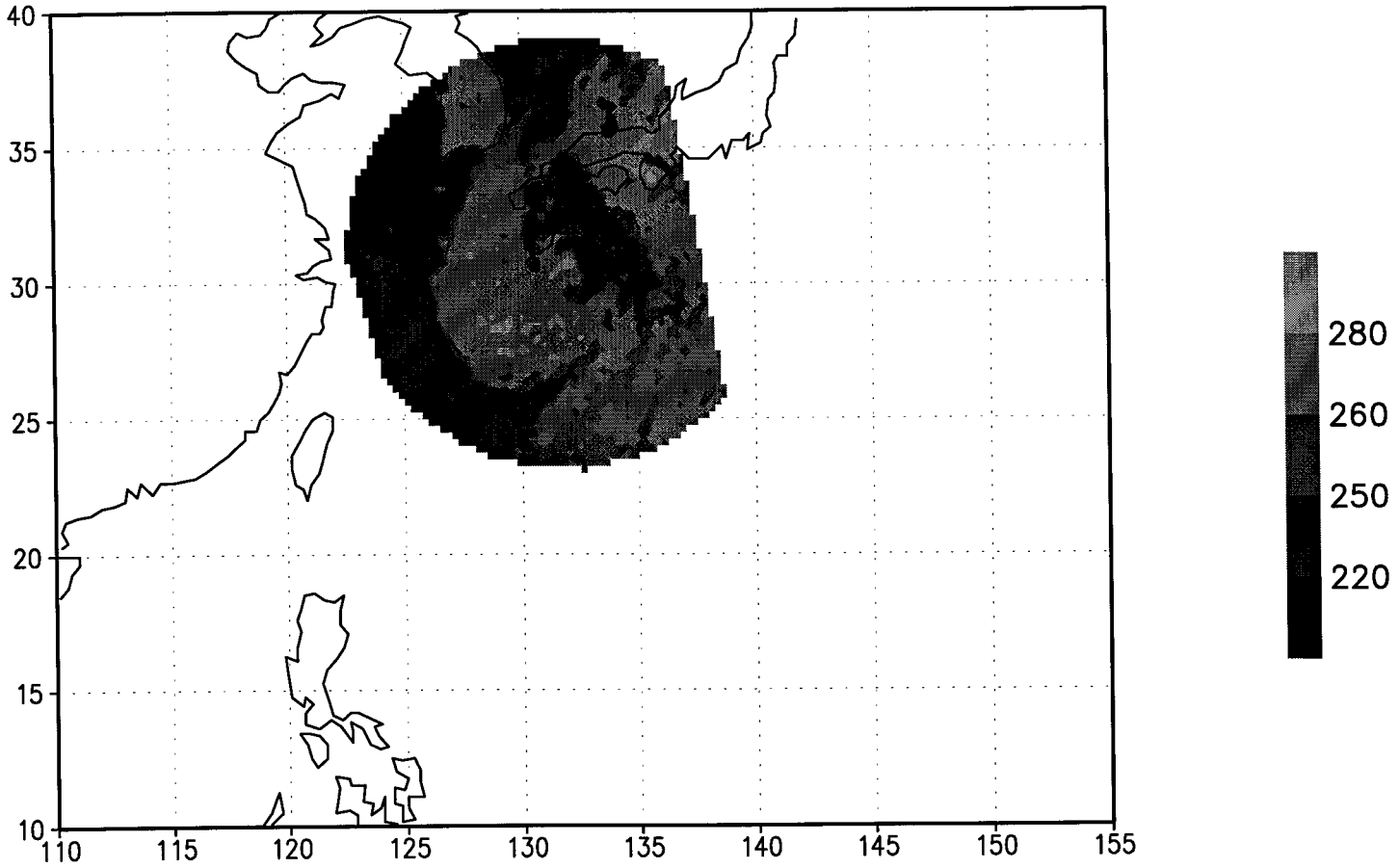

Figure 4.8. (a) The last available SSM/I 85-Ghz image at 2100 UTC, 18 September 1990. There are no longer indications of an eyewall feature.

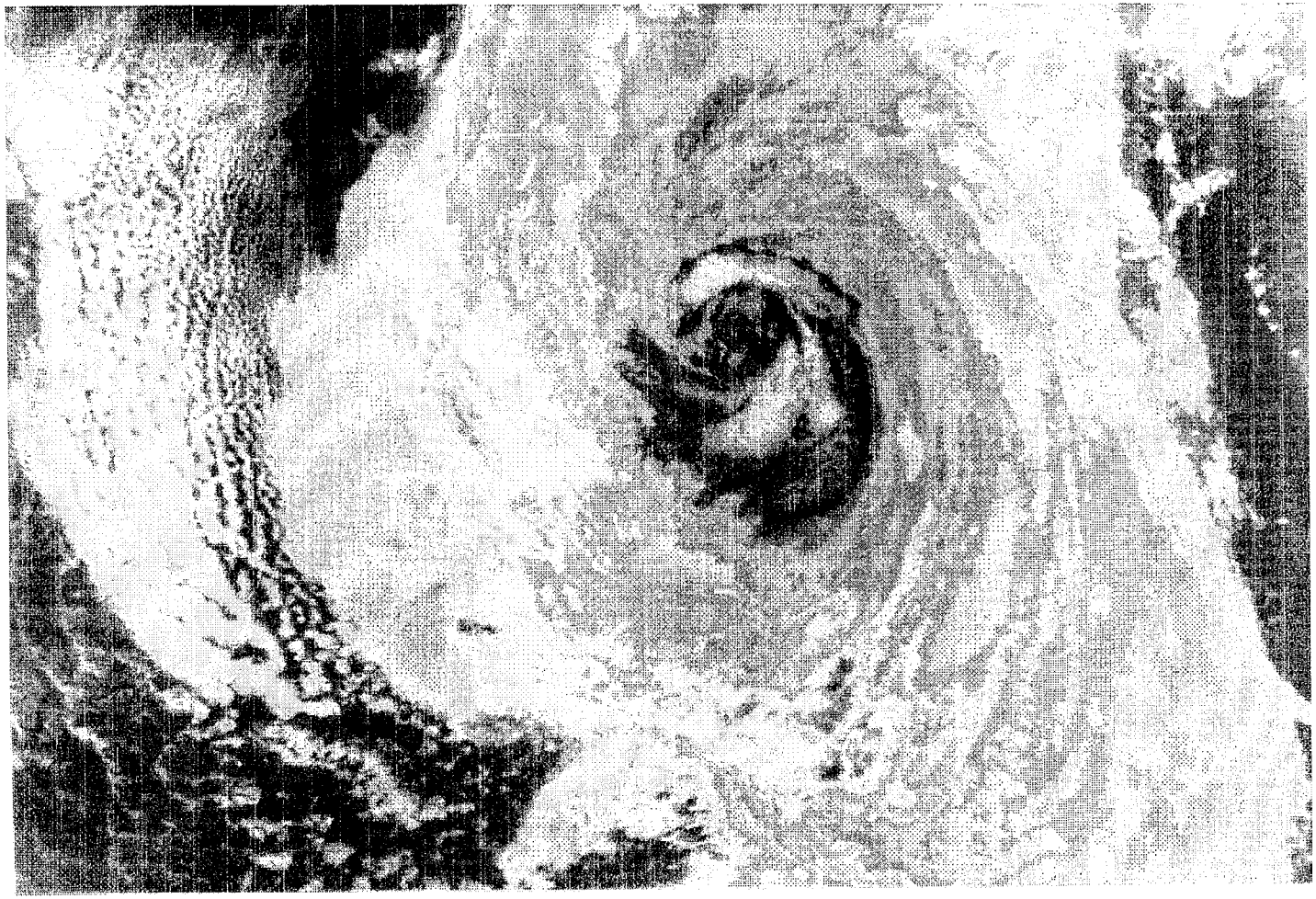

Figure 4.8. (b) Enhanced IR OLS imagery from the same DMSP satellite pass provides more detail of Flo's central features. Two prominent curved bands north and south provide a reasonable estimate of Flo's low-level circulation center.

caused extensive damage on the island of Honshu. Finally, at 0000 UTC, 20 September, Flo was downgraded to tropical storm strength due to extensive interaction with land, strong shear, and initial signs of extratropical transition.

4.2 Position Fixing with 85-Ghz (H) Data

The importance of accurate tropical cyclone center position fixes cannot be overstated. Each 6-hourly 72-hour storm forecast must be initialized with the most precise, and highest confidence center estimates. Since the end of aircraft tropical cyclone reconnaissance in the western North Pacific, JTWC has relied primarily on satellite data to provide location and intensity information. To a proportionately small extent, weather radar provides a secondary source of position information when tropical cyclone proximity allows. In 1990, 76% of all fixes were derived from satellite platforms with the remainder coming primarily from weather radar observations. Some other information sources may include ship reports, fixed and drifting buoys, and radiosonde data. Also included were several aircraft reconnaissance fixes courtesy of the TCM-90 field experiment.

At JTWC, satellite data processing capabilities and analysis methods have steadily improved, increasing the accuracy of satellite derived location estimates. The Meteorological Imagery Data Display and Analysis System (MIDDAS) now in use at JTWC, allows more accurate and efficient tropical cyclone fixing. Analysis applications such as looping of GMS IR and VIS images, super-imposing the log 10 spiral over convective banding features, and determining Dvorak intensity estimates permit higher

confidence fixes (Stetina et al. 1993). The system is also capable of processing OLS and SSM/I data from polar orbiting DMSP satellites. In addition, JTWC relies heavily on other members of the DMSP satellite reconnaissance network. Unfortunately, the other network locations do not possess these advanced capabilities. They do, however, process and display real time SSM/I data.

The SSM/I 85-Ghz (H) channel allows observations of convective organization at high resolution. Convective detail provides a characterization of the low-level circulation pattern of tropical cyclones. This capability makes the 85-Ghz (H) channel especially useful for locating the tropical cyclone low-level circulation center (LLCC). Velden et al. (1989), Sandlin and Spangler (1989), and Alliss et al. (1992, 1993) have all used specific cases to illustrate the merit of tropical cyclone center fixing using 85-Ghz data.

Data from SSM/I was first used operationally by the JTWC satellite reconnaissance network in 1990. Initially, geolocation difficulties in the ephemeris data processing software meant SSM/I data was only used reliably as a tool for determining the gale wind boundaries around tropical cyclones. However, with the geolocation software difficulties corrected, the SSM/I 85-Ghz (H) SDRs were used as a secondary source of position fixing information primarily to compliment DMSP OLS data. This data proved extremely useful when tropical cyclones were poorly organized during early stages and later during the dissipation phase. In these cases, locating the LLCC can be difficult using only OLS data. In some cases, the presence of a cold dense overcast (CDO) or cirrus shield can obscure the convective banding structure or hide the presence of an eye feature in a mature tropical cyclone. In these instances, a LLCC estimate is difficult using even high

resolution DMSP visible data while the need for an accurate center fix is most critical. In addition, poorly organized systems are even more difficult to analyze at night when the analyst is forced to rely almost exclusively on lower resolution infrared data.

Using 85-Ghz (H) observations of Super Typhoon Flo, position fix estimates were determined from each of the seven SSM/I passes. For five passes, the 85-Ghz center estimates and corresponding DMSP OLS fixes were each compared to the JTWC best track locations to determine track deviation distances. In one case, the best track error from an SSM/I center estimate was compared to the error between the best track and a NOAA infrared satellite image fix from 28 minutes earlier. Since there was no conventional satellite data avialable, the best track error determined from the final SSM/I pass could not be compared. Conventional satellite data best track errors were found in the Super Typhoon Flo post storm summary and final best track data provided by JTWC. Subjective analysis techniques were used to locate the LLCC or eye in the SSM/I data before calculating the deviation from best track. It should be noted that the JTWC final best track may have smoothed eye wobbles and some minimal erratic motion. Also, since there is no longer dedicated aircraft reconnaissance in the wester North Pacific basin, final best track data is usually based primarily on satellite information. However, because Super Typhoon Flo was the subject of two TCM-90 IOPs, four high quality aircraft fixes were also recorded. In addition, Flo's proximity to land from 1000 UTC, 16 September until dissipation, resulted in an unusually high percentage (62%) of high quality land based weather radar fixes. Land based weather radar position fixes are almost always considered more precise than satellite fixes because radar antenna elevation angle can be

adjusted low enough to accurately identify the LLCC. Satellite fixes must be corrected for parallax error caused by the targets distance from the satellite subtrack. Furthermore, even if an eye is evident in VIS or IR satellite data, the upper level cloud top signature may not correspond to the low level center if the eye column is tilted with height. Table 4.1 shows the error comparisons with JTWC final best track for each of the SSM/I 85-Ghz fixes along with DMSP OLS and NOAA Advanced Very High Resolution Radiometer (AVHRR) data. Distance deviations (best track errors) are given in kilometers. Mean error and standard deviation are also noted for the two sources of center estimates. The data in the table demonstrate a general improvement in fix error when the SSM/I data is compared to conventional satellite derived location estimates. The mean fix errors for the 85-Ghz SSM/I and OLS/AVHRR data are 13.0 km and 17.7 km respectively. Standard deviations are near 11.5 km for both.

From this point, it was also important to determine the significance of the difference in the average fix errors calculated. To accomplish this, an equal variance, one-sided t-test for unequal sample sizes was conducted. The variances of the two data sets were assumed to be equal only after completing a F-test at the significance level of $\alpha = 0.20$. T-test results indicated the mean best track error difference between SSM/I and conventional satellite data could be considered significant at level $\alpha = 0.24$. However, due to the small sample sizes, the difference was not necessarily meaningful when the t-test is conducted at significance levels smaller than $\alpha = 0.24$. In other words, there is a 76% probability that the difference in mean best track errors between SSM/I and conventional data will be greater than 4.7 km given a larger sample size.

Table 4.1. Error comparisons with JTWC final best track for each of the SSM/I 85-Ghz fixes shown with DMSP OLS and NOAA AVHRR fixes. Distance deviations from best track are given in kilometers. Mean errors and standard deviations are also included.

Pass Time	85-Ghz Error	OLS/AVHRR Error
13/2030	33.1	20.8
14/0900	15.6	36.1
16/2130	0.0	9.9
17/1000	15.6	19.3
17/2120	15.6	19.3
18/1000	0.0	0.7*
18/2100	11.0	
Mean Error:	13.0	17.7
Standard Deviation:	11.3	11.9

*NOAA AVHRR Data Final Best Track Error

The differences found in the small sample from Super Typhoon Flo are still quite significant given the relatively minor fix errors noted in the conventional satellite data. The available data generally provided observations of Flo as a mature tropical cyclone with very distinct features. In the cases involving an 85-Ghz (H) retrieval and an OLS image from the same pass, the low level center was usually easy to locate in both products. However, in the recent studies mentioned, even greater error differences were noted in fixes determined from conventional satellite imagery due primarily to either poor storm organization or high clouds obscuring the LLCC.

4.3 85-Ghz (H) Intensity Statistics

As previously mentioned, there is a general scarcity of conventional data over the western North Pacific. Moreover, there are no longer any "ground truth" tropical cyclone observations collected by reconnaissance aircraft. Therefore, the burden of accurately determining tropical cyclone intensity rests with the skilled satellite analyst and the application of the Dvorak technique. The Dvorak technique (Dvorak 1977,1984) is a statistically derived method of determining tropical cyclone intensity from cloud patterns and cloud top temperatures in VIS and enhanced IR satellite imagery. The accuracy of this technique has been verified with aircraft data. However, the analysis is often subjective and relies heavily on continuity. It may falter on occasions when the tropical cyclone is embedded in the monsoon trough or accelerating rapidly. Sometimes, off season systems don't behave according to Dvorak rules because environmental pressure gradients tend to indirectly intensify the winds on the periphery of the tropical cyclone.

Several recent SSM/I research efforts (Alliss et al. 1992,1993; Felde and Glass 1991; Rodgers et al. 1994) have also emphasized developing more objective methods for remotely measuring tropical cyclone intensity. In these studies, SSM/I SDRs have been tested as indicators for tropical cyclone intensity and intensity changes. The magnitude of latent heat release due to convection is considered to be one of the main conditions required for tropical cyclone intensification. The 85-Ghz (H) channel provides a good gauge of convective activity because the large ice particles and water droplets effectively scatter and attenuate upwelling microwave energy. The result is observed cold BTs relative to weak convection and the ocean background. Two recent studies have used

85-Ghz (H) retrievals to determine a correlation between BTs and tropical cyclone intensity.

Felde and Glass (1991) compared 85-Ghz (H) retrievals to estimates of intensity for 11 different western North Pacific tropical cyclones. A total of 17 SSM/I passes were used in the sample. A 1.0 degree latitude box positioned over the tropical cyclone center was used to determine the percentage area covered by a certain threshold 85-Ghz (H) BT. A threshold temperature of 220 K was determined to have the highest correlation with intensity for the entire sample. That study demonstrated that for the 1.0 degree latitude box, the percentage area coverage of BTs $<$ 220 K increased as the maximum sustained wind speed increased. For the set of all SSM/I passes regardless of storm stage, the study found a correlation coefficient of 0.73 between storm intensity and the percent portion of the $1^{\circ}x1^{\circ}$ box area covered by 85-Ghz (H) brightness temperatures less than the threshold temperature of 220 K.

Alliss et al. (1992) compared 85-Ghz (H) retrievals to the NHC best track intensity evolution of Hurricane Hugo (1989). In that application, the percent area coverage of horizontally polarized 85-Ghz BTs $<$ 220 K within a 1.0 degree circular radius around the storm center was determined for eight SSM/I passes over Hugo. For each of the eight overpasses, percent area coverage increased as central pressure decreased. Conversely, when central pressure increased, the percent area coverage of 85-Ghz BTs $<$ 220 K decreased. A high negative correlation value of -0.93 was found between the two parameters for the Hurricane Hugo case.

The concepts from the studies mentioned above were applied to SSM/I retrievals of Super Typhoon Flo. Additional evidence is needed to prove the results noted in the referenced research to determine their performance in other instances. This section was initiated to contribute additional information to meet the goal of devising a more objective method of remotely sensing tropical cyclone intensity. Two methods were used to determine a correlation between intensity and the threshold 220 K 85-Ghz (H) brightness temperature. The first method was similar to the studies cited above. The percent area coverage of BT pixels < 220 K was calculated for circular areas of radii 2.0, 1.5, and 1.0 degrees for each of the seven SSM/I passes over Flo. Figure 4.9 shows the plot of pixel percentage and maximum sustained wind speed (ms^{-1}) at each SSM/I observation time. JTWC uses maximum sustained winds to record tropical cyclone intensity and to classify tropical cyclones for their final best track data records. winds to classify tropical cyclone intensity. Poor correlation values and the absence of a discernible pattern between the two plots indicates very little if any association. Of the seven SSM/I observations of Flo, the data from the passes 8 1/2 hours before, then 4 hours after the recorded maximum intensity at 0600 UTC, 17 September both show percent area coverage for radii of 2.0 and 1.5 degrees at their lowest values instead of highest as expected.

The second method used to determine a possible correlation between tropical cyclone intensity and 85-Ghz (H) brightness temperatures was slightly different. An area averaged 85-Ghz (H) BT value was determined for each SSM/I pass. Circular areas defined by radii of 2.0, 1.5, 1.0, and 0.5 degrees were positioned over the storm center and then average 85-Ghz (H) BT values were calculated. Although the 220 K threshold value comparisons

did not produce favorable results, it was hoped that a negative correlation or a general pattern of decreasing 85-Ghz (H) BT averages and increased wind speeds could be determined based on the principles mentioned earlier in the section.

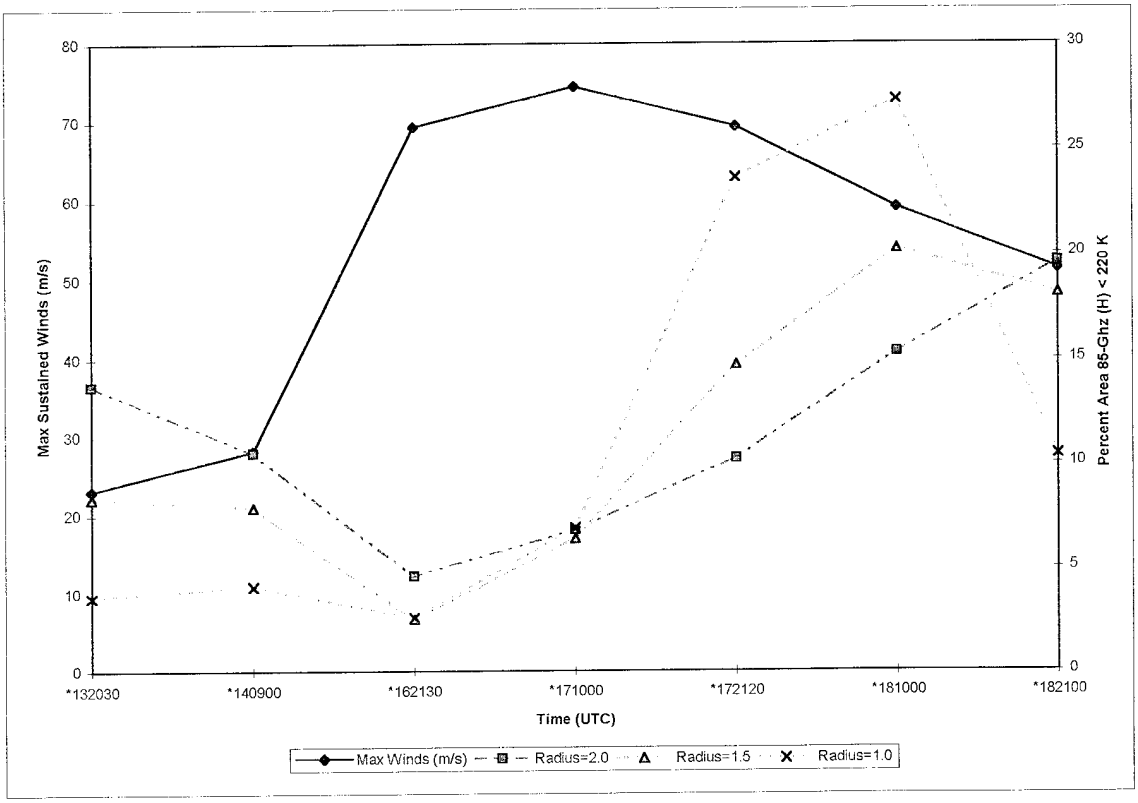

Figure 4.9. Percentage of 85-Ghz (H) pixels less than 220 K within radii of 2.0,1.5, and 1.0 degrees of Flo's center with maximum sustained winds (m/s) as a function of time. Low correlation values of r = -0.42, 0.03, and 0.38 indicate poor association between 85-Ghz (H) data and tropical cyclone intensity for this case.

In Figure 4.10, a plot of the average brightness temperatures and maximum sustained wind speed (ms^{-1}) at each SSM/I pass time is displayed. Unfortunately, the average brightness temperatures versus tropical cyclone intensity plot again, does not yield a conclusive pattern. Divergent correlation values verify the absence of association between

the two parameters. Additionally, observations at 2130 UTC, 16 September and 1000 UTC, 17 September, nearest the time of Flo's maximum recorded intensity, produced the highest average brightness temperatures of the seven calculated. Based on previous studies, the average brightness temperatures should have been at their lowest values near peak intensity.

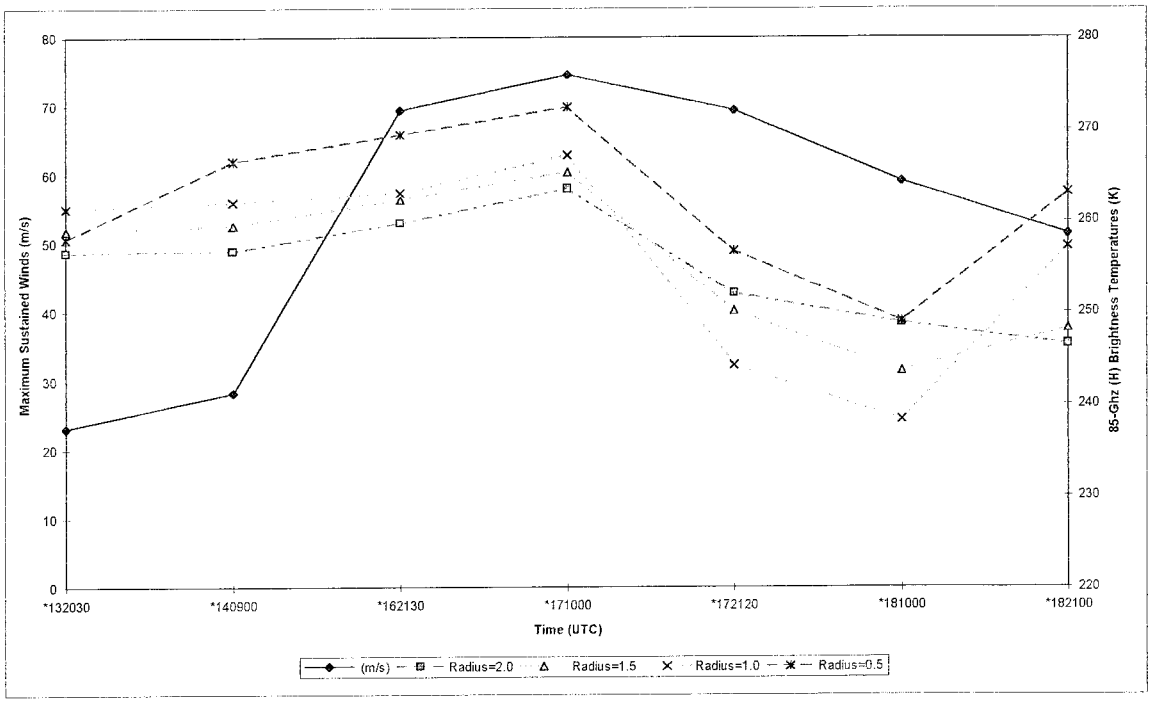

Figure 4.10. 85-Ghz (H) average brightness temperatures (K) at radii of 2.0, 1.5,1.0, and 0.5 degrees from Flo's center with maximum sustained winds (m/s) as a function of time (UTC). Correlation coefficients of r = 0.14, -0.02, -0.19, and 0.18 respectively represent divergent values indicating low correlation between 85-Ghz (H) BT averages and tropical cyclone intensity for this case. Winds are derived from JTWC best track data.

It appears that in each of the analyses presented above, expected results were not realized when the same principles and techniques from previous studies were applied to the Flo data set. Furthermore, opposite trends were found in Flo's SSM/I 85-Ghz (H)

statistics. For this case, it can be concluded that SSM/I retrievals of Super Typhoon Flo provided little if any evidence of a significant correlation between the 85-Ghz indicators and tropical cyclone intensity. As indicated in the final best track data, the Dvorak technique provided the most accurate assessment of Flo's intensity. The technique was validated by dropsonde observations at the time of peak intensity during the second TCM-90 aircraft mission on 17 September. The Dvorak analysis yielded a maximum intensity of 135 kts (69 ms^{-1}) while the uncorrected minimum sea-level pressure of 891 mb measured by the NASA DC-8 correlated to maximum sustained winds of 145 kts
(75 ms^{-1}).

5. 19-GHZ SENSOR DATA RECORDS

The 19-Ghz frequency provides the lowest resolution of all the SSM/I channels (near 55 km). However, this frequency has been found to be very sensitive to atmospheric parameters such as water vapor, cloud water, precipitation, and sea spray over the ocean. A SSM/I analysis of tropical cyclone structure has included observations of size and shape characteristics in 19-Ghz retrievals (Felde and Glass 1991). This same study also demonstrated a possible correlation between 19-Ghz data and tropical cyclone intensity. The following sections apply these two selected concepts from the referenced study to analyze Super Typhoon Flo in 19-Ghz SSM/I data.

5.1 19-Ghz (V) Observations of Flo's Horizontal Structure

The horizontal structure of a tropical cyclone refers to the size and shape of the active storm region. The active tropical cyclone region in turn, is defined by the presence of heavy wind driven seas, high water vapor content, and condition ranging from rain free to heavy precipitation. Felde and Glass (1991) applied this definition to fit the sensor capabilities of the vertically polarized 19-Ghz SSM/I channel.

Observing and forecasting the radius of gale force winds surrounding a tropical cyclone is an ongoing challenge. Combinations of synoptic data, SSM/I information, and empirical techniques are employed to determine the extent of tropical cyclone gale force winds (>15 ms^{-1}). An empirical technique developed by Martin and Holland (1988) relies on storm size and shape parameters to characterize wind radii extent. Size and shape parameters are determined from VIS and IR satellite imagery and then used in an

analytical formula to resolve the radius of gale force winds as well as realistic wind-distribution asymmetries (Guard et al. 1992). However, there are many occasions when the cloud shield of a tropical cyclone does not accurately depict the active region of a storm. The cirrus shield, viewed as bright white in IR satellite imagery, may extend beyond what is considered the active tropical cyclone region. In other instances such as the case of increased shear, the cloud shield may not cover the extent of the active storm region. With this in mind, a more accurate method of characterizing the size and shape of the active storm region may help to improve the analysis of tropical cyclone wind distribution.

Felde and Glass (1991) used SSM/I 19-Ghz (V) SDRs to examine the horizontal dimensions of the active tropical cyclone region. The goal of their research was to develop an objective method of characterizing general storm size and shape. The 19-Ghz (V) channel was especially suited for this task because of its importance in both the marine surface wind algorithm and the two over ocean rainfall rate algorithms described earlier. Investigating the mesoscale features that define the horizontal structure of a tropical cyclone does not require resolution higher than the 55 km afforded by the 19-Ghz frequency. In their study, Felde and Glass (1991) used RADTRAN model (described by Falcone et al. 1979) simulations to determine a threshold 19-Ghz (V) BT value that could define the boundary of the active tropical cyclone region. This model was employed because it accurately simulates satellite measured upwelling microwave energy and attenuation for realistic meteorological conditions. A threshold 19-Ghz (V) BT value of 220 K appeared to establish the boundary between the periphery of the tropical cyclone

disturbance and the relatively smooth ocean surface, moderate water vapor, and clear or non-convective cloud conditions outside the active region. The region between the periphery and the active tropical cyclone region was characterized by values between 220 K and 230 K. Brightness temperatures warmer than 230 K indicated areas where rough seas (sea spray), high water vapor, and conditions ranging from clear to heavy precipitation where present. The extremely intense region of the tropical cyclone was found to be associated with values warmer than 300 K.

In this section, similar thresholds are applied to SSM/I 19-Ghz (V) SDR retrievals of Super Typhoon Flo. These images characterize the shape and size of Flo during it's evolution. Available GMS IR images available close to SSM/I overpass times are used to compare the cloud shield shape to Flo's active region described by the 230 K boundary in the 19-Ghz (V) data. Storm size is subjectively determined by averaging maximum and minimum storm diameter for the 230 K boundary in SSM/I data and the cloud shield boundary in GMS data. Figure 5.1 (a) shows the 19-Ghz (V) image of Flo at 2030 UTC, 13 September. Although at this time Tropical Storm Flo was embedded in the monsoon trough, it is easy to identify the general size and shape of the storm. Unfortunately, the southern periphery of the storm and the full extent of the eastern and western boundaries cannot be determined. The noticeable straight edge on the northwest quadrant agrees well with the position of the TUTT cell. The diameter of the active tropical cyclone region is approximately 550 km. In Figure 5.1 (b), Japanese GMS geostationary IR imagery from 1830 UTC shows the same general shape represented in the cloud shield. However, the diameter of Flo's cloud shield in the GMS image appears to be slightly

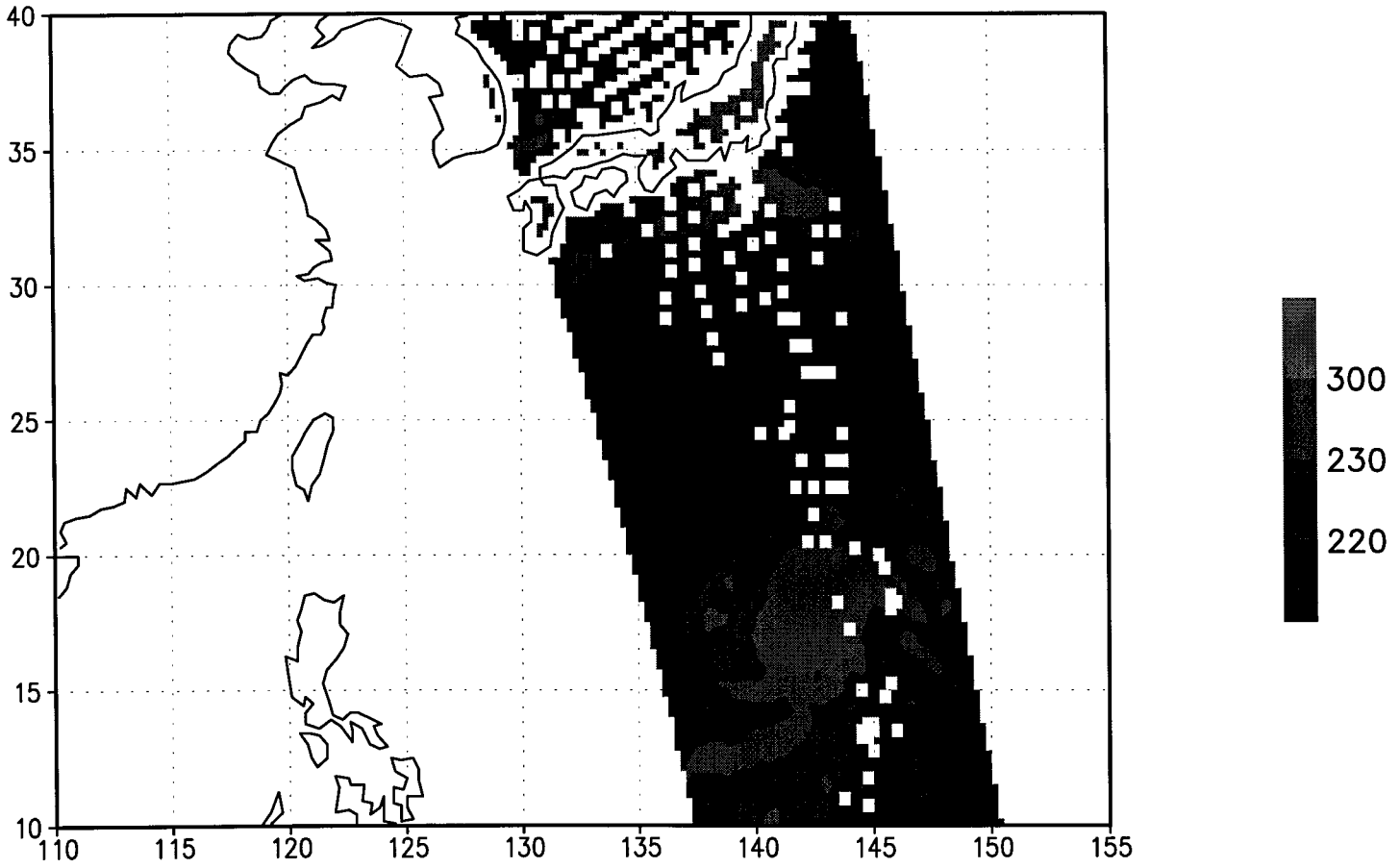

Figure 5.1. (a) The 19-Ghz (V) image of Flo at 2030 UTC, 13 September. Although at this time Tropical Storm Flo was embedded in the monsoon trough, it is easy to discern it's general size and shape.

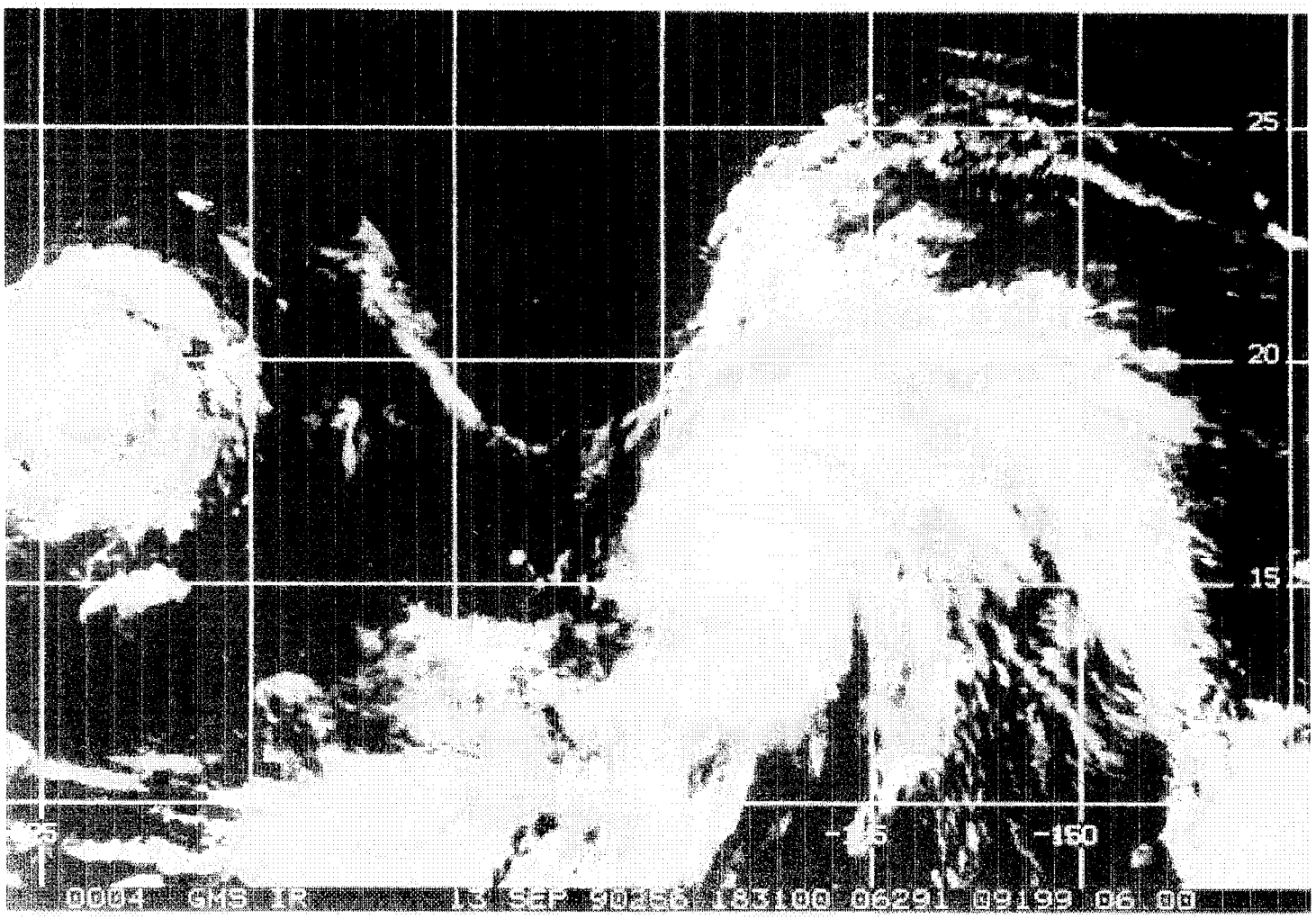

Figure 5.1. (b) The Japanese GMS geostationary IR imagery from 1830 UTC shows the same general shape represented in the cloud shield. This image reveals the presence of the TUTT cell northwest of Flo's position.

larger. The diameter of Flo defined by the cloud shield is approximately 620 km. A flat edge is evident along the periphery of Flo's western boundary. This noticeable feature may be due to the proximity of the TUTT causing shear along the storm's northwest quadrant. Although clouds may not appear visible in this region, rough seas caused by high winds may be present.

The 19-Ghz (V) data from the 0900 UTC 14 September SSM/I pass is shown in Figure 5.2 (a). Except for Flo's southern quadrant embedded in monsoon trough, the storm appears better organized with a much more symmetric shape. There is no longer an abrupt edge visible along Flo's northwest quadrant. The diameter of the active storm region now measures approximately 650 km neglecting Flo's extension into the monsoon trough south of 15° N latitude. The corresponding GMS IR image from 0630 UTC appears in Figure 5.2 (b). A general shape comparison between each image shows the same general characteristics. In this image the cirrus outflow extends to 25° N latitude or about 2° beyond what is observed in the SSM/I data. Differences in coverage between the cloud shield and the 19-Ghz (V) 230 K boundary are significant even if some minimal westward movement occured over the 2 1/2 hours (approximately 1.0 degree) between the GMS and SSM/I observations. In Flo's western semicircle, the active region described in the 19-Ghz data extends to near 134° E longitude while in the GMS IR data the cloud shield terminates near 137° E longitude. Although difficult to define, the estimated cloud shield diameter is near 775 km.

SSM/I data available 2 1/2 days later at 2130 UTC 16 September is shown in Figure 5.3 (a). Flo, now a typhoon, has an elongated shape oriented north-south as viewed in the

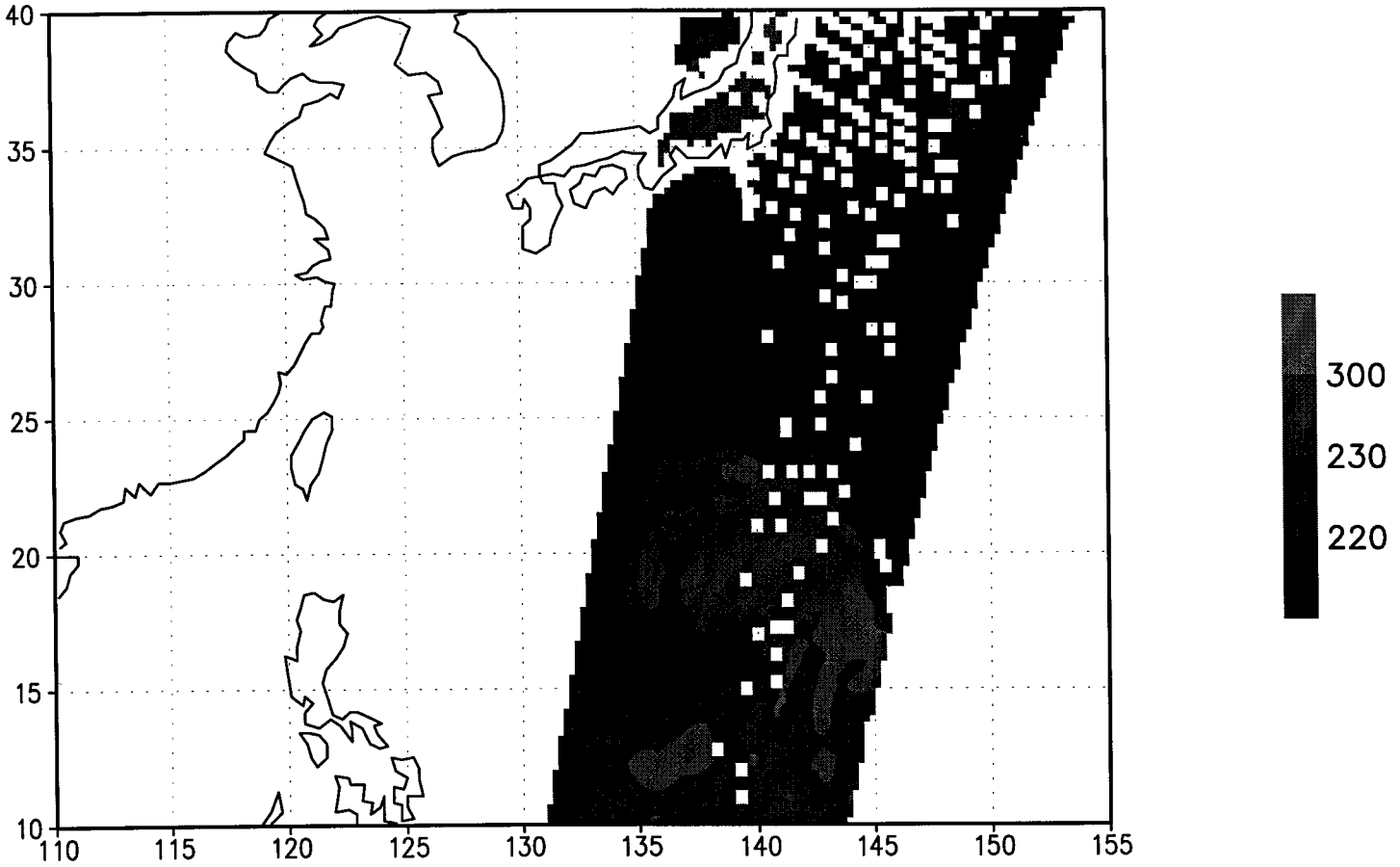

Figure 5.2. (a) shows the 19-Ghz (V) data from the 0900 UTC, 14 September SSM/I pass. Although the southern extent of Tropical Storm Flo embedded in the monsoon trough, the storm appears better organized with a much more symmetric shape.

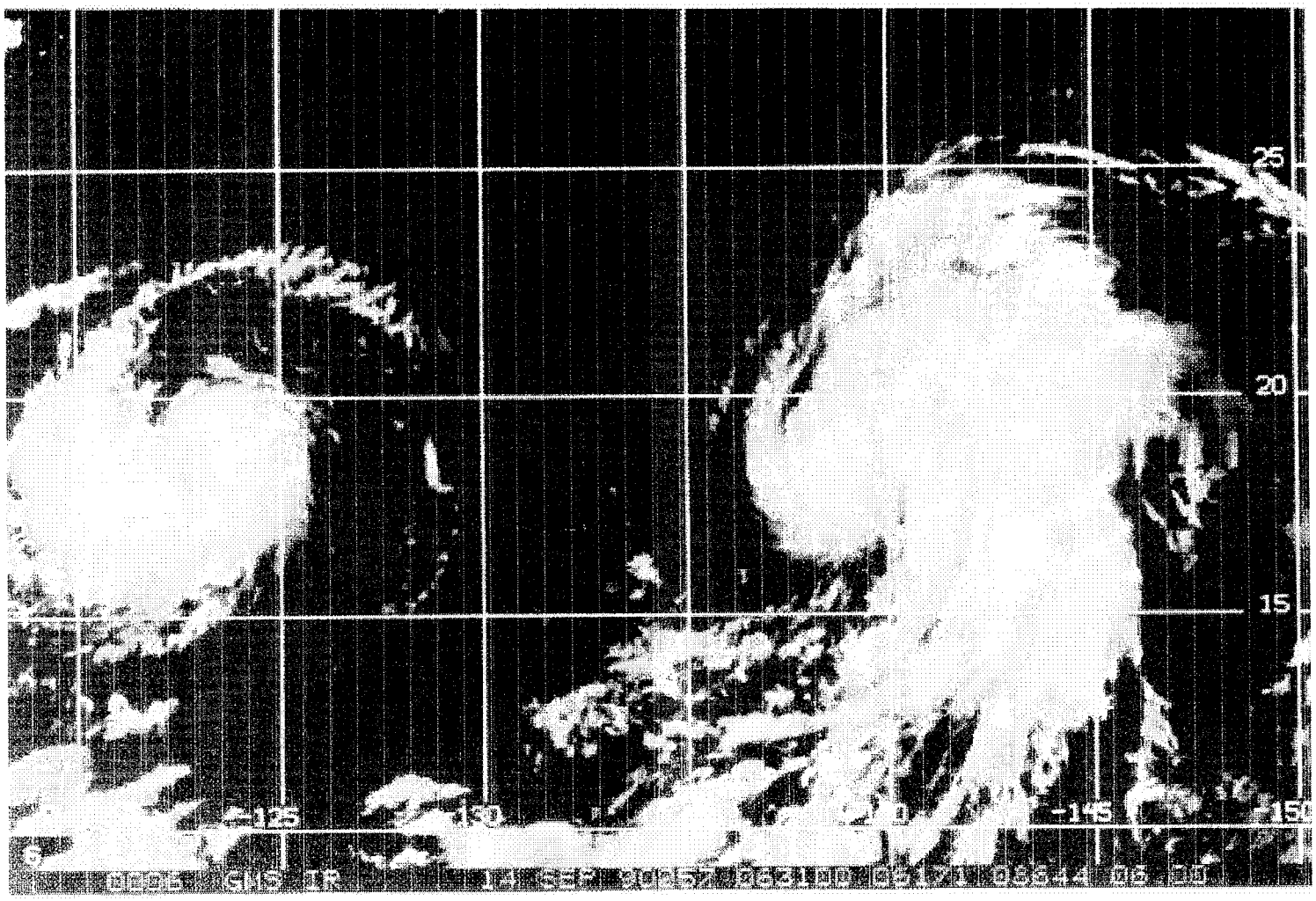

Figure 5.2. (b) The corresponding GMS IR image from 0630 UTC. Comparing patterns between images reveals the same general storm shape.

19-Ghz (V) data. In this pass, the active storm region extends from 21° N to near 30° N latitude and two degrees longitude west of the best track center. An average storm diameter of 700 km can be estimated from this image. In Figure 5.3 (b), the GMS IR image from 1830 UTC shows more symmetric organization in the cloud pattern. Here, the estimated storm diameter is also close to 700 km. In this image, the clouds associated with Typhoon Flo only extend to near 28° N latitude in contrast with the SSM/I data. The active storm region may extend beyond the boundary of the cloud shield due to an increased environmental pressure gradient associated with the passing trough. In the two images, the western extent of both the cloud shield and the 230 K boundary are almost coincident.

The 1000 UTC, 17 September 19-Ghz (V) SSM/I image is shown in Figure 5.4 (a). Super Typhoon Flo has a nearly circular shape in the SSM/I data. There is an extension of the active region visible north of the main circular organization. The diameter of the average active storm region measured in this image is approximately 700 km. Figure 5.4 (b) shows the GMS IR image from 1230 UTC. Likewise, Super Typhoon Flo has a very symmetric circular shape in this image. The GMS IR representation of the cloud shield has an estimated diameter of close to 700 km. This image also provides an explanation for the extension of the active region north of the main circular organization viewed in the 19-Ghz (V) data. The southern extent of an eastward migrating trough is coupled with the northern boundary of Super Typhoon Flo.

The 19-Ghz (V) image from 2120 UTC, 17 September is presented for analysis in Figure 5.5 (a). In this image, Super Typhoon Flo's shape has changed slightly. Although

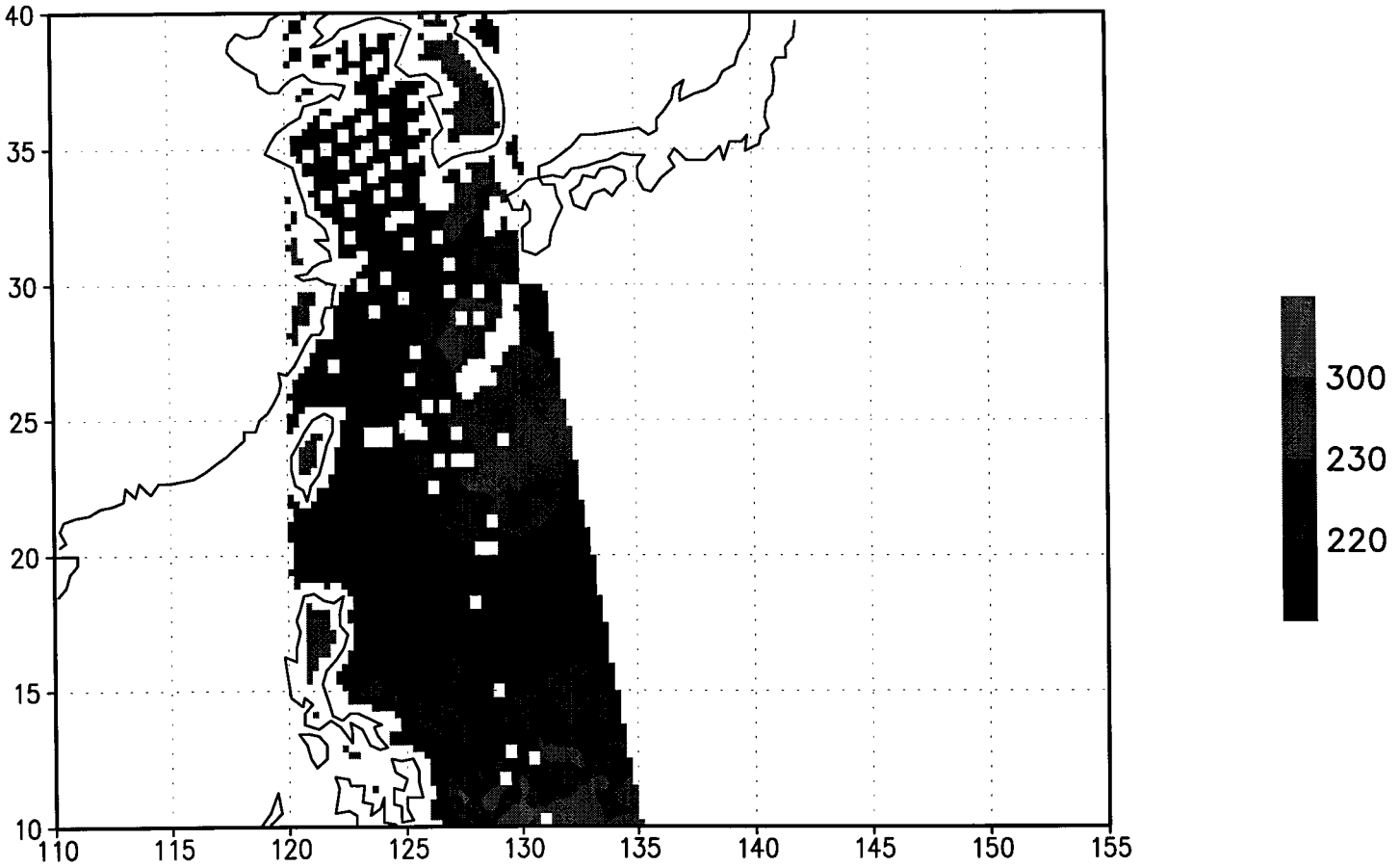

Figure 5.3. (a) The 19-Ghz (V) SSM/I data available 2 1/2 days later at 2130 UTC, 16 September shows Flo at typhoon intensity. The data depicts an elongated shape in the north-south direction.

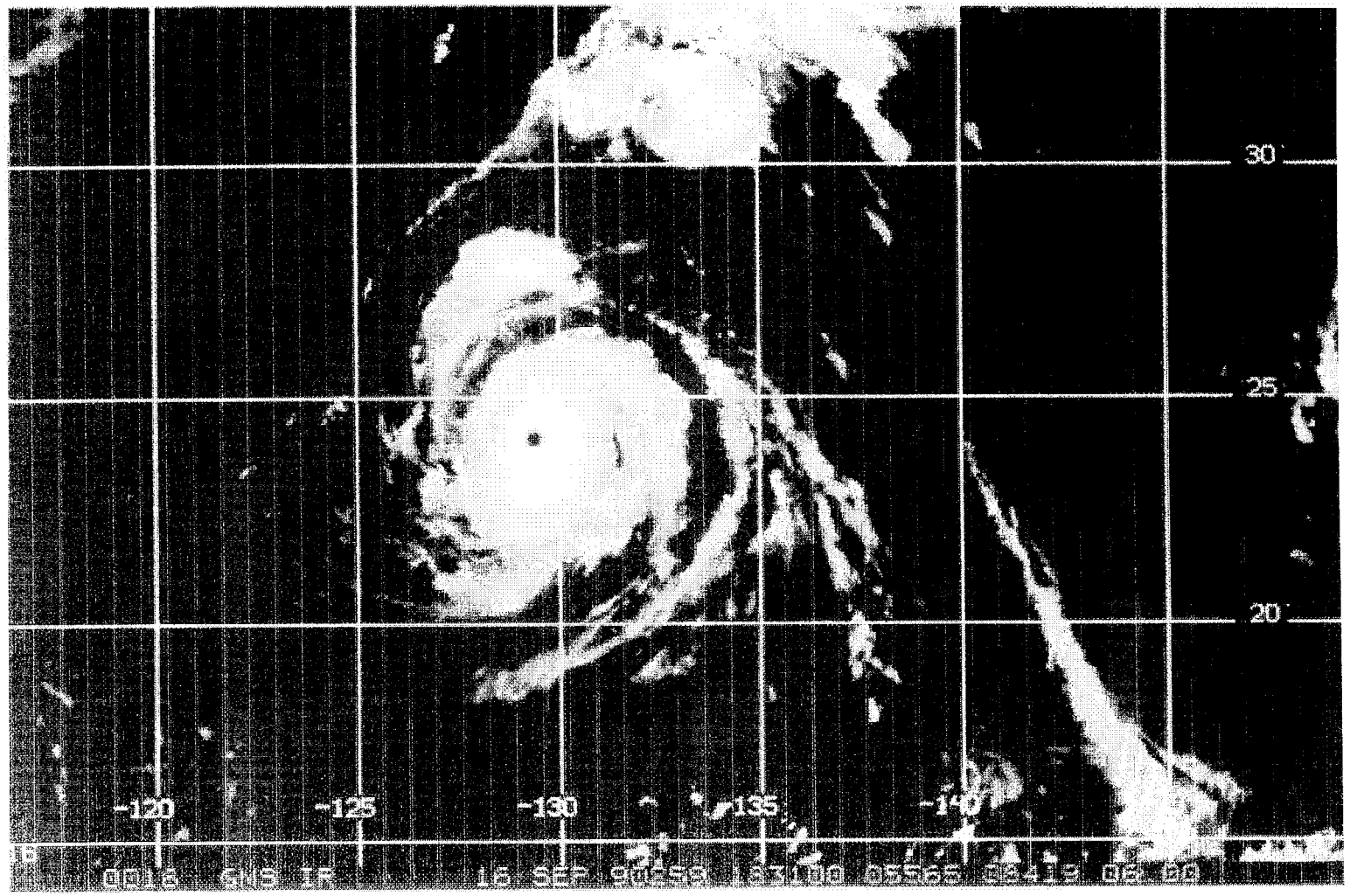

Figure 5.3. (b) The GMS IR image from 1830 UTC shows more symmetric organization in the cloud pattern compared to the SSM/I data.

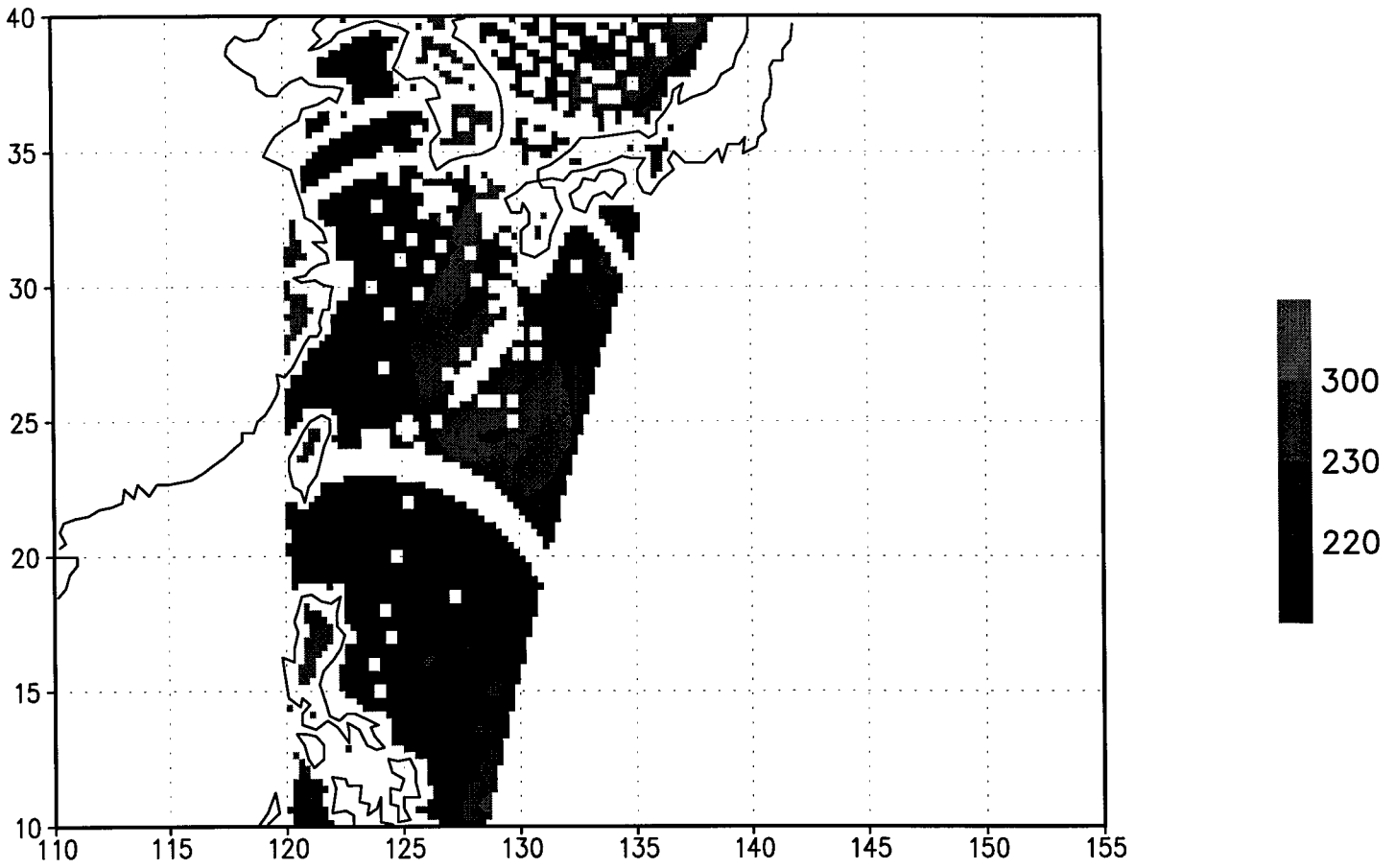

Figure 5.4. (a) The 1000 UTC, 17 September 19-Ghz (V) SSM/I image of Super Typhoon Flo. Flo now has a very circular appearance in the SSM/I data. There is an extension of the active region evident north of the main circular organization.

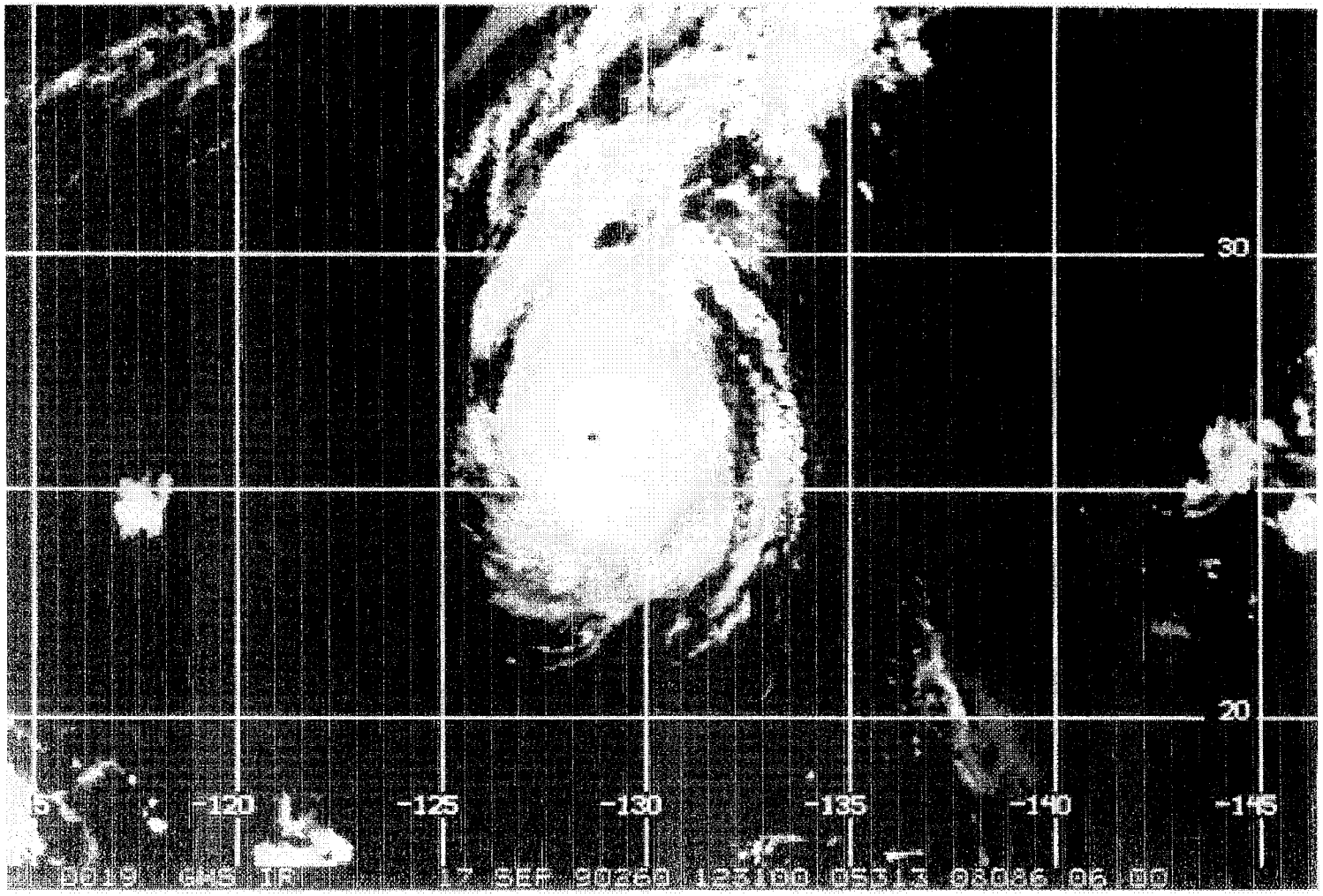

Figure 5.4. (b) The GMS IR image from 1230 UTC. Super Typhoon Flo has a very symmetric circular shape in this image.

the storm is still elongated, the orientation is now north-northwest through south-southeast. The average active storm region diameter measures near 750 km. Figure 5.5 (b) shows the GMS IR image of Flo less than three hours earlier at 1830 UTC. In this image the cloud shield edge directly associated with Flo's circulation appears symmetric about the eye. Increased convection north of the main cloud shield provides evidence of Flo's interaction with the passing trough and the land mass of southern Japan. The estimated diameter of Flo's cloud shield in the GMS image is roughly 800 km.

The next SSM/I pass was available at 1000 UTC, 18 September and is shown in Figure 5.6 (a). The 19-Ghz (V) image shows the active region of Super Typhoon Flo interacting with the Ryukyu Islands and southern mainland Japan. The general shape of Flo is now elongated north-northeast through south-southwest. In this image the active region diameter is approximately 650 km. The corresponding GMS image from 1230 UTC shown in Figure 5.6 (b), again provides evidence of Flo's interaction with the passing short wave. Flo also has an elongated shape in the GMS image. However, in this image, there is a north-northwest south-southeast elongation in contrast to the orientation noted in the 19-Ghz (V) data. Flo's approximate cloud shield diameter is about 750 km in the GMS data.

The final SSM/I 19-Ghz (V) image from 2100 UTC, 18 September is presented in Figure 5.7 (a). At this time, a large portion of the active region is affecting mainland Japan. Flo's southern semicircle exhibits a rounded shape while the northern quadrant appears to show signs of interaction with the passing trough. The storm diameter is approximately 600 km neglecting the active region associated with the midlatitude trough.

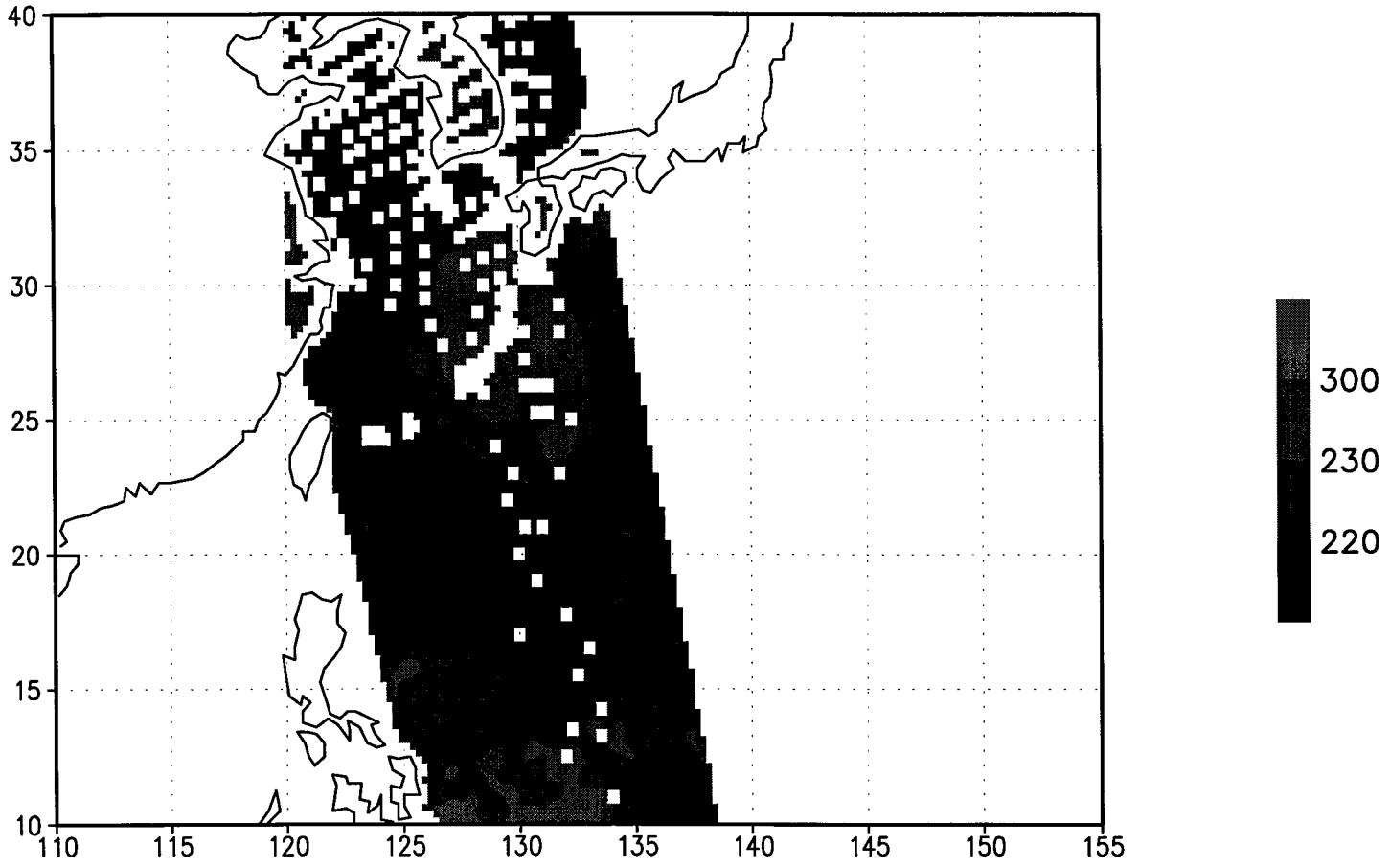

Figure 5.5. (a) The 19-Ghz (V) image from 2120 UTC, 17 September. In this image, Super Typhoon Flo's shape is in more elongated in a north-northwest south-southeast orientation.

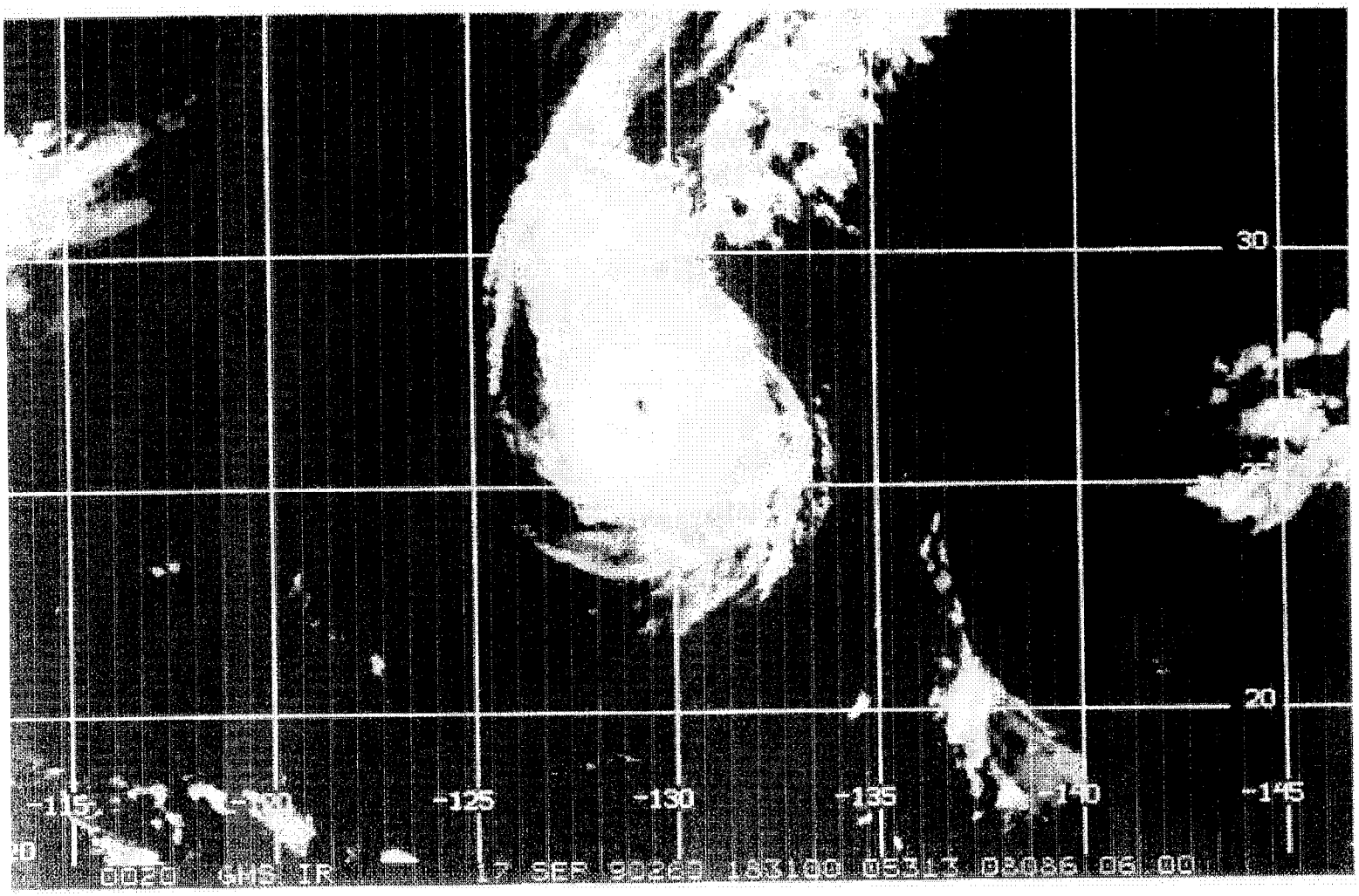

Figure 5.5. (b) The GMS IR image of Flo less than three hours earlier at 1830 UTC. In this image the edge of the dense white clouds associated directly with Flo's circulation appears symmetric about the eye.

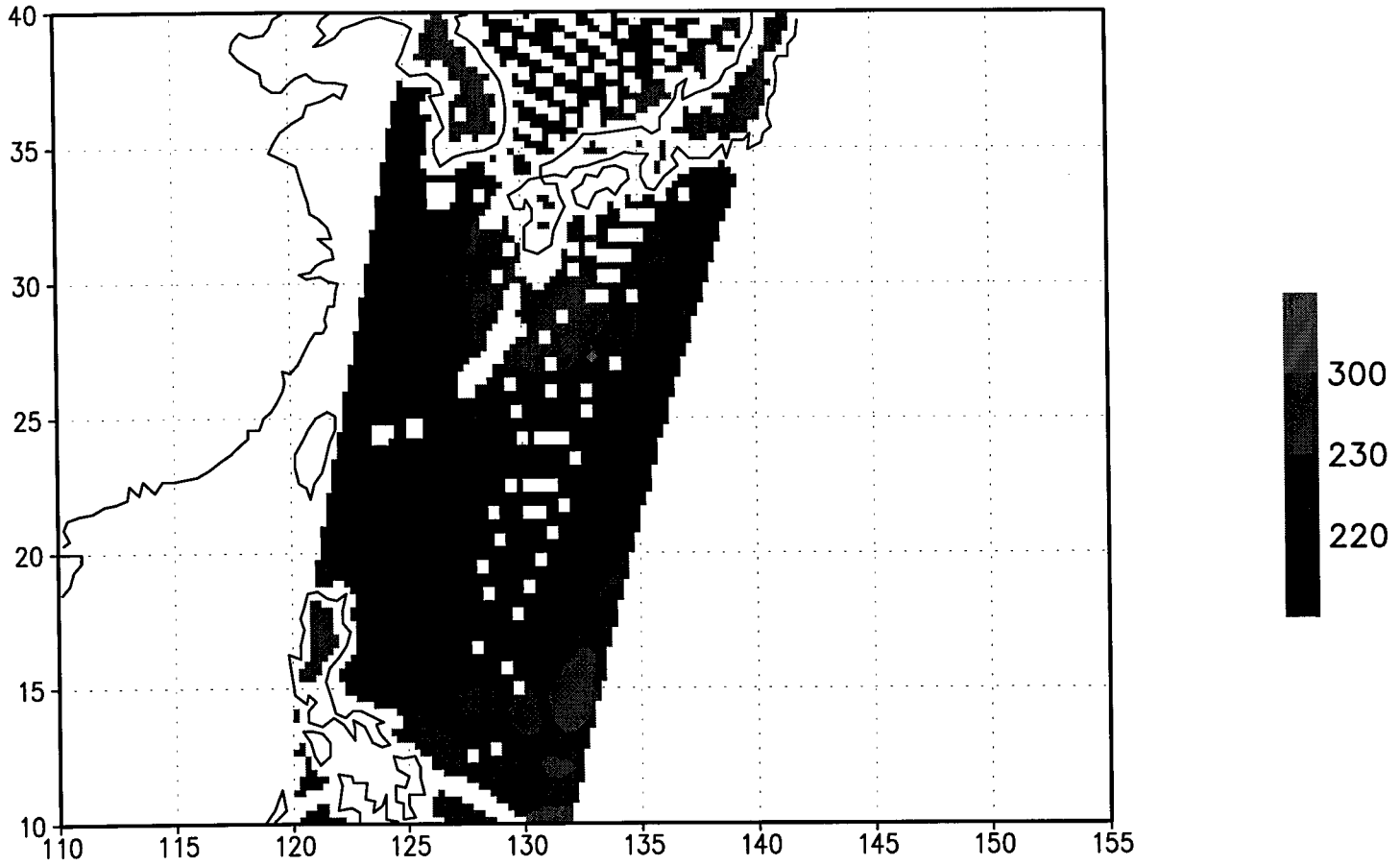

Figure 5.6. (a) The 1000 UTC, 18 September 19-Ghz (V) image shows the active region of Super Typhoon Flo interacting with the Ryukyu Islands and southern mainland Japan. The general shape of Flo is now elongated north-northeast through south-southwest.

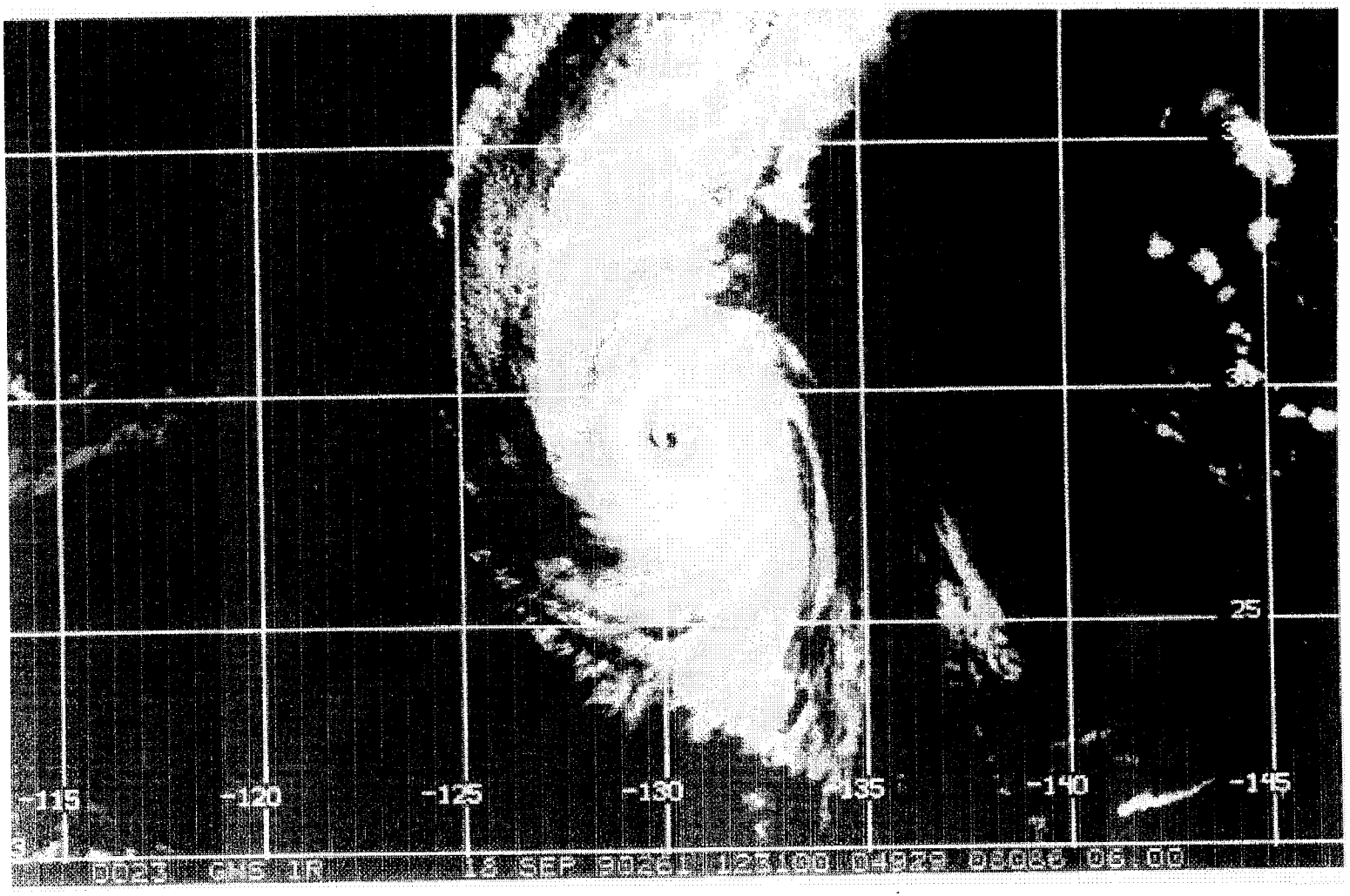

Figure 5.6. (b) The corresponding GMS image from 1230 UTC shows Flo's interaction with the passing short wave. This is the first evidence of the elongated shape in the GMS image.

Figure 5.7 (b) shows the corresponding GMS image from 1830 UTC, just 2 1/2 hours earlier. In this data the southern semicircle does not have the same rounded shape. There is howver, good agreement between the two images with the respect to signs of coupling with the midlatitude trough. In addition, the detached band along the eastern semicircle of Flo viewed in the GMS image can also be seen in the previous 19-Ghz (V) data as a detached band of 220-230 K BTs. A cloud shield diameter of roughly 650 km was measured by also neglecting the northern extent of convection associated with the short-wave.

The qualitative analysis of SSM/I and GMS images suggest that the 19-Ghz (V) data may provide a more accurate characterization of the general size and shape of the active tropical cyclone region of Super Typhoon Flo. At the very least it also contends that storm size and shape may not be accurately characterized solely in conventional satellite data. In the comparisons presented, the cloud shield pattern in infrared data often extended beyond the active region depicted in the microwave images. In infrared GMS imagery, Super Typhoon Flo's diameter was an average of 50 km larger than the diameter observed in the 19-Ghz (V) data. In conclusion, relying only on the infrared cloud top signature to estimate size and shape parameters may unnecessarily impact wind radii forecasts by exaggerating the extent of the active tropical cyclone region.

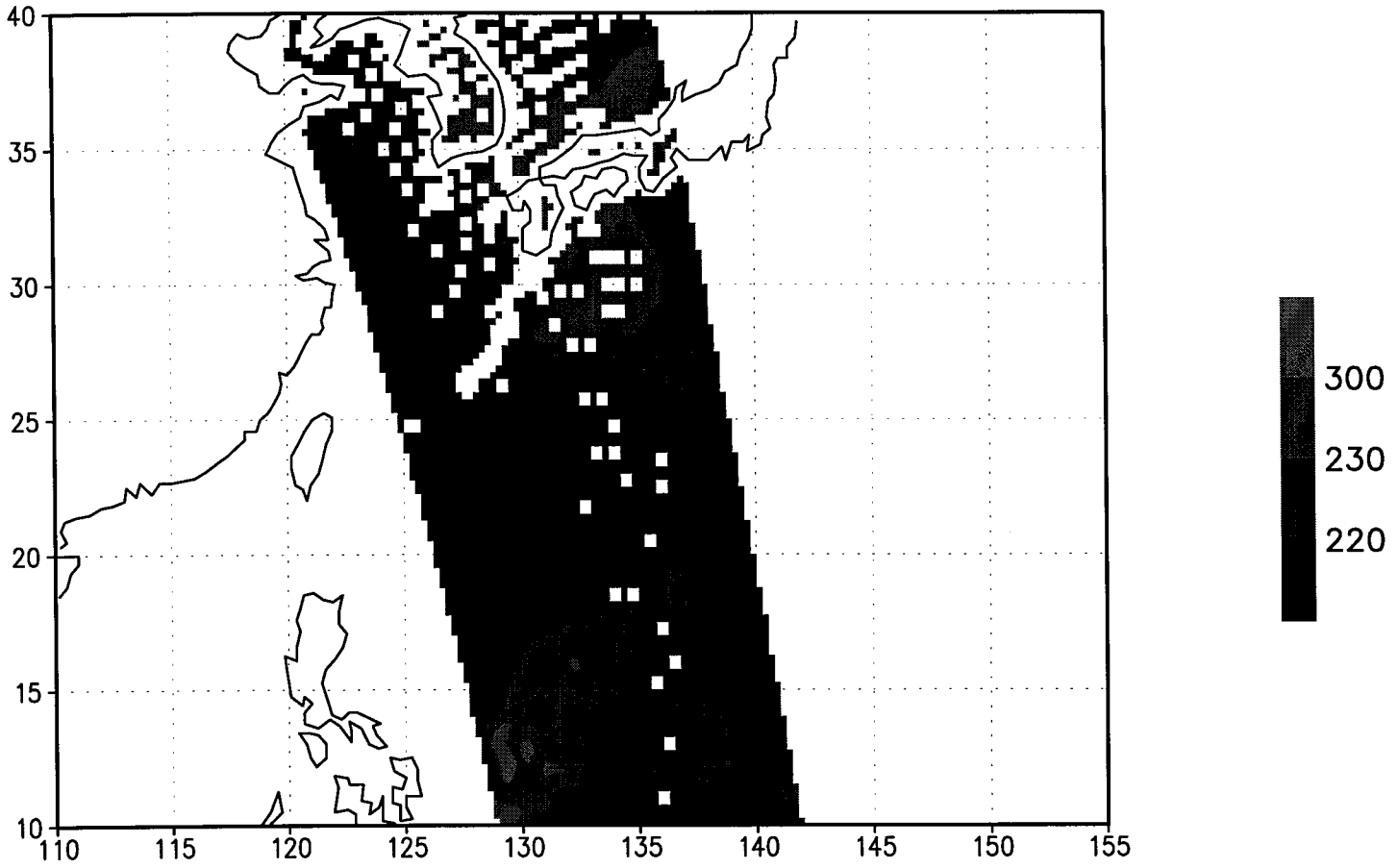

Figure 5.7. (a) The final SSM/I 19-Ghz (V) image from 2100 UTC, 18 September. It is apparent that a large portion of the active region is now located over mainland Japan. The southern semicircle exhibits a rounded shape while the northern quadrant appears to be coupling with the passing trough.

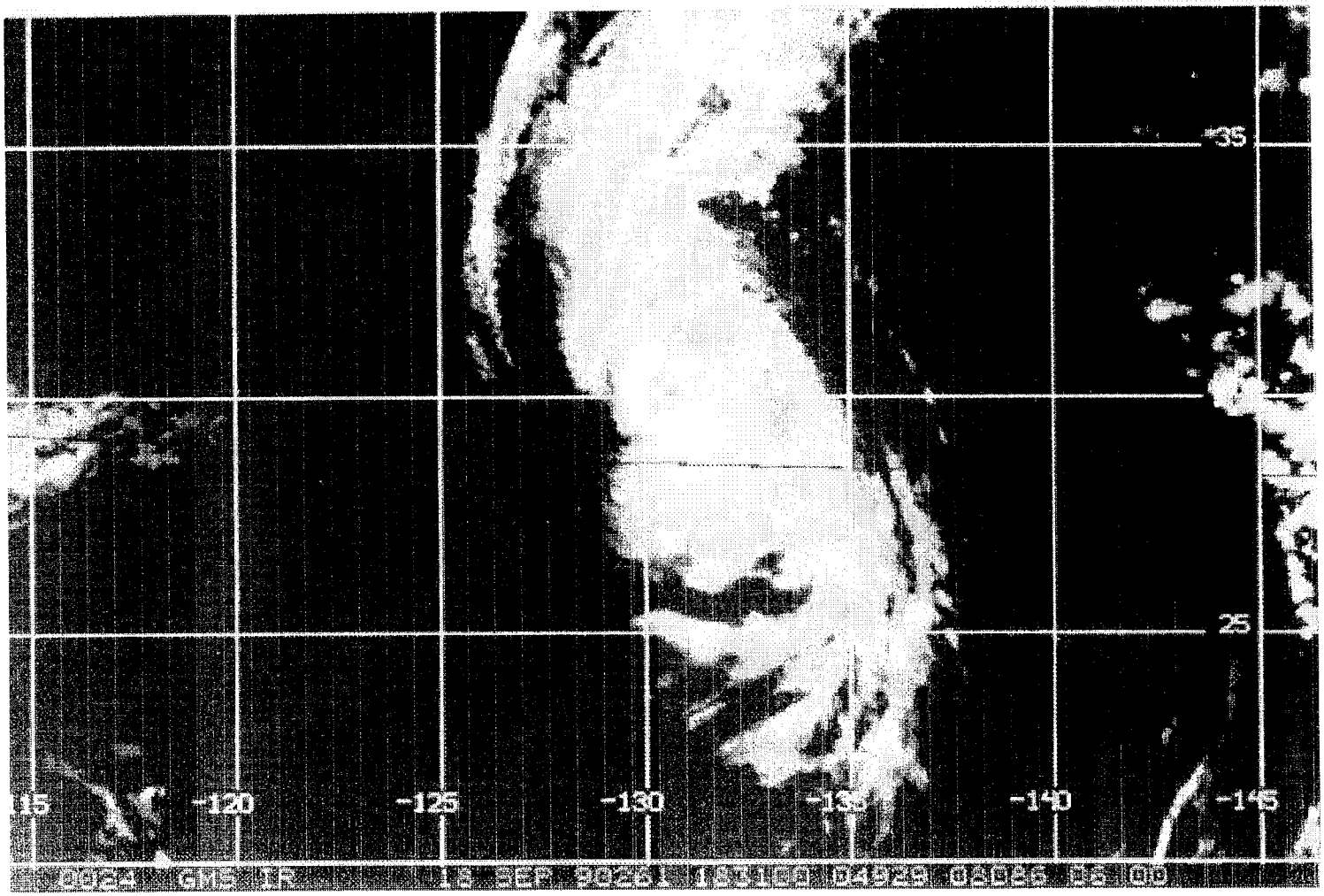

Figure 5.7. (b) The GMS IR image 2 1/2 hours earlier at 1830 UTC. In this image the southern semicircle does not have the same rounded appearance.

5.2 19-Ghz (D) Intensity Statistics

Felde and Glass (1991) demonstrated a favorable correlation between tropical cyclone intensity and 19-Ghz retrievals. As mentioned previously, this frequency is very sensitive to attenuation and emissions by atmospheric constituents such as water vapor, convective precipitation, and sea spray. For this reason, 19-Ghz BTs were investigated as a possible indicator of tropical cyclone intensity.

In their study of 17 SSM/I overpasses of 11 different western North Pacific tropical cyclones, 19-Ghz BTs were investigated as a possible indicator of tropical cyclone intensity. Microwave energy emitted and reflected by the ocean is highly polarized while microwave energy emitted and scattered by atmospheric constituents is unpolarized. The 19-Ghz polarization difference (V-H) was used to isolate the microwave signature attributed only to the atmospheric constituents related to tropical disturbances. The lower the 19-Ghz (D) value, the greater the attenuation, providing an indication of the degree of convective precipitation and other parameters related to tropical cyclone intensity.

For the sample of 17 SSM/I passes, average 19-Ghz (D) values were determined for 1.0, 2.0, and 4.0 degree latitude boxes positioned over the circulation centers. Their research discovered the most significant correlation when the average was calculated over the 1.0 degree latitude box. A correlation coefficient of 0.78 was determined for the 1.0 degree latitude box for the sample of all storms. For intensifying storms, the correlation was slightly higher (0.85), and lower (0.69) for weakening systems.

Conclusions from the composite study were similarly applied to Super Typhoon Flo SSM/I data. A method similar to that described above was used to calculate average 19-

Ghz (D) values. In this investigation, intensity evolution was correlated with 19-Ghz (D) data averaged over circular areas with radii of 0.5, 1.0, 1.5, and 2.0 degrees for each of the 7 SSM/I passes. Figure 5.8 is a plot of maximum sustained wind speed (ms^{-1}) and 19-Ghz (D) BT averages for each circular area as a function of time. Based on the results indicated in the referenced study, there should be at least a general pattern of decreasing 19-Ghz (D) BT averages and increasing wind speeds. Although correlation coefficients are negative for each radius, low values indicate there is no significant relationship between the two parameters. In fact, two out of three of the highest 19-Ghz (D) values correspond to the SSM/I observations at 2130 UTC, 16 September and at 1000 UTC, 17 September, the two passes closest to peak intensity.

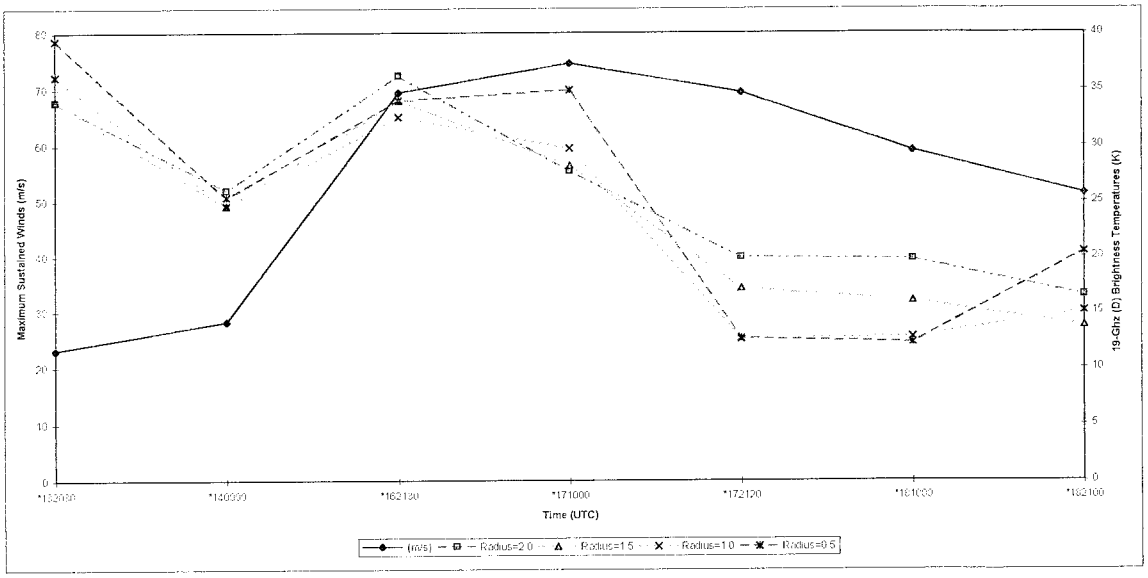

Figure 5.8. The 19-Ghz (D) average brightness temperatures (K) at radii of 2.0, 1.5, 1.0, and 0.5 degrees from Flo's center with maximum sustained winds (ms^{-1}) as a function of time (UTC). Correlation coefficients of r = -0.17, -0.19, -0.29, and -0.26 respectively, indicate there is no association between 19-Ghz (D) BT averages and tropical cyclone intensity for this case. Winds are from JTWC best track data.

Once again, earlier studies relating a derived SSM/I SDR parameter to tropical cyclone intensity failed when it was applied to Super Typhoon Flo. The 19-Ghz (D) BT averages could not have been used to objectively determine Flo's intensity. Although a sample of only 7 SSM/I passes was available, Flo's intensity evolution did not appear to be a function of increased convective activity signaled by increased attenuation and lower 19-Ghz (D) values.

6. SSM/I RAINFALL RATE ENVIRONMENTAL DATA RECORDS

Recent studies have characterized tropical cyclone structure in SSM/I rainfall rate environmental data records. Some of these same studies have also identified a relationship between tropical cyclone intensity and SSM/I retrieved rainfall rates. Alliss et al. (1992, 1993) characterized the precipitation patterns of Hurricane Hugo (1989) and Hurricane Florence (1988) in SSM/I rainfall rate data. In both tropical cyclones, increases in total latent heat release derived from SSM/I rainfall rate retrievals occurred simultaneously with intensification. In Hugo, a strong correlation between the eyewall's maximum rainfall rate and coincident intensification was also noted. Additionally, SSM/I rainfall rate averages within the inner-core region of Florence were found to be strongly associated with intensity changes as the system strengthened from depression stage to a strong tropical storm.

A recent study by Rodgers et al. (1994) stated that the intensification and maintenance of a mature tropical cyclone (storm stage and greater) depend on the amount and distribution of precipitation within the inner core region, i.e., within 111 km. In that study, SSM/I data from 18 named western North Atlantic tropical cyclones were used to determine a relationship between inner-core diabatic heating and intensity change. Results indicated that the more intense tropical cyclones had higher rainfall rates and therefore greater inner-core diabatic heating brought about by the release of latent heat. The highest correlation coeffiecient was found when inner-core latent heat release and corresponding intensity changes occurred during the hurricane stage. Much lower correlation coefficients were found in the case of less intense tropical depressions and storms.

In the introduction, it was mentioned that as Flo recurved within 60 nm (110 km) east of Okinawa, Japan, enough rain fell to end the island's mandatory day-on-day-off water rationing. However, actual rainfall totals measured during this event were much lower than expected, given Flo's extreme intensity and slow translation speed as it skirted Okinawa. In comparison with similar studies of other tropical cyclones, Flo displayed a lower than normal convective signature as indicated by the 85 and 19-Ghz SSM/I retrieved intensity statistics described in the two preceeding chapters. As shown in Chapter 3, each of the two channels is an important variable in the regression equations that descibe the SSM/I rainfall rate algorithms used in this research. Therefore, it is expected that observed SSM/I rainfall rate retrievals of Super Typhoon Flo might also verify less than expected precipitation amounts, primarily during peak intensity.

In the next section, the overall performance of the two original SSM/I rainfall rate algorithms, descibed by Hollinger (1989,1991), is evaluated to determine the most realistic representation of Flo's rainfall rates. In the section following, retrievals from the most reliable SSM/I rainfall rate algorithm are used to characterize Super Typhoon Flo's precipitation structure. In addition, SSM/I rainfall rates are used to determine if an association with intensity can be identified. Finally, an explanation is offered for the lower than expected rainfall generated during the period of Flo's peak intensity.

6.1 SSM/I Rainfall Rate Algorithms

A realistic characterization of Flo's precipitation structure in SSM/I data depends to some extent on the performance and accuracy of the rainfall rate EDR algorithm selected

to perform the analysis. The two algorithms cited in Chapter 3 were first compared to determine the one that best reflects the actual rainfall rates observed during Super Typhoon Flo's most intense episode as it passed east of Okinawa. The two SSM/I rainfall rate algorithms evaluated exhibit one primary difference. The Volume I (Hollinger 1989) alternate algorithm employs the horizontally polarized 85-Ghz frequency in the rainfall rate regression equation while the Volume II (Hollinger 1991) alternate algorithm uses no 85-Ghz data. Raingage measurements and model analysis data provided a method of identifying the most realistic SSM/I rainfall rate algorithm of the two evaluated.

SSM/I Rainfall rate averages (mmh^{-1}) were calculated over a $5^{o}x5^{o}$ box centered on the JTWC final best track position. Average rainfall rates were also computed over the same area in NOGAPS and NMC analyses. For the NOGAPS analyses, the box was centered on the minimum sea-level pressure analyzed in the data while the JTWC final best track position was used to center the box in NMC analyses. However, given the large box used in the calculation, any discrepancies in storm position did not seem to result in large differences in the computed area averaged rainfall rate values.

A water vapor budget calculation was used to determined average rainfall rates in the NOGAPS data. Evaporation was calculated over a $5^{o}x5^{o}$ box positioned over the tropical cyclone center. Moisture convergence was then calculated around the boundary of the $5^{o}x5^{o}$ box from the surface through each level of the column. Assuming constant storage within the enclosed volume, the rainfall rate was computed by applying the following formula:

$$\textbf{Precipitation} = -\frac{1}{g}\int\int\left(u\frac{\partial q}{\partial x}+v\frac{\partial q}{\partial y}\right)dpdA + \int \rho C_d|V|(q_s - q)\,dA$$ where,

g = gravity (m s^{-2})
u = u-wind component (m s^{-1})
v = v-wind component (m s^{-1})
p = pressure level (mb)
q = specific humidity (air)(g kg^{-1})
A = area (m^2)
ρ = density of air (kg m^{-3})
C_d = surface drag coefficient (dimensionless)
$|V|$ = magnitude of wind velocity (m s^{-1})
q_s = saturation specific humidity (at the sea-surface)(g kg^{-1})

The first term on the right-hand side of the equation represents the total moisture convergence defined by the box area. The last term on the right hand side is the bulk aerodynamic formula for evaporation (moisture flux) at the surface over the defined square area. After computing the average convergence and evaporation over the defined 5°x5° area, the two results were added and then divided by the density of water to determine the final rainfall rate. The resolution of NOGAPS is considered coarse compared to the relatively higher (25 km) resolution SSM/I rainfall rate retrievals. However, since average rainfall rate was determined over a large 5°x5° area, meaningful comparisons were possible between the two products. Average rainfall rates were computed for the NOGAPS analyses closest to SSM/I overpass times. In all but one case, time differences were less than 3 hours.

In the NMC data, the six hour accumulated precipitation (mm) field was used to compute the average rainfall rate for the 5°x5° box area. To determine the overall mean rainfall rate, the box averaged accumulated rainfall was further time averaged over the six hour period. Average rainfall rates were computed for the NMC analyses closest to each available SSM/I overpass. In most cases, the time differences were less than three hours.

SSM/I rainfall rate data was also compared to raingage totals from three observing sites. The three sites are all within a 20 km radius of 26.3° N and 127.7° E and are situated in the southern third of the small Japanese island of Okinawa. Their locations are significant given the varying terrain on the island. Each site is located within 1.6 km of the ocean. Also, the southern portion of the island has only small hills and relatively flat terrain compared to the significant terrain features of the island's northern region. Therefore, it can be assumed that the rainfall measured during Super Typhoon Flo at the three southern observing sites was not significantly enhanced by topography. Rainfall totals associated with Flo's passage were measured over a 48 hour period. Rainfall measurements provided by Naha Air Base, Futemna Marine Corps Air Station, and Kadena Air Base were 96.3, 127.3, and 126.5 mm, respectively.

For comparison purposes, rainfall rates were derived from the raingage measurements directly associated with Flo's passage. This was accomplished by time averaging the rainfall measured for the total period (48 hours) by the 42 hour duration the three stations remained within the window of Flo's 5°x5° box. It was estimated that approximately 88% of the total rainfall amount was measured during this period. Once the time averaged rainfall rates were determined, they were further spatially averaged over the three sites. An average rainfall rate of 2.45 mmh^{-1} was derived from the available raingage information.

To further standardize the comparison, SSM/I, NOGAPS, and NMC data were time averaged from 1200 UTC, 16 September through 0600 UTC, 18 September. This was the same 42 hour period used to determine the average rainfall rate from the raingage

information. Straight line interpolations were applied to estimate rainfall rates for the start and stop times in the analysis and SSM/I data. Table 6.1 shows the results of these computations.

Table 6.1. Space and time averaged rainfall rate comparisons.

Rainfall Rate Method	Average Rainfall Rate (mmh^{-1})
SSM/I Volume I Alternate	2.2
SSM/I Volume II Alternate	0.5
NOGAPS Analysis	2.0
NMC Analysis	1.6
Raingage	2.5

For Super Typhoon Flo, the Volume I Alternate algorithm provided a rainfall rate estimate very close to the raingage data and model analyses. In comparisons between individual observations, correlation coefficients of 0.87 and 0.84 were found between the Volume I alternate algorithm and the NOGAPS and NMC rainfall rate averages, respectively. According to these comparisons, the Volume II alternate algorithm performed poorly, underestimating the rainfall rate by an average factor of four.

Average SSM/I rainfall rate retrievals from Super Typhoon Flo were further compared to results from similar tropical cyclone precipitation research. This was done to determine if the SSM/I observations of Flo could be considered representative. Table 6.2 shows comparisons of time and space averaged rainfall rates from this study and other SSM/I tropical cyclone research as well as earlier raingage studies of hurricane

precipitation. The studies were grouped by the total area to provide the most worthwhile comparisons.

Table 6.2. Time and space averaged rainfall rate comparisons. The first group compares average rainfall rates within the eyewall. The next area comparisons integrate rainfall rates over the eyewall and the inner rainband region. The last two groups of comparisons cover a large area of the active tropical cyclone region including the outer rainbands.

Study	Storm	Observation Method	Average RR (mmh^{-1})	Area Method	Total Area (10^3 km^2)
Present	Flo	SSM/I	3.3	1°x1° Box	12
Alliss et al. (1992)	Hugo	SSM/I	14.4	R=60 km Circle	11
Miller (1958)	16 Storm Composite	raingage	6.6	1°x1° Box	12
Present	Flo	SSM/I	3.8	2°x2° Box	49
Alliss et al. (1992)	Hugo	SSM/I	12.1	R=111 km Circle	39
Alliss et al. (1993)	Florence	SSM/I	5.4	R=111 km Circle	39
Rodgers et al. (1994)	18 Storm Composite	SSM/I	5.7	R=111 km Circle	39
Present	Flo	SSM/I	3.2	3°x3° Box	111
Miller (1958)	16 Storm Composite	raingage	3.8	3°x3° Box	111
Present	Flo	SSM/I	2.3	5°x5° Box	308
Rodgers et al. (1994)	18 Storm Composite	SSM/I	2.7	R=333 km Circle	348

Using SSM/I data, Alliss et al. (1992) computed time and space averaged rainfall rates of Hurricane Hugo (1989) within the eyewall and inner-core region at radii of 60 and 111 km, respectively. In a similar study, Alliss et al. (1993) computed the time composite SSM/I rainfall rate average for Hurricane Florence (1988) over a circular area with a radius of 111 km. Miller (1958) determined average rainfall rates from raingage observations of 16 Florida Hurricanes for square areas of 1 and 3 degrees latitude. Using composites of SSM/I data from 18 western North Atlantic tropical cyclones, Rodgers et al. (1994) computed the average rainfall rates for circular areas defined by 111, and 222 km.

Within the eye wall (1°x1° Box), Super Typhoon Flo's rainfall rates are 4 1/2 times less than Hurricane Hugo's and a factor of 2 lower than Miller's (1958) storm composite average. For the inner-core region (2°x2° Box), the rainfall rate average for Flo is more in line with the other studies, except for the 12.1 mmh^{-1} rate computed for Hurricane Hugo. For the larger area comparisons that comprise a significant portion of the active tropical cyclone region including outer rainbands, Flo's average rainfall rates appear to be very close to the averages found in the multiple storm composite studies. Comparisons with these studies indicate that Super Typhoon Flo probably produced below average rainfall given the similarity in data and methods used to determine the time and space averaged rainfall rates.

6.2. Radial Precipitation Distribution

Rodgers et al. (1994) studied the radial distribution of SSM/I rainfall rates in 27 observations of 12 western North Atlantic hurricanes. Results indicated that rainfall rates generally decreased as the radius from the hurricane centers increased. Alliss et al. (1993) used six SSM/I passes to describe the precipitation pattern evolution of Hurricane Florence (1988). The radial distribution of Florence's rainfall pattern was investigated by determining the average SSM/I rainfall rates over circular areas at 20 km radius increments from the circulation center. As expected, there was a general pattern of decreasing rainfall rates with increasing radial distance from the storm center. In addition, a significant difference in the maximum average rainfall rates was observed between the tropical storm and hurricane stages of Florence. Alliss et al. (1992) discovered a comparable pattern in a similar SSM/I analysis of Hurricane Hugo (1989).

The analysis of Super Typhoon Flo's radial rainfall distribution was constructed to account for the three definitive areas of the active tropical cyclone region; the eyewall, the inner-core region, and the outer-core (outer rainband) region. To isolate the SSM/I rainfall rates in each of these regions, annular squares (square rings) were created around the storm center bounded by radial distances of 0.0-0.5, 0.5-1.0, and 1.0-2.5 degrees. A total area defined by the radial distance of 0.0-2.5 degrees (5°x5° box) was also included in the analysis. Average rainfall rates were then calculated for the areas within each of the square rings. Figure 6.1 shows the results of those computations for each SSM/I pass over Super Typhoon Flo. With the exception of the second and third passes, it appears maximum rainfall rates occurred within the inner-core region and not the immediate

eyewall area. This may have been due to the presence of a relatively large rain free region within the eye. It is also noted that the maximum rainfall rates within the inner-core did occur during the period of peak intensity (75 ms^{-1}), although the magnitudes were far lower than some other studies. For example, Alliss et al. (1993) found an SSM/I retrieved area averaged maximum rainfall rate of 16 mmh^{-1} within a 70 km radius of the center of Tropical Storm Florence (1988). In the other study by Alliss et al. (1992), a mean rainfall rate of 19 mmh^{-1} was detected for the area within a 30 km radius of Hurricane Hugo (1989) near peak intensity (approx. 70 ms^{-1}).

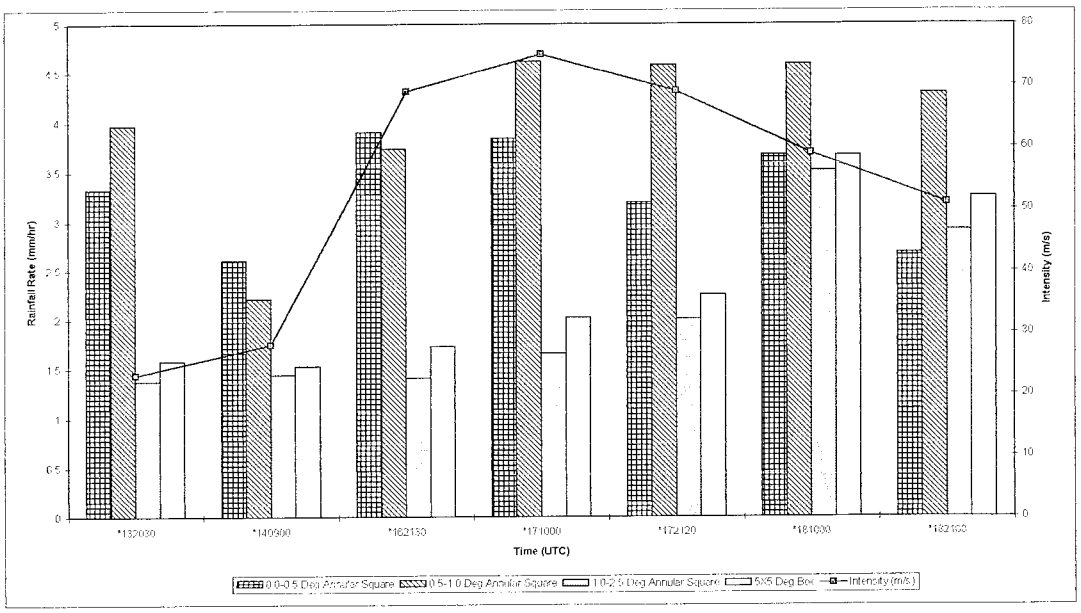

Figure 6.1. Average rainfall rates within the selected areas described by annular squares of 0.0-0.5, 0.5-1.0, 1.0-2.5, and the total 5x5 degree area for each pass. Maximum sustained winds (m/s) are also plotted.

However, when inspecting the composite study by Rodgers et al. (1994), the area averaged rainfall rates for 27 hurricanes were near 6.4 and 5.4 mmh^{-1} at radii of 55 and

111 km, respectively. Flo's maximum average rainfall rates within the inner-core region were slightly less than the composite study but they were more closely compared.

Radial precipitation distribution was also examined by determining mean rainfall rate values over increasing box sizes. Figure 6.2 shows area averaged rainfall rates for the last five passes over Super Typhoon Flo as a function of increasing square areas. The same general pattern of decreasing rainfall rates with increasing distance from the storm center is consistent with similar studies.

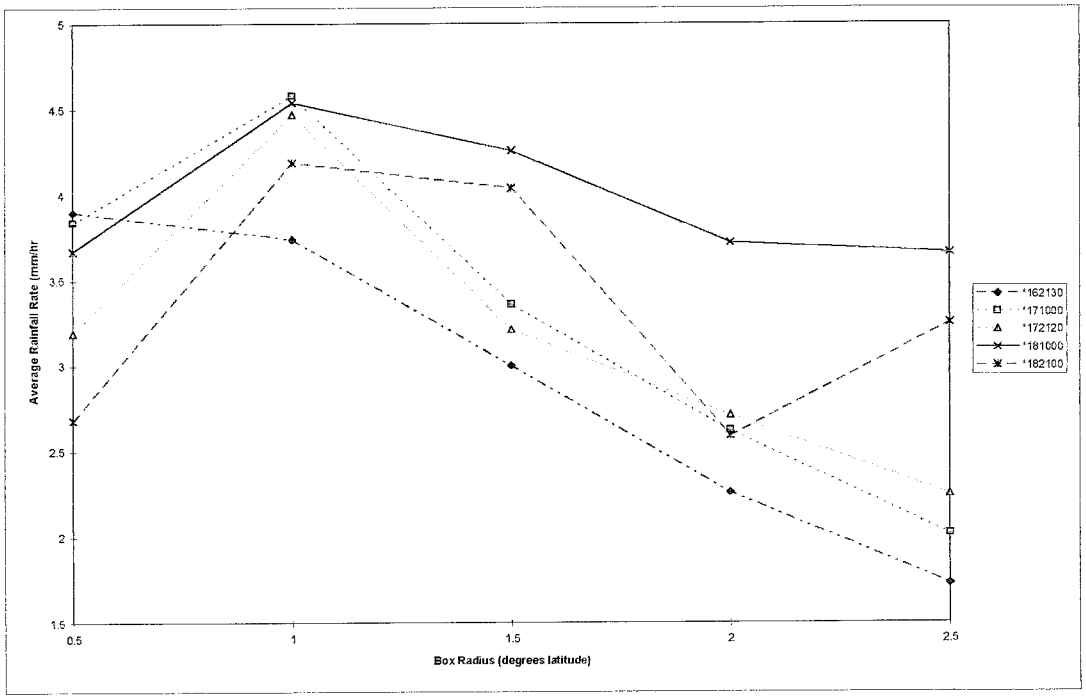

Figure 6.2. Box averaged rainfall rates as a function of radial distance from Flo's center during typhoon, super typhoon, and dissipating typhoon stages.

The last two observations during Flo's weakening phase give indications that the rainfall is beginning to spread away from the inner-core region. It is also obvious from the figure

that the range of average rainfall rates is comparatively small considering extent of intensity change over the period.

6.3. Sectored Precipitation Distribution

The asymmetric nature of the precipitation distribution around tropical cyclones has been widely studied. Most studies have suggested a relationship between the storm movement and the distribution of the heaviest rainfall around the vortex center. A boundary layer model study by Shapiro (1983) found that tropical cyclone motion affects the boundary layer flow over the ocean. Results indicated that storm motion causes enhanced convergence within the boundary layer leading to more intense rainfall in the front portion of a moving tropical cyclone. In examining the asymmetric precipitation distribution of Hurricane Allen (1980), Marks (1985) found that time averaged rainfall rates were highest in the right front quadrant relative to storm motion. Burpee and Black (1989) discovered a similar distribution in an investigation of Hurricane Elena (1985) for a composite foreward motion of 4.9 ms^{-1}. However, in the same study, Burpee and Black (1989) found the highest time averaged rainfall rates located in the left front quadrant of the slower moving (average speed = 1.7 ms^{-1}) Hurricane Alicia (1983).

To investigate Super Typhoon Flo's spatial rainfall distribution, a slightly different method was employed by partitioning the previously defined square ring enclosing the inner-core region. Using the smallest 0.5-1.0 degree annular square, the area was sectored into six equal rectangular areas or sextants. With this sector area convention, it was decided to examine the spatial distribution of Flo's rainfall rates before and after

recurvature. Three SSM/I passes were available prior to recurvature, one during, and three more after. The three passes before recurvature comprise the first time composite. The one pass during and three after Flo's recurvature are time averaged for the second composite. The results of these computations are shown in Figures 6.3 (a) and (b). The time composite prior to recurvature is consistent with previous studies. It shows the larger rainfall rates located in the NW and W sectors, coincident with the forward area relative to Flo's motion. Although there is a noticeable shift in higher rainfall rates to the east, the second composite shows the highest rainfall rates remained in the NW and W sectors or the left-hand side relative to storm motion.

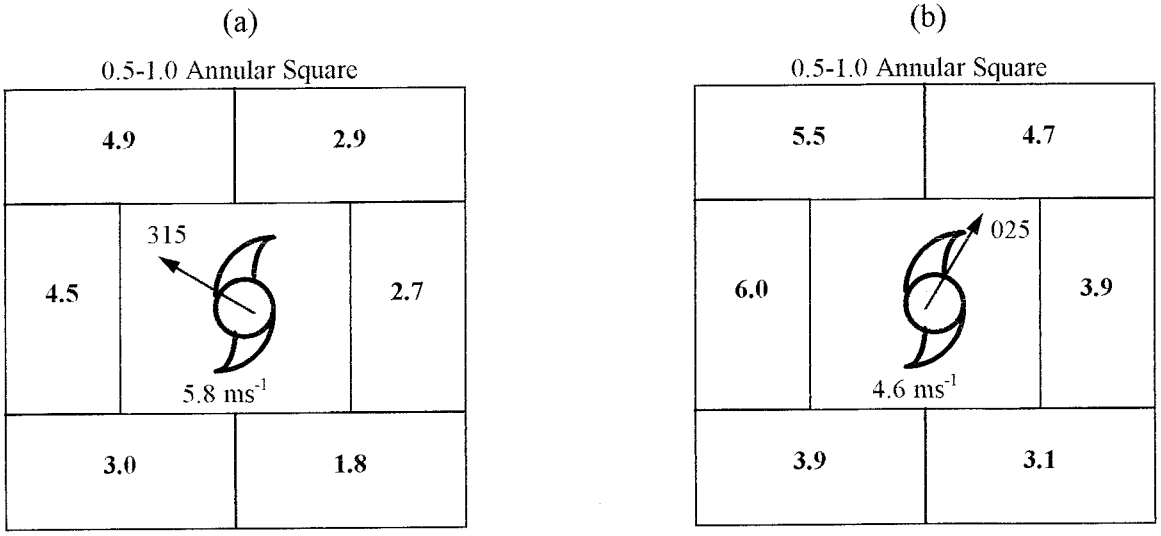

Figure 6.3. Super Typhoon Flo time composite rainfall rate (mmh^{-1}) distribution by sextant for SSM/I passes (a) before recurvature, and (b) during and after recurvature. Forward speed and direction are shown for each.

This result appears to be inconsistent with a similar recent investigation by Rodgers et al. (1994), In that study, a threshold speed of less than 4.1 ms^{-1} was used to categorize slow

moving tropical cyclones. For that composite category of slow moving tropical cyclones results showed the heaviest rainfall located in the front quadrant relative to storm motion.

In examining sectored spatial rainfall rate distributions for individual SSM/I passes, there was a noticeable shift in rainfall rates near the time of recurvature. The SSM/I passes available immediately before and during recurvature exhibited an interesting rainfall rate distribution pattern. The spatial rainfall rate distributions of the pass before and during recurvature are shown for examination in Figures 6.4 (a) and (b). Just before and during recurvature, tropical cyclones normally exhibit a slowing in their relative forward speed. As expected, Super Typhoon Flo reached it's slowest forward motion at the apex of recurvature. Flo's forward speed was approximately 3.5 ms^{-1} at the time of each SSM/I pass.

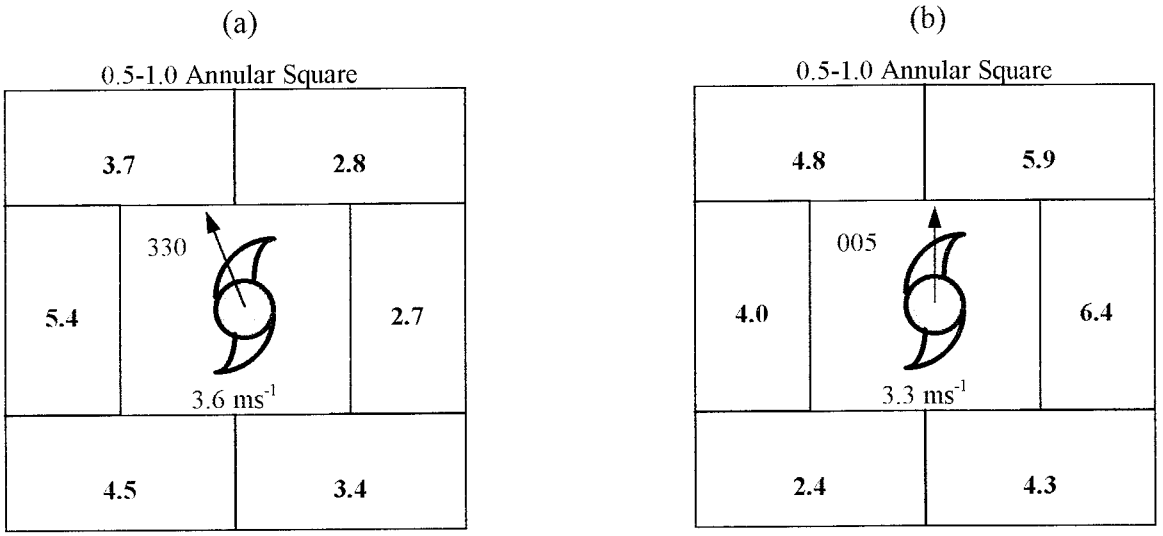

Figure 6.4. Inner-core region sectored rainfall rates for Super Typhoon Flo (a) at 2130 UTC, 16 September before recurvature and, (b) at 1000 UTC, 17 September during recurvature. Flo's forward speed and direction for each pass are also indicated.

In comparing the two observations, there is a notable shift in the precipitation pattern. In the pass prior to recurvature, the highest rainfall rates are generally located in the eastern half of the inner-core region or to the left relative to storm motion. However, the precipitation pattern appears to have migrated relative to storm movement in the next pass. In this observation, the highest rainfall rates have shifted into the NE and E sections or to the right of forward motion. This sector shift in rainfall rates is also coincident with Flo's northeasterly motion after recurvature.

6.3. Rainfall Rates and Typhoon Intensity

Several recent studies have shown a strong association between tropical cyclone intensity and total latent heat release within the inner-core region (Rodgers et al. 1994; Alliss et al. 1992,1993; Marks 1985). Noting that the rainfall rate is linked to total latent heating total latent heating, some of these same studies have also illustrated a strong correlation between rainfall rate magnitudes and tropical cyclone intensity. Weatherford (1987) went as far as to state that the intensification and maintenance of a mature tropical cyclone are dependent on the amount and distribution of rain within the inner-core. Some of these same studies have also established a relationship between rainfall rate changes and subsequent intensity changes in tropical cyclones. However, in investigating the rainfall rates associated with Super Typhoon Flo, a correlation between the rainfall rate magnitude and storm intensity was not readily apparent. The available SSM/I rainfall rate retrievals (confirmed by comparisons with raingage measurements, model output, and similar rainfall

rate studies) suggest Flo produced less than normal rainfall. For example, based on a comparison with Alliss et al. (1992), Flo's SSM/I derived rainfall rates were as much as a factor of four lower than Hurricane Hugo within the eyewall and inner-core region. Providing the avialable SSM/I rainfall rate estimates are representative, other more important mechanisms must have contributed to the rapid intensification of Super Typhoon Flo.

Schubert and Hack (1982) advanced a theory based on tropical cyclone inertial stability that may explain Flo's extreme intensity in the absence of observed high rainfall rates in SSM/I data. They demonstrated that the development of a tropical cyclone-scale circulation could not just be explained by a linear coupling with latent heating caused by increased cumulus convection and precipitation. The linear conditional instability of the second kind (CISK) theory advanced by Ooyama (1964, 1969a) and Charney and Eliassen (1964) may effectively explain the initial phase of tropical cyclone development. However, this linear theory does not account for changes in the two stabilizing mechanisms present within the vortex of a mature tropical cyclone. In intense tropical cyclones, static and inertial stability tend to suppress convergent flow and vertical motion within the inner-core. However, with eye evolution, inertial stability was found to have an unexpected positive effect on continued tropical cyclone intensification. During the period of rapid intensification, a positive nonlinear feedback was discovered between increased inertial stability and the increasing efficiency of the inner-core diabatic heating. Consequently, when the tropical cyclone intensifies, a corresponding increase in latent heat release is not required to bring about continued local warming within the vortex. This

positive feedback begins as hydrostatically lowered surface pressures caused by column warming result in increased tangential winds, and even greater inertial stability. These dynamic and thermodynamic processes may explain the relatively low precipitation rate in Flo. However, a detailed analysis of Flo's energetics and inertial stability require a highly detailed internal structure analysis not practical in the avialable data.

Comparisons have shown Super Typhoon Flo's SSM/I observed rainfall rates were lower than in similar studies of other tropical cyclones. However, it is still of interest to determine whether the changes in rainfall rates from pass to pass would correspond to changes in Flo's intensity. Figure 6.5 shows rainfall rate retrieval averages for box sizes of $1^{\circ}x1^{\circ}$ and $2^{\circ}x2^{\circ}$ plotted with maximum sustained winds at each of the seven SSM/I pass times. The $2^{\circ}x2^{\circ}$ box area is closely compared to the area of the 111 km radius circle used by Alliss et al. (1993) to calculate mean rainfall rates in Hurricane Florence (1988). This larger area most likely encloses both the eyewall and the inner-core region. There appears to be a relatively strong correlation between the $2^{\circ}x2^{\circ}$ box averaged rainfall rates and maximum sustained winds, particularly during intensification. A statistical comparison between rainfall rates and maximum sustained winds yielded a correlation coefficient of 0.7. This indicates a relatively strong association compared to the low correlation results found in the 85 and 19-Ghz data. While the SSM/I observed rainfall rates in Super Typhoon Flo are relatively low, rainfall rate changes do appear to be coincident with intensity changes and are consistent with those observed in previous tropical cyclone research.

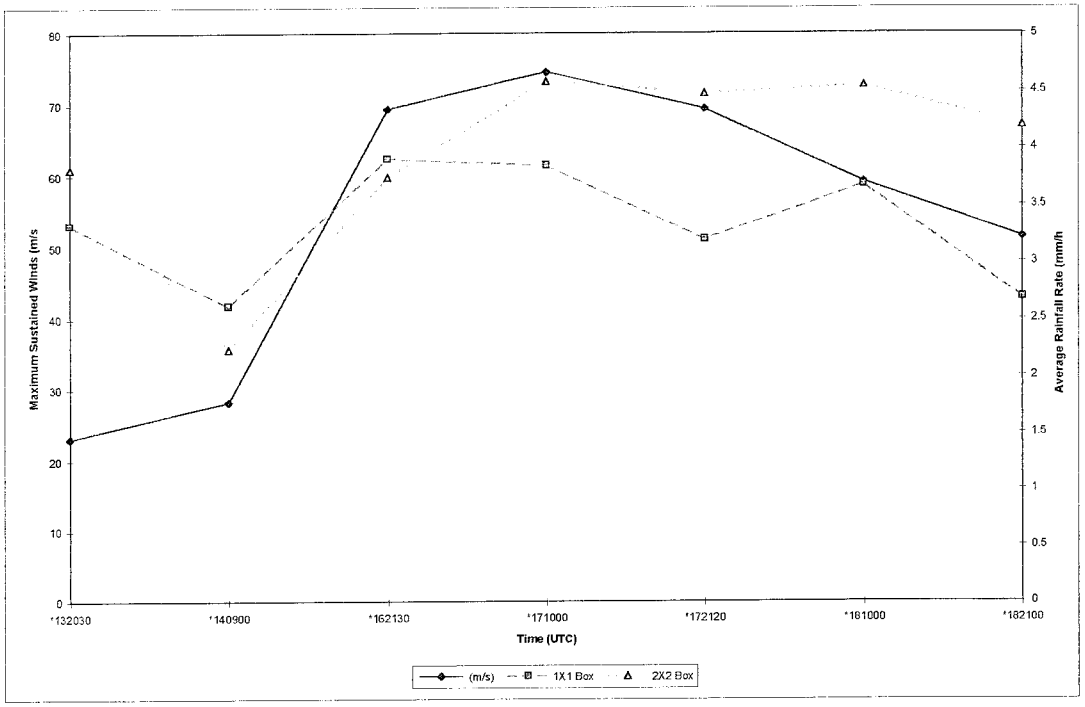

Figure 6.5. Average rainfall rates within 1x1 and 2x2 degree box areas and maximum sustained winds as a function of time. A positive correlation between changes in rainfall rates and changes in maximum sustained winds is most evident for the 2x2 degree box.

7. CONCLUSIONS

SSM/I retrievals and TCM-90 data have been used to observe and analyze the structural characteristics and intensity evolution of Super Typhoon Flo (1990). Qualitative comparisons were made between microwave data and conventional satellite data. Possible tropical cyclone intensity indicators found in similar studies were applied to the SSM/I observations of Flo. In addition, position fix estimates using horizontally polarized 85-Ghz imagery were compared with the Joint Typhoon Warning Center final best track. Finally, two SSM/I rainfall rate retrieval algorithms were compared and then used to quantitatively analyze Flo's precipitation distribution and intensity evolution.

Differences and some similarities were found in the qualitative comparisons between SSM/I 85-Ghz (H) and DMSP OLS data. The microwave data provided a much more detailed picture of Flo's convective structure particularly with respect to the central features. However, the larger swath viewed in OLS data still affords significant advantages in storm coverage. In some instances, enhanced IR imagery provided a better depiction of Flo's eye. Center fixing in horizontally polarized 85-Ghz was shown to offer improved accuracy over fixes in visible and infrared OLS data from the same DMSP pass. The average fix deviation from best track was 13 km for the SSM/I data while it was near 18 km for the OLS data. Unfortunately, little if any correlation was found between tropical cyclone intensity and previously studied SSM/I 85-Ghz brightness temperature statistics. Despite the Dvorak technique's shortfalls, it still provides fairly accurate tropical cyclone intensity estimates.

Accurate descriptions of the size and shape of a tropical cyclone's active region are important in the wind radius forecasts issued by the Joint Typhoon Warning Center. The cloud shield, as depicted in conventional satellite data, is normally used to describe the size and shape parameters of the active tropical cyclone region. These parameters are then used in an empirically derived wind radius equation. According to Felde and Glass (1991), observations of the active tropical cyclone region can be defined as the boundary of 230 K brightness temperatures in vertically polarized 19-Ghz retrievals. Therefore, vertically polarized 19-Ghz retrievals were compared with GMS infrared imagery to establish differences in the observed active tropical cyclone region. Significant differences between the two data types were observed. The diameter of Flo's active region in the SSM/I imagery was an average of 50 km less than the diameter of the cloud shield observed in GMS data. Over estimating the extent of the active tropical region may have lead to unrealistic wind radii forecasts. Differences in the vertical and horizontal 19-Ghz data were also processed to establish a possible relationship with tropical cyclone intensity as shown in other studies. Computed 19-Ghz polarization difference statistics did not correlate favorably with Super Typhoon Flo's intensity evolution.

SSM/I rainfall rate retrievals were also used to characterize Flo's precipitation structure. Two rainfall rate retrieval algorithms described by Hollinger (1989,1991) were first compared with selected data from the TCM-90 field experiment. The Cal/Val Volume I (Hollinger 1989) alternate algorithm, employing the 85-Ghz frequency, was shown to be more accurate when compared to rainfall rates derived from NOGAPS and NMC model analyses and limited raingage information. SSM/I rainfall rate averages over

Super Typhoon Flo were likewise contrasted with previous tropical cyclone studies. Flo's average rainfall rates within the eyewall and inner-core were lower than indicated in other studies. However, more agreeable rainfall rate values were found when larger area averages were compared. SSM/I rainfall rate retrievals from the Volume I (Hollinger 1989) algorithm were also used to characterize Flo's radial and spatial precipitation distribution. Flo's highest rainfall rates were found within the inner-core region defined by the annular squares created by a square of 0.5-1.0 degrees from the storm center. Rainfall rates averaged over increasing box sizes yielded a similar result. The highest average rainfall rates were found in the 2^{o}x2^{o} box centered on the storm. Flo's spatial or sectored precipitation distribution was generally similar to previous studies. The highest rainfall rates were usually located in the foreward sectors relative to storm motion. Although during recurvature, the distribution of highest rainfall rates shifted to the sectors aligned with subsequent recurvature.

Other studies have shown an association between higher rainfall rates and tropical cyclone intensification. However, SSM/I data revealed rainfall rate magnitudes within Flo's eyewall and inner-core were comparatively low. More complicated dynamics might explain Floe's extreme intensity in the absence of higher rainfall rates. A possible explanation was found in a diagnostic analysis of tropical cyclone dynamics by Schubert and Hack (1982). Their theory showed a nonlinear positive feedback exists between increased inertial stability and the increased efficiency of diabatic heating. Further investigation of Flo's average rainfall rate distributions showed changes in inner-core

precipitation rates correlated relatively well with intensity changes even though rainfall rate magnitudes were comparitively low.

REFERENCES

Adler, R. F., and E. B. Rodgers, 1977: Satellite-observed latent heat release in a tropical cyclone. *Mon. Wea. Rev.*, **105**, 956-963.

Alliss, R. A., S. W. Chang and S. Raman, 1992: Special Sensor Microwave/Imager (SSM/I) observations of Hurricane Hugo (1989). *Mon. Wea. Rev.*, **120**, 2723-2737.

Alliss, R. A., S. W. Chang and S. Raman, 1993: Applications of SSM/I data in the analysis of Hurricane Florence (1988). *J. Appl. Meteor.*, **32**, 1581-1591.

Atkinson, G. D., and C. H. Holliday, 1977: Tropical cyclone minimum sea level pressure/maximum sustained winds relationship for the western North Pacific. *Mon. Wea Rev.*, **105**, 421-427.

Black, T. L., 1988: The step-mountain, eta coordinate model: a documentation. NOAA/NWS/NMC Washington, 47 pp. (Available from NOAA/NWS/NMC Washington, Development Division, W/NMC22, Room 204, Washington, DC 20233)

Burpee, R. W. and M. L. Black, 1989: Temporal and spatial variations of rainfall near the centers of two tropical cyclones. *Mon. Wea. Rev.*, **117**, 2204-2209.

Chang, S. W. and T. R. Holt, 1991: Impact of SSM/I rainfall rates on numerical predictions of cyclones: an observing system simulation. *Prec, First International Symposium on Winter Storms*, 151-153, New Orleans.

Charney, J. G., and A. Eliassen, 1964: On the growth of the hurricane depression. *J. Atmos.Sci.*, **21**, 68-75.

Dunnavan, G., R. L. Elsberry, L. Ritchie, G. Holland, and D. Lauritsen, 1991: Structure of Supertyphoon Flo during TCM-90, *Proc., 19th Conference on Hurricanes and Tropical Meteorology*, 21-26, Miami, FL.

Dvorak, V. R., 1975: Tropical cyclone intensity analysis and forecasting from satellite imagery. *Mon. Wea. Rev.*, **103**, 420-430.

Dvorak, V. F., 1984: Tropical cyclone intensity analysis using satellite data. NOAA Technical Report NESDIS 11, Satellite Applications Laboratory, NESDIS, NOAA, Dept. of Commerce, Washington D.C., 47 pp.

Elsberry, R. L., B. C. Diehl, J. C.-L. Chan, P. A. Harr, G. J. Holland, M. Lander, T. Neta, and D. Thom, 1990: ONR Tropical cyclone motion research initiative: Field experiment summary. Technical Report NPS-MR-91-001, Naval Postgraduate School, Monterey, CA 93943, 107 pp.

Falcone, V. J., L. W. Abreau, and E. P. Shettle, 1979: Atmospheric Attenuation of Millimeter and Submillitmeter Waves: Models and Computer Code. AFGL Technical Report AFGL-TR-79-0253, AFGL, Hanscom AFB, MA.

Felde, G. W., and M. Glass, 1991: SSM/I brightness temperatures analysis of tropical cyclones, *Proc., 19th Conference on Hurricanes and Tropical Meteorology*, 400-404, Miami, FL.

Fiorino, M., and T. T. Warner, 1981: Incorporating surface winds and rainfall rates into the initialization of a mesoscale hurricane model. *Mon. Wea. Rev.*, **109**, 1914-1929.

Glass, M., and G. W. Felde, 1989: The structure of tropical cyclones and surrounding regions as determined from OLS and SSM/I imagery analysis. *Prec., Fourth Conference on Satellite Meteorology and Oceanography*, 35-38, Boston, MA.

Guard C. P., L. E. Carr, F. H. Wells, R. A. Jeffries, N. D. Gural, and D. K. Edson, 1992: Joint Typhoon Warning Center and the challenges of multibasin tropical cyclone forecasting. *W. and Forecasting*, **7**, 328-352.

Hogan, T. F., and T. Rosmond, 1991: The description of the Navy Operational Global Atmospheric Prediction System's Spectral Forecast Model. *Mon. Wea. Rev.*, **119**, 1789-1815.

Hogan, T. F., T. Rosmond, and R. Gelaro, 1990: The NOGAPS forecast model: A technical description. NOARL Report #13, 212 pp. (Available from Naval Research Lab, Monterey, CA 93943-5006.

Holliday, C. R., and K. R. Waters, 1989: SSM/I observations of tropical cyclone gale force vicinity winds, *Proc., 4th Conference on Satellite Meteorology and Oceanography*, , San Diego, CA.

Holliday, C. R., and A. H. Thompson, 1979: Climatological characteristics of rapidly intensifying typhoons. *Mon. Wea. Rev.*, **107**, 1022-1034.

Hollinger, J., R. Lo, G. Poe, R. Savage, and J. Peirce, 1987: Special Sensor Microwave/Imager User's Guide. (available from the author at Naval Research Laboratory, Washington, DC 20375)

Hollinger, J. P., 1989: DMSP Special Sensor Microwave/Imager Calibration Validation, Final Report Vol. I. (available from the author at Naval Research Laboratory, Washington, DC 20375)

Hollinger, J. P., 1991: DMSP Special Sensor Microwave/Imager Calibration Validation, Final Report Vol. II. (available from the author at Naval Research Laboratory, Washington, DC 20375)

Marks, F. D., Jr., 1985: Evolution of the structure of precipitation in Hurricane Allen (1980). *Mon. Wea. Rev.*, **113**, 1268-1285.

Martin, J. D., and G. J. Holland, 1988: Wind-radii profiler and beta motion tool. [Documentation available from Techniques Development Officer, Detachment 1, PACAF, COMNAVMAR, Box 20, FPO AP 96540-0051.]

McMorrow, D., 1989: Forecasting typhoons without aircraft reconnaissance at the Joint Typhoon Warning Center, *Proc., 19th Conference on Hurricanes and Tropical Meteorology*, J32-J35, Miami, FL.

Mesinger, F., 1984: A blocking technique for representation of mountains in atmospheric models. *Riv. Meteor. Aeronautica*, **44**, 195-202.

Miller, B. I., 1958: Rainfall rates in Florida hurricanes. *Mon. Wea Rev.*, **86**, 258-264.

Molinari, J., 1982: Numerical hurricane prediction using remotely-sensed rainfall rates. *Mon. Wea. Rev.*, **110**, 553-571.

Olson, W. S., 1989: Physical retrieval of rainfall rates over the ocean by multispectral microwave radiometry-application to tropical cyclones. *J. Geophys Res.*, **94**, 2267-2280.

Ooyama, K., 1964: A dynamical model for the study of tropical cyclone development. *Geofis. Int.*, **4**, 187-198.

Ooyama, K., 1969a: Numerical simulation of the life cycle of tropical cyclones. *J. Atmos. Sci.*, **26**, 3-40.

Peng, M., and S. W. Chang, 1994: Impacts of SSM/I retrieved rainfall rates on the numerical prediction of tropical cyclones. Submitted to *Mon. Wea. Rev.*

Rappaport, E. N., 1991: Operational applications of SSM/I data at the National Hurricane Center, *Proc., 19th Conference on Hurricanes and Tropical Meteorology*, 179-183, Miami, FL.

Rappaport, E. N., and P. G. Black, 1989: The utility of Special Sensor Microwave/Imager data in the operational analysis of tropical cyclones. *Proc., Fourth Conf. on Satellite Meteorology and Oceanography,* San Diego, Amer. Meteor. Soc., J21-J24.

Rogers, E., G. J. DiMego, and S. J. Lord, 1991: Data assimilation and forecasting for the tropical cyclone motion experiment (TCM-90) at the National Meteorological Center, *Proc., 19th Conference on Hurricanes and Tropical Meteorology*, Miami, Amer. Meteor. Soc., 7-9.

Rodgers, E. B., S. W. Chang, and H. F. Pierce, 1994: A satellite observational and numerical study of precipitation characteristics in western North Atlantic Tropical Cyclones. *J. Appl. Meteor.*, **33**, 129-139.

Rodgers, E. B., S. W. Chang, J. Stout, J. Steranka and J. J. Shi, 1991: Satellite Observations of variations in tropical cyclone convection caused by upper-tropospheric troughs. *J. Appl. Meteor.*, **30**, 1163-1184.

Sandlin, G. D., and D. J. Spangler, 1989: SSM/I imagery, center-fixes, and wind fields for tropical cyclones, Naval Research Laboratory Report, (available from the author at Naval Research Laboratory, Washington, DC 20375).

Schubert, W. H., and J. J. Hack, 1982: Inertial stability and tropical cyclone development. *J. Atmos. Sci.*, **39**, 1687-1697.

Shapiro, L. J., 1983: The asymmetric boundary layer flow under a translating hurricane. *J. Atmos. Sci.*, **40**, 1984-1998.

Velden, C. S., W. S. Olson, and B. A. Roth, 1989: Tropical cyclone center-fixing using SSM/I Data, *Proc., 19th Conference on Hurricanes and Tropical Meteorology*, J36-J39, Miami, FL.

Vermillion, C. H. , F. L. Stetina, E. H. Shaffer, R. L. Mahoney, C. P. Guard, 1993: Joint Typhoon Warning Center, MIDDAS system development case study, *Proc., 20th Conference on Hurricanes and Tropical Meteorology*, San Antonio, Amer. Meteor. Soc., 185-188.

Weatherford, C., 1987: Typhoon structural evolution. *Proc., 17th Conf. on Hurricanes and Tropical Meteorology*, Miami, Amer. Meteor. Soc., 337-340.

Willoughby, H. E., J.A. Clos, and M. G. Shoreibah, 1982: Concentric eye wall, secondary wind maxima, and the evolution of the hurricane vortex. *J. Atmos. Sci.*, **39**, 395-411.